

HUMAN ANTIBODY RESPONSE TO ZONOTIC INFLUENZA A VIRUSES

By

Sandhya Bangaru

Dissertation

Submitted to the Faculty of the  
Graduate School of Vanderbilt University

in partial fulfillment of the requirements

for the degree of

DOCTOR OF PHILOSOPHY

in

Microbiology and Immunology

May 11, 2018

Nashville, Tennessee

Approved:

James W. Thomas, M.D.

Kathleen L. Gould, Ph.D.

Maria Hadjifrangiskou, Ph.D.

Christopher R. Aiken, Ph.D.

James E. Crowe, Jr., M.D.

To my parents for their unconditional love and infinite support  
To my husband who put his dreams behind so I could pursue mine

## ACKNOWLEDGEMENTS

I would first like to thank my mentor, Dr. James Crowe for being a wonderful teacher, a guide and a friend. Ever since my first day in Crowe lab, he has given me complete scientific freedom to explore and pursue my research, which has helped me grow as an independent scientist. He has always been there to share my excitement and provide encouragement when needed. I could not have imagined a better advisor for my PhD research. His expectations and faith in me has helped me become a better scientist.

I would also like to express my sincere gratitude to my dissertation committee, Dr. Tom Thomas (Chair), Dr. Kathy Gould, Dr. Christopher Aiken, Dr. Maria Hadjifrangiskou, and my previous chair John Williams for all their guidance and support over the last four years. I am very grateful for their insightful suggestions and contributions to this work.

I am greatly indebted to my wonderful colleagues for their support and friendship over these years. They have contributed immensely to my personal and professional time at Vanderbilt. I want to specially thank Nurgun Kose who has been more than a friend to me during my time in Crowe lab. The long hours in the lab always seemed better with her company. I am very grateful to Natalie Thornburg and Jennifer Pickens whose friendship and guidance played a significant role in my research during my early years in Crowe lab. My deep appreciation for Hannah King whose patience and helping nature were my saving grace during times of heavy experimental burden. Also, a huge thanks to my fellow graduate students for providing scientific as well as moral support and for all the fun we had during the last four years. A special thanks to Jessica Finn for making my life easier with her sequencing and coding help. I would also like to acknowledge the managers and the administrative staff of Crowelab for their technical

assistance. My sincere thanks to Lorie Franklin and the graduate school for all the assistance and support provided by them.

My sincere thanks goes to my collaborators, Dr. Ian Wilson and Dr. Andrew Ward from the Scripps research institute, without whom I couldn't have successfully completed my projects. I thank all the Scripps researchers, Heng Zhang, Shanshan Lang, Xueyong Zhu, Travis Nieusma and Hannah Turner, who have contributed towards my thesis work. I want to extend my thanks to Dr. Sheng Li, Dr. Randy Albrecht, Dr. Adolfo Garcia Sastre, Dr. Webby Richard and Dr. Juergen Richt for the support I received from the collaborative work done with their groups. Besides my collaborators, I would also like to express my sincere gratitude to all the participants and researches involved in the vaccine clinical trials that made my research possible.

I am grateful to the Vanderbilt International Scholar Program (VISP) for the funding provided towards my PhD. I want to thank Dr. Kathy Gould for giving me the opportunity to be a part of this program. Kathy has been a pillar of support to me ever since my joining Vanderbilt. I want to thank her for her guidance and support during these last 5 years. I want to also thank the National Institute of Health (NIH) and the National Institute of Allergy and Infectious Diseases (NIAID) for funding my research.

Finally, I want to thank my family who were with me during every step of this journey. I am forever grateful to my parents and my sister for their unconditional love and understanding. Their support, dedication and sacrifice are the true reasons behind my success. I was very fortunate to have had my husband during the crucial years of my PhD. Your unwavering love and patience gave me the courage to embark on this journey and to finish what I started. Thank you for always being there for me through thick and thin.

## TABLE OF CONTENTS

	Page
DEDICATION .....	ii
ACKNOWLEDGEMENTS .....	iii
LIST OF TABLES .....	vii
LIST OF FIGURES .....	viii
LIST OF ABBREVIATIONS.....	ix
Chapter	
<b>I. Introduction.....</b>	<b>1</b>
Thesis overview.....	1
Introduction to influenza.....	3
Influenza isolation and classification .....	3
IAV structure and morphology.....	6
Influenza life cycle .....	9
Immune response to influenza.....	12
Current influenza vaccines and therapeutics .....	15
Influenza pandemics and epidemics.....	16
Influenza viruses with pandemic potential .....	17
Influenza A hemagglutinin and universal vaccine .....	19
Influenza A neuraminidase .....	23
<b>II. Recognition of influenza H3N2v virus by human neutralizing antibodies.....</b>	<b>26</b>
Introduction .....	26
Study of B cell response before and after vaccination with H3N2v vaccine .....	28
Isolation and functional characterization of H3N2v-reactive human mAbs.....	31
Competition-binding studies.....	35
Epitope mapping by mutagenesis experiments and electron microscopy .....	35
The H3N2v HA is antigenically related to that of older human seasonal H3N2 IAVs .....	40
Discussion.....	43
Experimental methods.....	46
<b>III. A broad H3 human monoclonal antibody that targets influenza HA head exploits multiple antiviral strategies.....</b>	<b>54</b>
Introduction .....	54
MAb H3v-47 exhibits broad neutralizing activity against human and swine H3N2 strains .....	56
Prophylactic administration of H3v-47 reduced pulmonary viral load in mice.....	60
Epitope mapping and structural characterization of H3v-47-HA complex reveals a unique neutralizing epitope on H3 head domain .....	62

Mechanism of neutralization by mAb H3v-47 .....	65
H3v-47 mAb exhibits ADCC activity.....	70
Discussion.....	72
Experimental methods .....	74
<b>IV. A broadly protective human antibody for influenza type A viruses recognizes a hidden epitope on the hemagglutinin head domain .....</b>	<b>83</b>
Introduction .....	83
Donor vaccination history.....	85
Isolation and characterization of human mAb FluA-20 .....	86
Identification of clonal lineages.....	87
FluA-20 exhibits prophylactic efficacy in vivo against viruses of influenza type A H1N1, H3N2, H5N1 or H7N9 subtypes.....	90
FluA-20 lacks neutralizing function but possesses ADCC activity.....	92
Epitope binning, DXMS and structural studies reveal FluA-20 epitope.....	94
Mutation experiments to identify critical residues in the FluA-20 IgG paratope .....	97
FluA-20 binding to HA is substantially reduced after HA cleavage.....	100
Discussion.....	104
Experimental methods.....	107
<b>V. Human antibody responses to influenza A H7N9 virus.....</b>	<b>115</b>
Introduction .....	115
Comparison of human B cell response following vaccination or natural infection with H7N9.....	118
Cross-reactive response elicited by H7N9 infection or vaccination .....	120
Isolation of N9-specific human antibodies.....	124
Functional analysis of N9-specific mAbs .....	124
Epitope mapping of human N9 mAbs.....	128
Discussion.....	132
Experimental methods.....	134
<b>VI. Conclusions and future directions.....</b>	<b>139</b>
Study of human antibody response to IAVs.....	139
Human antibody response to H3v HA.....	140
Human antibody response to H7 HA and N9 NA.....	141
Future directions: Towards universal influenza vaccines .....	143
Induction of broadly cross-reactive antibodies by exposure to H7 HA .....	143
Broad H3 mAbs that target vestigial esterase domain and inhibit viral egress .....	146
Targeting HA trimer interface for heterosubtypic breadth .....	147
LIST OF PUBLICATIONS .....	149
BIBLIOGRAPHY.....	150

## LIST OF TABLES

### Table

3-1.	H3v-47 IgG breadth of HA binding and virus neutralization for human or swine H3N2 viruses .....	58
4-1.	Binding of FluA-20 paratope mutants to HA from indicated strain .....	99
6-1.	Binding breadth of H7-induced heterosubtypic mAbs .....	145

## LIST OF FIGURES

### Figure

1-1.	Phylogenetic trees of HA and NA genes from all known subtypes .....	5
1-2.	Schematic diagram of influenza A virus particle .....	8
1-3.	Influenza life cycle .....	11
1-4.	Antigenic sites mapped on the surface representation of H3 A/Aichi/2/1968 HA .....	22
1-5.	Surface representation of N9 A/Shanghai/1/2013 NA .....	24
2-1.	H3N2v specific and cross-reactive B cell response .....	30
2-2.	Characterization of 17 neutralizing monoclonal antibodies .....	33
2-3.	Neutralization titers for four H3v-reactive human mAbs against swine IAVs .....	34
2-4.	Competition binding of neutralizing antibodies to MNv HA protein .....	36
2-5.	Binding of H3 variant specific-antibodies to mutated Minnesota HA proteins .....	38
2-6.	Negative stain EM images of Hemagglutinin-Fab complexes .....	39
2-7.	H3N2v is antigenically similar to older seasonal strains .....	42
3-1.	Comparison of neutralizing activity exhibited by H3v-47 Fab, F(ab') <sub>2</sub> or IgG against A/Minnesota/11/2010 H3N2v virus .....	59
3-2.	Prophylactic efficacy of H3v-47 in mice .....	61
3-3.	Competition binding of H3v-47 with other influenza head- or stem-binding antibodies .....	63
3-4.	Crystal structure of antibody H3v-47 Fab in complex with H3N2v HA (A/Minnesota/11/2010) and identification of the epitope .....	64
3-5.	Inhibition of egress of A/Minnesota/11/2010 H3N2v virus by IgG of mAbs H3v-47 or CR8020 or by the small molecule neuraminidase inhibitor zanamivir .....	67
3-6.	H3v-47 localizes to interfaces between virus and cell surface or between viral particle .....	69
3-7.	H3v-47 mAb exhibits ADCC activity .....	71
4-1.	Network analysis of sequences clonally related to FluA-20 .....	89
4-2.	Binding of FluA-20 to group 1 and group 2 HAs .....	90
4-3.	FluA-20 antibodies prophylactically protect mice from sub-lethal challenge from pathogenic IAV for humans .....	91
4-4.	FluA-20 likely protects by ADCC activity .....	93
4-5.	Epitope mapping by competition binning and HDX-MS studies .....	95
4-6.	FluA-20 targets the 220-loop and the 90-loop at the trimer interface of the H1 head domain .....	98
4-7.	Flow cytometric analysis of antibody binding to cell-surface expressed HA .....	102
4-8.	FluA-20 does not neutralize HA0 virus .....	103
5-1.	Frequency of H7- and N9-reactive B cells in 30 H7N9 vaccinated donors .....	120
5-2.	Breadth of HA response in H7N9 vaccinees and survivors .....	122
5-3.	Breadth of NA response in H7N9 vaccinees and survivors .....	123
5-4.	Binding breadth of NA-reactive mAbs isolated from H7N9 survivors and vaccinees .....	126
5-5.	Functional characterization of N9-specific antibodies .....	127
5-6.	N9 NA-reactive mAbs target at least two distinct antigenic regions on NA .....	130
5-7.	Epitope mapping of N9-specific mAbs by HDX-MS and EM .....	131



## LIST OF ABBREVIATIONS

ADCC	Antibody-dependent cell-mediated cytotoxicity
APC	Antigen-presenting cells
Ab	Antibody
BCR	B cell receptor
BLI	Bio-layer interferometry
CDC	U.S. Centers for Disease Control
CDR	Complementarity-determining regions
cRNA	Complementary RNA
EC <sub>50</sub>	Half-maximal effective concentration
ELISA	Enzyme linked immunosorbent assay
ELLA	Enzyme linked lectin assay
EM	Electron microscopy
Fab	Fragment-antigen binding
FACS	Fluorescence-activated cell sorting
Fc	Fragment crystallizable
FcγR	Fcγ receptors
HA	Hemagglutinin
HA0	Hemagglutinin precursor protein
HA1	Hemagglutinin subunit 1
HA2	Hemagglutinin subunit 2
Hb site	Hemadsorption site on neuraminidase
HAI	Hemagglutination-inhibition
HC	Heavy chain
HDX-MS	Hydrogen deuterium exchange mass spectrometry
H3N2v	H3N2 variant
IAV	Influenza A virus

IC <sub>50</sub>	Half-maximal inhibitory concentration
IFN	Interferon
Ig	Immunoglobulin
IgA	Immunoglobulin A
IgG	Immunoglobulin G
IgM	Immunoglobulin M
kDa	Kilodalton
LC	Light chain
LCL	Lymphoblastoid cell lines
mAb	Monoclonal antibody
MDCK	Madin-Darby canine kidney cells
mRNA	Messenger RNA
M1	Matrix 1 protein
M2	Matrix 2 protein
MN <sub>v</sub>	Minnesota H3N2 <sub>v</sub>
NA	Neuraminidase
NCBI	National Center for Biotechnology Information
NEP	Nuclear export protein
NI	Neuraminidase enzymatic inhibition
NP	Nucleoprotein
O.D	Optical density
PA	Polymerase acidic protein
PB1	Polymerase basic protein 1
PB2	Polymerase basic protein 2
PBS	Phosphate buffered saline
PBMC	Peripheral blood mononuclear cells
PFU	Plaque forming units

RBS	Receptor-binding site
SA	Sialic acid
$\alpha$ -2,6-linked	Sialic acid attached to the galactose by an $\alpha$ 2,6 linkage
$\alpha$ -2,3-linked	Sialic acid attached to the galactose by an $\alpha$ 2,3 linkage
SEM	Standard error of the mean
SPR	Surface plasmon resonance
ssRNA	Single-stranded RNA
TCID <sub>50</sub>	Median tissue culture infectious dose
TEM	Transmission electron microscopy
TLR	Toll-like receptor
TPCK	L-(tosylamido-2-phenyl) ethyl chloromethyl ketone
UCA	Unmutated common ancestor
vRNP	Viral ribonucleoprotein
WHO	World Health Organization

# CHAPTER I

## INTRODUCTION

*“However, as bad as things were, the worst was yet to come, for germs would kill more people than bullets. By the time that last fever broke and the last quarantine sign came down, the world had lost 3-5% of its population.”*

*Charles River Editors, The 1918 Spanish Flu Pandemic: The History and Legacy of the World's Deadliest Influenza Outbreak (2014)*

### **Thesis overview**

This document contains the results and conclusions of my work investigating the human antibody response to pandemic-potential influenza A viruses (IAV). It is divided into six chapters; chapter I contains the required background information on IAVs, the pandemic potential of zoonotic IAVs, the structural and antigenic diversity of the viral glycoproteins hemagglutinin (HA) and neuraminidase (NA), the mechanisms by which antibodies to HA and NA mediate protection, and current vaccination strategies.

My thesis work begins in chapter II, which focuses on the human antibody response to swine-origin influenza A H3N2 variant (H3N2v) viruses. In this chapter, I describe the isolation and characterization of H3N2v-reactive monoclonal antibodies from adult donors who were vaccinated with an H3N2v subunit vaccine candidate. Using these mAbs, I was able to identify the important viral residues responsible for antigenic differences between swine-origin H3N2v and the H3N2 strains circulating in humans. I was also able to provide evidence as to why children had no pre-existing immunity to H3N2v virus making them the most susceptible subset

of the population.

Chapter III focuses largely on the characterization of a human monoclonal antibody designated H3v-47 that exhibits potent cross-reactive neutralization activity against a majority of human and swine H3N2 viruses making it a promising therapeutic candidate. I provide detailed structural and functional evidence to support that H3v-47 binds to a novel epitope on influenza hemagglutinin (HA) and functions in a unique manner by inhibiting viral egress, a mechanism distinct from that of any known IAV antibody.

In chapter IV, I describe the discovery of a naturally occurring pan-influenza A human monoclonal antibody FluA-20 that provides *in vivo* protection against diverse IAV subtypes. FluA-20 recognizes a conserved site on the HA head domain that is occluded in the HA trimer interface, suggesting previously unrecognized dynamic features of the HA head domains in the trimeric protein.

In chapter V, I focus on human antibody-mediated immunity to highly lethal avian-origin H7N9 viruses. I compare the antibody responses to HA and NA in H7N9 vaccine donors and survivors of natural H7N9 infection. While most influenza antibody research has been focused on HA, my studies have shown that antibodies to NA play an equally important role in providing anti-viral immunity and are particularly critical in individuals who develop significantly higher antibody titers against NA compared to HA.

In chapter VI, I summarize all my findings on antibody-mediated immunity to influenza viruses and propose future direction for this work. Majority of my thesis work has been focused on studying the human antibody response to diverse influenza antigens and understanding the molecular mechanisms by which cross-reactive influenza antibodies provide protective immunity.

## **Introduction to influenza**

Influenza A viruses are highly contagious respiratory pathogens associated with high morbidity and mortality rates. The most common symptoms for uncomplicated influenza illness are fever, myalgia, malaise, headache, sore throat and non-productive cough (1, 2). Influenza infections also exacerbate underlying medical conditions like pulmonary or cardiac disease and are the primary cause of viral pneumonia (3). Although influenza epidemics affect people of all age groups, the highest risk of complications occurs among the elderly, children, pregnant women and individuals with chronic diseases (2). Annual outbreaks of influenza in humans are one of the major health problems worldwide, causing 3-5 million cases of severe illness and up to 500,000 deaths every year (4). In addition to its social impact, influenza viruses also pose a huge economic burden due to the resulting health-care costs and loss of productivity.

## **Influenza isolation and classification**

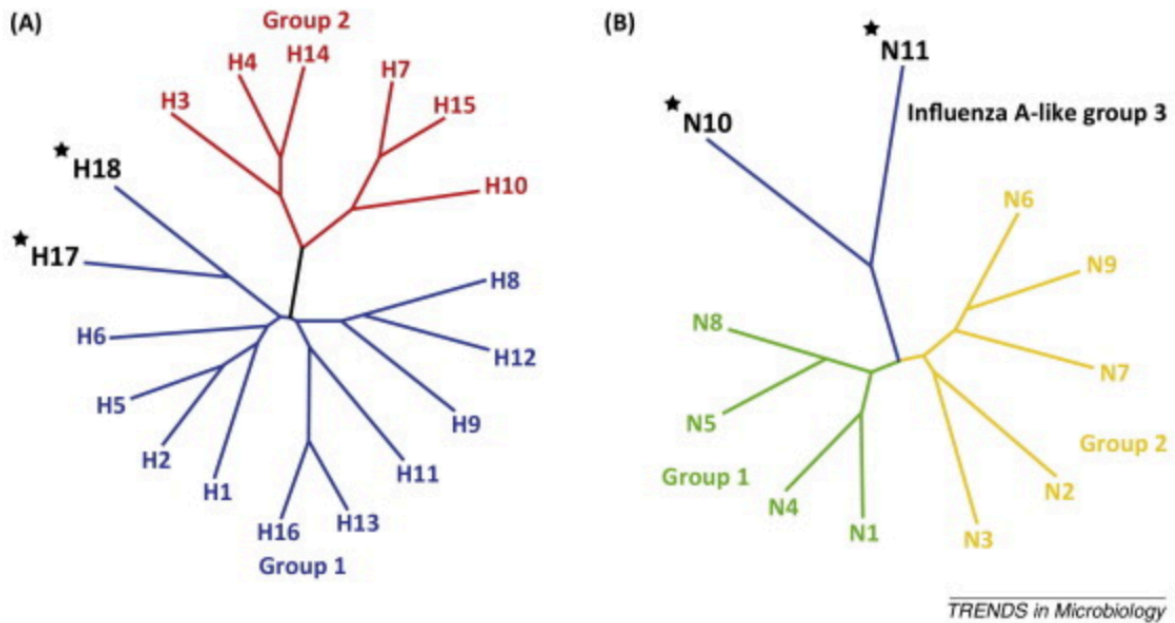
Beginning from the 5<sup>th</sup> century B.C, reports have consistently described epidemics and pandemics with influenza-like symptoms. However, it was not until 1931 that influenza was isolated for the first time from infected pigs by Richard Shope, an investigator from the Rockefeller Institute (5, 6). The first human influenza virus was isolated at the National Institute for Medical Research, UK by Wilson Smith, Christopher Andrewes, and Patrick Laidlaw in 1933 (7). Influenza B, C and D types were isolated in 1940, 1947 and 2011 respectively (8-10).

Influenza are enveloped, segmented, single-stranded, negative-sense RNA viruses belonging to the *Orthomyxoviridae* family that includes seven genera: *Influenza virus A*, *Influenza virus B*, *Influenza virus C*, *Influenza virus D*, *Isavirus*, *Thogotovirus* and *Quaranjavirus*. Influenza viruses A, B and C are classified on the basis of their core proteins and

only influenza A viruses are further classified into serologically distinct subtypes based on the combination of their two viral surface glycoproteins HA and NA (11). Both influenza A and B viruses cause annual epidemics in the human population while type C viruses cause mild upper respiratory infections and are not thought to cause epidemics. Among the different influenza types, IAVs are the most virulent human pathogens and the only type with the ability to cause human pandemics due to their broad host-range. My research work has focused on the immune responses to influenza A viruses.

The IAV genome consists of 8 RNA segments that encode 11 viral proteins including glycoproteins, matrix proteins, nonstructural proteins, nucleoproteins, and polymerase proteins. The 2 major surface glycoproteins HA and NA are the principal antigenic components on the virus and form the basis for IAV classification. Currently, there are 18 known HAs that fall into 2 broad groups based on their sequence and phylogeny (12-14). Similarly, the 11 known NAs also fall under 2 major groups and a third minor group that includes two neuraminidase-like proteins N10 and N11 (13, 14). Several combinations of HA and NA are possible. For example, IAVs designated as H3N8 contain HA3 and NA8 proteins on its surface. Members of all HA and NA subtypes can be found within wild aquatic birds, which serve as a natural reservoir for IAVs. By contrast, only 2 subtypes, H1N1 and H3N2, currently circulate in the human population.

To ensure accurate naming of influenza viruses, WHO established a standard naming convention in the year 1980. The influenza nomenclature consists of: the antigenic type (A, B, C or D), host origin (no designation needed for human origin), geographical origin, strain number and year of isolation followed by the subtype. For example, A/duck/Czechoslovakia/1956 (H4N6) is an influenza A virus of subtype H4N6 isolated from a duck in Czechoslovakia during the year 1956.



**Figure 1-1. Phylogenetic trees of HA and NA genes from all known subtypes.** (A) The HA molecules are divided into 2 phylogenetic groups, group 1 and group 2. (B) The NA molecules are also divided into 2 major groups, group 1 and group 2. Bat-derived neuraminidase-like proteins, N10 and N11, fall under a separate group 3. The HA and NA subtypes that were recently derived from influenza-like viruses in bats are marked with a star. (14)



## **IAV structure and morphology**

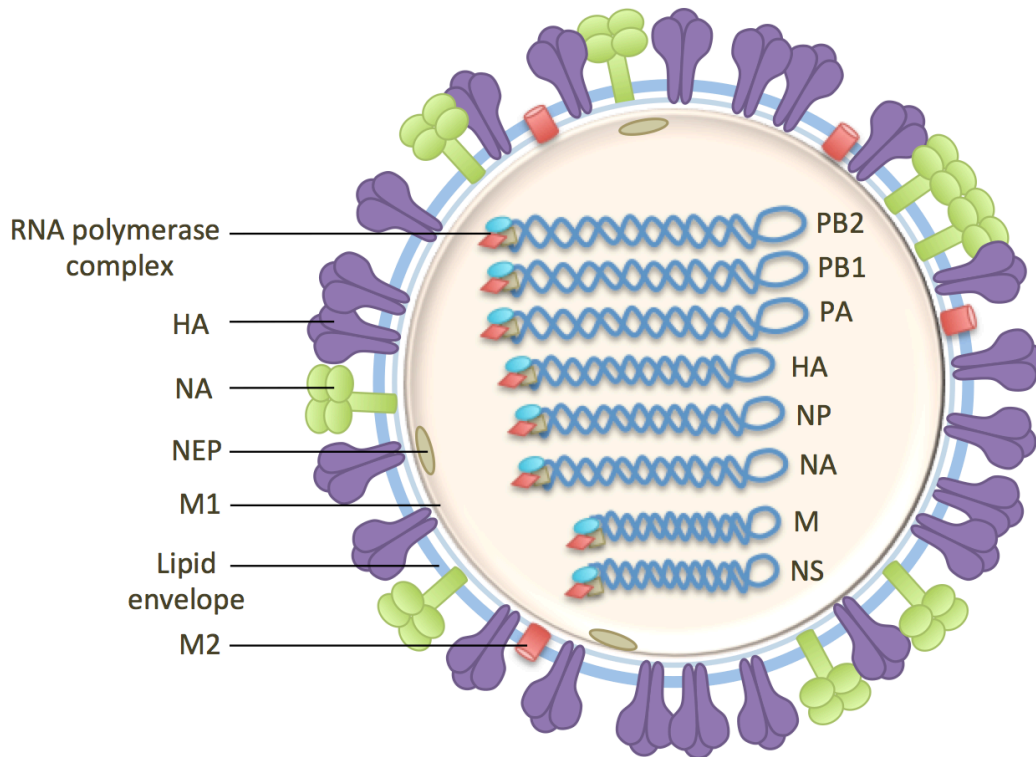
IAVs are pleomorphic with spherical (80-120 nm) or filamentous forms (>300 nm). The viral core contains eight single-stranded RNA (ssRNA) segments that encode at least 11 proteins: HA, NA, matrix 1 (M1), matrix 2 (M2), nucleoprotein (NP), non-structural protein 1 (NS1), non-structural protein 2 (NS2; also known as nuclear export protein, NEP), polymerase acidic protein (PA), polymerase basic protein 1 (PB1), polymerase basic protein 2 (PB2) and polymerase basic protein 1-F2 (PB1-F2).

The genome segments exist as individual rod-shaped viral ribonucleoprotein complexes (vRNP). Each helical vRNP complex contains a viral RNA segment coated with several copies of NP associated with the heterotrimeric RNA polymerase complex consisting of PA, PB1 and PB2 (15, 16). Only RNA that is bound to NP serves as a template for transcription and replication, therefore NP is essential for these steps. NP also interacts with PB1 and PB2 subunits of the polymerase complex and M1 matrix protein. PB1 is the catalytic subunit of RNA polymerase and forms the structural backbone of the complex while PB2 subunit plays a role in replication, transcription initiation and 5' capping (17-19). PA has been implicated in several functions including RNA synthesis, cap and promoter binding, viral RNA packaging, and protein nuclear localization (17, 20, 21).

The matrix protein (M1) forms a shell between the viral core and the envelope and plays a key role in virus assembly (22). The virus envelope surrounding M1 is a lipid bilayer derived from the host cell membrane during the budding process. IAV envelope contains three viral transmembrane proteins: HA, NA and M2. HA is the most abundant protein on the virus surface, comprising 80% of the total surface protein. An influenza virion usually contains between 350-400 HA trimers and ~50 NA tetramers on its surface (23). HA plays a major role in viral

attachment to sialic acid receptors on the cell surface and membrane fusion, while NA is involved in the release of newly formed virions from the cell surface by cleaving sialic acid residues from the cell surface (23, 24). M2 is the least abundant envelope protein with around 16-20 molecules per virion. M2 traverses the lipid envelope and functions as an ion channel that facilitates acidification and dissociation of the viral core during the fusion process (25, 26).

The two non-structural proteins, NS1 and NS2, play key roles in replication. NS1 plays a critical role in escape from host immunity by inhibiting  $\alpha/\beta$  interferon synthesis and antagonizing the interferon mediated anti-viral response (27). NS1 also inhibits host mRNA polyadenylation, export of polyadenylated mRNA, and mRNA splicing (28). The NS2 or NEP protein has been shown to mediate export of viral ssRNA from the nucleus and has also been implicated in other functions (29).



**Figure 1-2. Schematic diagram of influenza A virus particle.** The 3 envelope proteins HA, NA and M2 are shown in purple, green and orange on the lipid envelope. Each of the eight negative sense single-stranded RNA segment is associated with the RNA polymerase complex (PB1, PB2 and PA).

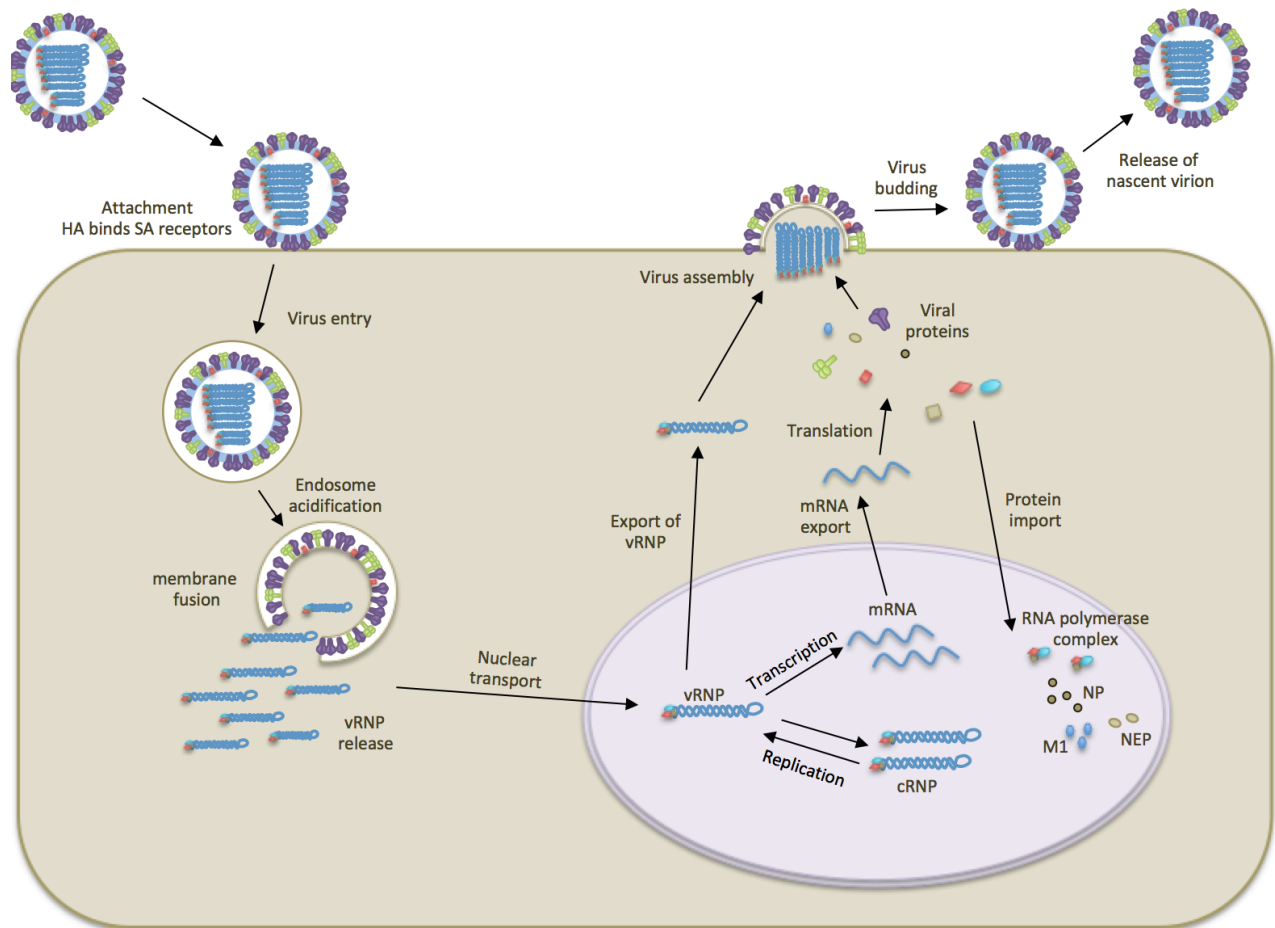
## Influenza life cycle

Influenza viruses are transmitted mainly via respiratory droplets generated by sneezing, coughing or talking. The seasonal IAV strains in human circulation generally replicate in the epithelial cells of the respiratory tract. The first stage of viral infection is the recognition and attachment of N-acetylneuraminic (sialic) acid receptors on host cells by influenza HA. Although sialic acids (SA) are present on most cell types, the carbon-2 of the terminal SA can form different type of linkages with galactose ( $\alpha$ -2,3- and  $\alpha$ -2,6-linkages) resulting in various steric conformations of the terminal SA. The preferential binding of HA to these SA conformations on the host cells is the major determinant of host range (30). The HAs of avian IAVs have high affinity for  $\alpha$ -2,3-linked SA receptors, whereas those of human IAVs have high affinity for  $\alpha$ -2,6-linked SA receptors, which are predominantly expressed in the upper respiratory tract of humans (30-33). Importantly, swine have abundant  $\alpha$ -2,3- and  $\alpha$ -2,6-linked sialic acids in their respiratory tracts, making them susceptible to influenza viruses from various hosts.

Upon attachment to SA-receptors, the virus particle enters the host cell by receptor-mediated endocytosis. A decrease in the pH in the endosome induces HA to undergo conformational changes that expose the HA fusion peptide, which then interacts with the endosomal membrane and facilitates fusion of viral and endosomal membrane (34-36). The pH drop in the endosome also opens the M2 ion channel that acidifies the viral core, allowing release of vRNP from M1 into the cell cytoplasm (37, 38). Once vRNPs are released in the cytoplasm, they are transported to the nucleus where the negative sense viral RNA is used as a template to synthesize viral messenger RNA (mRNA) and complementary RNA (cRNA) (39-41). The cRNAs are then transcribed to produce more copies of viral genomic negative-sense RNA. The viral mRNAs with 5'-methylated caps and poly(A) tails are transported and translated

to viral proteins (42). The newly synthesized envelope proteins HA, NA and M2 are first directed to the endoplasmic reticulum to be folded, and are then trafficked to the Golgi apparatus for post-translational modifications and finally transported to the plasma membrane. The export of vRNPs formed in the nucleus is mediated by interactions with viral proteins M1 and NEP. All the viral components are assembled and packaged for budding at the plasma membrane. When the budding process is complete, the HAs from the newly formed virion continue to bind to the SA receptors on the cell surface. NA, which possesses sialidase activity, cleaves the sialic acids bound to HA facilitating the release of newly formed virions (24). This process of release of nascent virions is also referred to as viral egress.

For the newly formed virions to become infectious, the HA glycoprotein, which is synthesized and oligomerized as an immature polypeptide protein HA0, must be cleaved into two subunits HA1 and HA2 by host proteases into its mature form (23, 43). The HA1 and HA2 subunits remain together linked by two disulphide bonds. The new N-terminal end of HA2 consists of the hydrophobic fusion peptide that allows HA to mediate fusion at low pH (35). The amino acid sequence variability at the cleavage site among diverse HAs determines their susceptibility to a variety of host proteases expressed by different cell types, which in turn regulates virus tropism. In general, most HAs carry an Arg or Lys at the proteolytic site and are restricted to cleavage by trypsin-like proteases expressed in the human respiratory tract (43). Consequently, the virus replication is restricted to the respiratory tract as seen for most seasonal strains circulating in the human population. However, HAs from highly pathogenic H5 and H7 viruses contain multibasic proteolytic sites that can be cleaved by ubiquitous proteases produced in various tissues (44, 45). As a result, these viruses have the ability to spread effectively to other organs and replicate systemically, making them highly pathogenic.



**Figure 1-3. Influenza life cycle.** Binding of influenza HA to sialic acid receptors on the cell surface mediate endocytosis of the virion. Low pH in the endosome triggers HA-mediated fusion of viral and cell membrane and release of vRNP. The vRNPs are transported to the nucleus where replication and transcription occurs. The newly synthesized mRNA that is 5' capped and 3' polyadenylated is exported to the cytoplasm for translation. Newly synthesized viral proteins, PB1, PB2, PA and NP are imported into the nucleus for assembly of vRNPs. Following export, vRNPs and viral proteins assemble at the cell membrane for budding. NA cleaves the sialic acids bound to HA on the cell surface to facilitate release of newly formed virions.

## **Immune response to influenza**

Influenza infections elicit both innate and adaptive immune responses in the host, which play an important role in controlling the virus. The innate immune response, important during the early stages of influenza infection, is primarily triggered by stimulation of at least two Toll-like receptors (TLR), TLR3 and TLR7, in the endosomes. TLR stimulation induces IFN responses to block viral replication and promotes activation of adaptive immune cells; TLR7 promotes antibody production by B cells (46-48). While the innate immune responses are not triggered by antigen-specific mechanisms, the antigen-specific adaptive immune response is initiated by presentation of viral peptides to T cells by antigen-presenting cells (APC) (primarily dendritic cells). The adaptive immune response is activated when immunoglobulin receptors on B cells (BCR) bind to the virus and facilitates differentiation of B cells into antibody-producing plasma cells. Activated T helper cells ( $T_H$  cells) stimulate B cell proliferation and differentiation into plasma cells.

Following influenza infection, the host immune system induces both systemic and mucosal secretion of antibodies to different influenza antigens, which provide major resistance to natural infection (49). Although presence of both serum and mucosal antibodies provide optimal protection against influenza, either mucosal or systemic antibody alone can be sufficient for protection. There are five different classes of antibodies (immunoglobulins): IgM, IgG, IgD, IgA and IgE. IgG is the most abundant immunoglobulin in serum and is a primary mediator of immunity to influenza. While secretory IgA is important for protection of the upper respiratory tract, serum IgG is involved in lower respiratory tract (50). Antibody responses to viral proteins can be categorized as primary (first response to the antigen) or secondary responses (response to pre-exposed antigen). The three major antibody classes, IgG, IgM and IgA, can be detected in

serum following primary infection. While IgM and IgA levels peak at 2 weeks and decline, IgG levels peak at 3-6 weeks following primary infection or vaccination (50). During secondary exposure, IgGs and IgAs dominate the response (51). During the course of the immune response, B cells produce antibodies with increasing affinity for the antigen through a process called affinity maturation. B cells with high affinity and specificity to viral antigens are selected to become memory B cells, which can be rapidly activated upon secondary exposure to the same antigen. In the case of influenza, a person is generally exposed to these viral antigens several times and the secondary exposures can be with an antigenically similar or a distinct influenza strain. The various influenza A hemagglutinin molecules share certain conserved antigenic determinants but also possess strain-specific and subtype-specific determinants. Therefore, when an individual who has been pre-exposed to an influenza A virus is vaccinated with an antigenically different virus, the response consists of two coincident events: a primary response to the new strain and a secondary recall response to the common antigenic determinants between the original and the new virus.

Antibodies are Y-shaped molecules composed of four polypeptide chains; the two arms of the Y end are involved in antigen binding. Each IgG (150 kDa) consists of 2 heavy chains (HC, 50 kDa) and 2 light chains (LC, 25 kDa) that are linked together by disulphide bonds. Cleavage of IgG by papain produces 3 fragments; 2 identical antigen-binding fragments referred to as Fragment-antigen binding (Fab) fragments. The third fragment that does not contain antigen-binding activity is referred to as Fc fragment, for Fragment crystallizable (52). The heavy and light chain of each Fab fragment consists of a variable domain (V) and a constant domain (C); the variable domains contain the antigen-binding site or the paratope. The V region shows great amino acid sequence variability with the highest variability, observed in areas called



hypervariable regions or complementarity-determining regions (CDRs). The V regions of the heavy ( $V_H$ ) and light chain ( $V_L$ ) each contain 3 CDRs: CDR1, CDR2 and CDR3 that define the antigen specificity of the antibody. Accumulation of mutations in CDRs by a process called somatic hypermutation alters the antigen specificity and affinity of the antibody. This plays an important role in defining the breadth of antibody response to HA and NA during exposure to influenza.

Antibodies to influenza proteins, HA and NA, are associated with resistance to infection (50). The Fab portions of the antibody that recognize HA or NA antigens mediate neutralizing functions. Antibodies to HA protein neutralize virus by blocking viral attachment and membrane fusion while antibodies to NA provide protection by preventing viral egress. In addition to neutralizing activity, antibodies to viral proteins also can facilitate additional Fc-mediated effector functions, including antibody-dependent cell-mediated cytotoxicity (ADCC), complement-mediated lysis, and phagocytosis by engaging Fc $\gamma$  receptors (Fc $\gamma$ Rs). ADCC responses play a role in protection against diverse human pathogens including human immunodeficiency virus (HIV), West Nile virus (WNV) and influenza virus (53-58). ADCC is mediated when the Fc region of antibodies bound to viral antigen on infected cells interacts with and subsequently cross-links Fc $\gamma$ RIIIa (CD16a) receptors on innate immune effector cells. The resulting effector cell activation triggers release of perforins and granzymes along with secretion of antiviral cytokines, mediating killing of virus-infected cells. Antibodies that target HA have been shown to possess the ability to interact with Fc $\gamma$ R on effector cells and to mediate ADCC activity and protection *in vivo* (59-62).

## **Current influenza vaccines and therapeutics**

Current influenza vaccines elicit neutralizing antibodies to HA and NA antigens and remain the most effective form of protection against influenza infections. Traditional seasonal influenza vaccines consist of three viruses: an influenza A H1N1 virus, an influenza A H3N2 virus, and an influenza B virus. These are referred to as trivalent vaccines. More recently, seasonal quadrivalent vaccines that contain an additional influenza B strain have also been made available. The majority of the licensed vaccines are inactivated influenza vaccines (IIVs) that are unadjuvanted. IIVs are standardized by their HA content and typically contain 15 µg of HA for each vaccine strain. The only live attenuated influenza vaccine (LAIV), commercially known as FluMist, is currently not recommended due to low vaccine efficacy. Recombinant influenza vaccines that contain 60 µg of HA for each vaccine strain are also available under the commercial name Flublok. The efficacy of seasonal vaccines however depends on how well the vaccine strain antigenically matches the circulating strains. Influenza vaccines are reformulated every year in an effort to ensure the vaccine strain matches the circulating strains; the vaccine strains are selected 9-12 months in advance so that the vaccine can be manufactured and approved before the influenza season. Strain mismatches can occur owing to emergence of new strains during the vaccine production period or due to inaccurate prediction of the vaccine strain.

There are currently three NA inhibitors, zanamivir, oseltamivir and peramivir, which are FDA approved to treat IAV infections. These antiviral drugs target the NA enzymatic site and block viral egress. Another class of drugs called adamantanes function by blocking the M2 ion channel and preventing viral uncoating. Adamantanes are currently not recommended for use against seasonal IAVs as more than 99 % of these strains have acquired drug-resistant mutations.

## **Influenza pandemics and epidemics**

The segmented genome and error-prone polymerase of influenza viruses allows continuous evolution by genetic reassortment and mutations, respectively. These mechanisms result in emergence of antigenically diverse strains and subtypes that can escape from host immunity. Antigenic drift refers to gradual accumulation of mutations in IAV genes that does not change the viral subtype. Antigenic drift in the two major envelope proteins, HA and NA, alters the immunological recognition of the virus within the host resulting in antigenically distinct strains within the same subtype (heterologous strains). Antigenic drift is the major reason why individuals require annual vaccinations against the same viral subtype as current vaccines only elicit protective antibodies against viruses antigenically similar to the vaccine strain (homologous protection). Alternatively, antigenic shift occurs during co-infection with two different influenza viruses. The segmented nature of the viral genome allows for genetic reassortment, or mixing of genes, from both influenza viruses within infected host cells. Antigenic shift resulting in new combinations of HA and NA genes can cause major antigenic changes resulting in pandemics. All of the pandemics that took place during last century have occurred due to antigenic shift.

During the last century, IAVs have caused four major pandemic outbreaks: in 1918 (H1N1), 1957 (H2N2), 1968 (H3N2) and 2009 (H1N1) (63, 64). The 1918 influenza pandemic or the “Spanish flu” was the most severe pandemic, which infected one-third of the global population and caused at least 50 million deaths worldwide. The H1N1 subtype, introduced in 1918, circulated in the human population for 39 years before being replaced by the H2N2 subtype following the 1957 pandemic. The H2N2 subtype only circulated for 11 years before being replaced by the H3N2 subtype that was introduced during the 1968 pandemic. During

1977, a H1N1 virus that was antigenically similar to those that circulated during the 1950s was reintroduced in the human population, resulting in an epidemic. It was considered a pandemic in children, who had no pre-existing immunity against this virus. Since this period, both H1N1 and H3N2 subtypes have circulated in the human population causing seasonal epidemics. The H1N1 and H3N2 strains that cause annual epidemics are referred to as seasonal strains. In April of 2009, a new swine-origin H1N1 virus that was antigenically closer to the 1918 pandemic virus emerged in Mexico and caused another H1N1 pandemic. By 2011, the 2009 H1N1 pandemic strain replaced all previously circulating H1N1 strains. The pandemic influenza 1918 virus has an avian-like genome and all the pandemic viruses that have emerged since then share genetic ancestry with the 1918 virus (65).

### **Influenza viruses with pandemic potential**

Influenza A viruses have a wide host-range that includes humans, pigs, cats, dogs, ferrets, horses, sea mammals and birds. Aquatic birds including gulls, waterfowl, terns and shorebirds serve as natural reservoirs for IAVs. In these birds, the virus replicates in the intestinal epithelial cells in contrast to mammalian IAVs that replicate in the respiratory tract (66). Avian IAVs are generally low-pathogenic viruses that cause mild to no disease in birds, indicating optimal adaptation in these hosts. Highly pathogenic IAVs rarely occur in wild birds and are seen primarily in land-based poultry. Avian IAVs are poorly transmitted to the humans owing to differences in SA-receptors between hosts. Despite the host-range restrictions, both low and high pathogenic avian IAVs with H5, H6, H7, H9 and H10 HAs have caused sporadic infections or outbreaks in the human population, raising concern about their potential to cause severe pandemics due to a lack of pre-existing immunity (67, 68). In particular, H5 and H7 strains have

been responsible for most avian IAV-related illnesses in humans. These human infections are generally caused by direct exposure to poultry with limited human-to-human transmission.

Unlike avian IAV H5N1 that has attracted a lot of research attention, the pandemic potential of H7 has been overlooked until recently. The first known case of human H7 infection was from contact with ducks in 1996, which confirmed the potential of H7 strains to cross host range restriction (69). Since then, H7N7, H7N2 and H7N3 strains have caused more than 100 infections in humans, causing conjunctivitis and some respiratory illness (69-71). However, the pandemic threat posed by H7 strains became apparent during the spring of 2013, when a lethal H7N9 influenza virus started infecting people, causing severe respiratory illness (72). Since 2013, H7N9 viruses have caused 5 annual epidemics in China with more than 1580 cases of human infection and greater than 600 deaths (> 30% mortality) (73). Although person-to-person transmission is thought to have occurred at multiple instances, the majority of the infections occurred from exposure to poultry (74). Genome analysis of avian H7N9 virus revealed a complex genetic background with gene segments derived from as many as four domestic and wild bird species (72, 75, 76). The pandemic potential of H7N9 viruses is reinforced by several factors: 1) their ability to remain in circulation and cause annual epidemics, 2) compatibility of H7 with different neuraminidases (N2, N3, N7 and N9) that have caused human infections, 3) presence of several mammalian-adapting mutations in HA and 4) lack of pre-existing immunity to viral envelope proteins, H7 HA and N9 NA (72, 77). The influenza risk assessment tool (IRAT) was developed by CDC to assess the pandemic potential of zoonotic viruses using several factors. Currently, avian H7N9 viruses pose the highest risk of potential emergence as identified by IRAT.

In addition to direct human transmission of avian IAV strains, genetic reassortment of

human, avian and swine IAVs in intermediate hosts like swine can also result in novel influenza A strains that can efficiently transmit in the human population (32, 78). Swine-origin H1N1 virus that caused the 2009 pandemic is a good example of a avian-swine-human reassorted IAV virus that effectively transmitted and established itself in the human population (79). Several swine-origin IAVs of H1 and H3 subtypes have caused sporadic human infections (80). When a swine IAV is detected in a person, it is referred to as a “variant” virus abbreviated “v”.

H3N2v viruses containing 7 genes from triple-reassortment influenza A viruses with inherited genes from classical swine, avian, and human influenza viruses and the M gene from H1N1 2009 pandemic strain have caused at least 414 cases of human infections since July 2011 (81-83). Most of these human infections have been associated with prolonged exposure to swine with limited person-to-person transmission. Children are particularly susceptible to infection with H3N2v viruses. Limited serological studies indicate the presence of some prior immunity to the H3 variant virus in the adult population, but not in children (84). H3N2v viruses are antigenically different from the current seasonal strains, therefore seasonal trivalent inactivated vaccination does not increase seroprotection to H3N2v viruses (85).

### **Influenza A hemagglutinin and universal influenza vaccine**

Influenza HA glycoprotein is a spike-shaped homotrimer that extends from the envelope surface of the virus. Each mature HA protomer consists of 2 subunits, HA1 (55 kDa) and HA2 (25 kDa), which are formed by cleavage of their precursor HA0. The HA molecule can be divided into the globular head domain and the stem domain (86-88). The head domain consists of 2 major regions: the receptor-binding site (RBS) at its membrane-distal tip and the vestigial esterase subdomain located lower down on the HA head. The receptor-binding site consists of

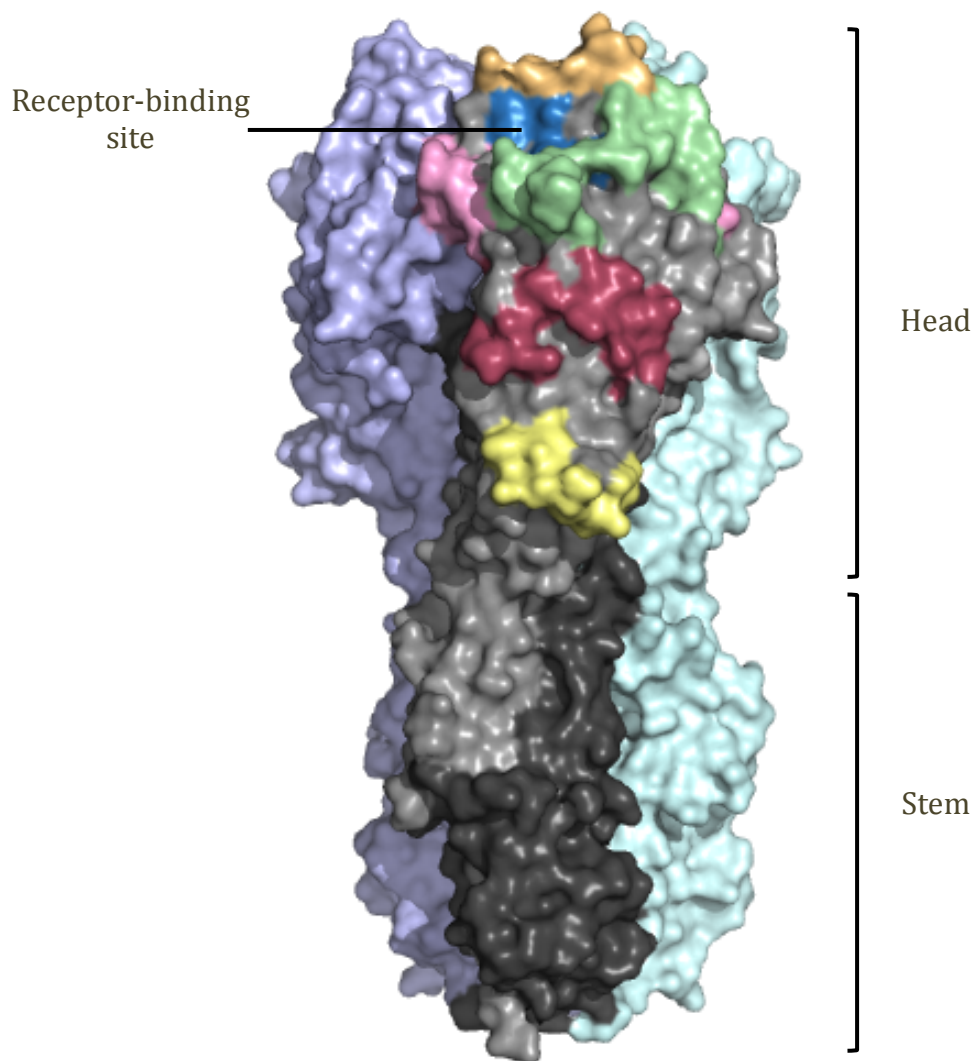
three conserved secondary structures, 190-helix, 130-loop and the 220-loop, at its edges and four conserved amino acids, Tyr-98, Trp-153, His-183, and Tyr-195, at its base (23, 89, 90). Amino acid changes that occur near the receptor-binding site can alter the affinity and specificity of receptor binding to different SA linkages. The HA from avian IAVs requires as little as one amino acid substitution to acquire binding to  $\alpha$ -2,6-linked SA receptors present in the human respiratory tract. Amino acid substitutions E190D and G225D for H1 HA and Q226L and G228S for H2 and H3 HAs are important for the switch in receptor specificity from avian to human SA receptors (91-94). While the head domain is required for receptor-binding, the membrane-proximal stem region contains the components responsible for the low pH-triggered membrane fusion activity of HA in the endosomal compartments (95, 96).

HA is the primary target for potent neutralizing antibodies induced by influenza vaccination or natural infection (97). The HA head domain tolerates high sequence variability and is the major antigenic portion of the HA; the antibodies that target head domain generally block the RBS and prevent viral attachment (98-101). Antigenic sites are sites on the HA molecule that are targeted by antibodies and undergo selective pressure to evade host immune response. Previous studies have recognized 5 antigenic sites on both H1 and H3 HAs (102-105). Antigenic sites mapped on H3N2 using murine monoclonal antibodies are designated as A, B, C, D and E and sites on H1N1 as Sa, Sb, Ca1, Ca2 and Cb (106). Nevertheless, antigenic sites mapped using human monoclonal antibodies are less distinct due to the contiguous nature of the epitopes targeted by human mAbs. All of these antigenic sites are present on the HA head domain. Due to the continuous antigenic drift occurring in the HA head domain, majority of the antibodies that target HA head only recognize antigenically related strains within a subtype.

Numerous broad-spectrum heterosubtypic influenza HA-specific antibodies have been

isolated and characterized in recent years, and the majority of these broad antibodies target conserved sites in the HA stem region. Antibodies that target the HA stem domain are present at low frequencies following seasonal vaccination in comparison to HA head domain antibodies. Antibodies that target the stem domain inhibit pH-induced conformational changes in HA and block membrane fusion (*107, 108*). Stem antibodies exhibit differing levels of cross-reactivity against IAV strains from group 1 (*109-111*), group 2 (*112-114*) or both (*60, 115-119*). These findings have led to the development of several stem-based immunogens for the purposes of “universal” influenza vaccination (*120-123*). However, inducing broad-spectrum stem antibodies through vaccination may be challenging due to reduced accessibility of this region on the viral surface, reduced immunogenicity due to structural features, or other reasons. As a class, anti-stem antibodies also tend to be less potent in virus neutralization assays in comparison to RBS-specific antibodies.



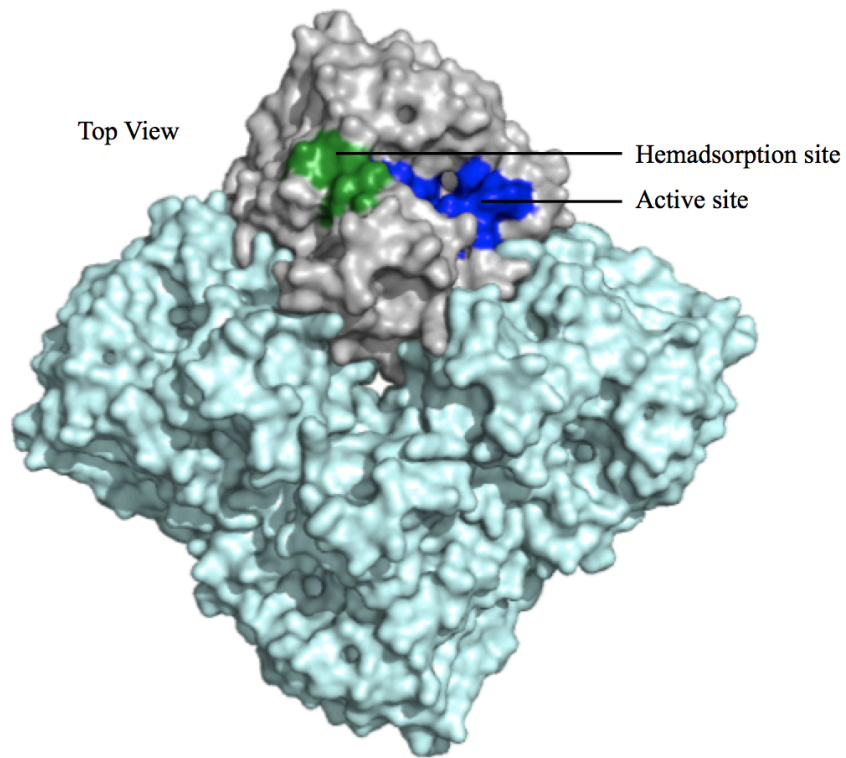


**Figure 1-4. Antigenic sites mapped on the surface representation of H3 A/Aichi/2/1968 HA trimer.** The three HA protomers are shown in grey, purple and cyan. The HA1 and HA2 subunits are illustrated on a single protomer in light grey and dark grey, respectively. The receptor binding site (blue) and H3 antigenic sites A (Green), B (Orange), C (Yellow), D (Pink) and E (Maroon) are mapped in the head region. (PDB ID: 3VUN)

## **Influenza A neuraminidase**

Influenza A neuraminidase is a homotetramer that resembles a mushroom on the viral surface. NA is an exosialidase that cleaves the  $\alpha$ -ketosidic linkage between sialic acid and the adjacent sugar residue (124). The enzymatic activity of NA is essential for release of viral progeny from the infected cell surface and is also important during the early stages of infection in the respiratory tract (24, 125). Protective mucus present in the respiratory tract contains several sialic acid coated glycoproteins that can trap virus by binding to viral HA. NA prevents this by cleaving the sialic acids from the glycoproteins (125). Because HA and NA have antagonistic functions, it is important that they are functionally compatible to achieve efficient replication and transmission (126). When HA binds to sialic acid receptors on the cell surface, the virus is rapidly internalized before NA can cleave the sialic acids.

Each NA protomer (60 kDa) consists of a globular head domain and a thin stalk of variable length (124). The head domain contains the enzymatic site, which is extremely conserved across several subtypes while the stalk domain is highly variable (127). In addition to the enzymatic site, NAs from avian IAV such as N9 were discovered to have a second sialic acid binding site, also known as Hb site, with hemadsorption activity similar to HA (128, 129). The function of this Hb site is not clearly understood. A recent study indicated that the Hb site on N9 NA could contribute to overall virus binding to SA receptors on the cell surface and may play an important role in enhancing the ability of avian H7N9 viruses to bind to human-like SA receptors (130).



**Figure 1-5. Surface representation of N9 A/Shanghai/1/2013 NA.** NA is a homotetramer; three protomers are shown in cyan and one protomer is shown in gray. The neuraminidase enzymatic site (residues in blue) and the hemadsorption site (residues in green) are mapped on one protomer. (PDB ID: 4MWL)

The presence of serum neutralizing antibodies to influenza HA following infection or vaccination has been well established as a correlate of protection against influenza (*131*). Yet, relatively little is known about the vaccine-induced antibody response to NA (*132*). The recent optimization of enzyme linked lectin assay (ELLA), a technique used to measure NA enzymatic inhibition activity, has allowed assessing the role of vaccine-induced NA antibodies in protection against influenza (*133*). A recent study, that compared the anti-NA antibody responses induced by six licensed vaccines in healthy adults, showed that all inactivated vaccines elicited NA antibodies with some better than others (*134*). Another group indicated that 2010-2011 trivalent inactivated vaccine was only modestly immunogenic for N1 and N2 (*135*). However, it is difficult to assess the quality and quantity of NA response to licensed vaccines because all current vaccine formulations are standardized by their HA content with varying levels of NA in them.

As antibodies to NA do not prevent viral attachment or entry, they are not considered neutralizing in the traditional sense but are thought to provide infection-permissive immunity. There are currently no known human monoclonal antibodies targeting influenza neuraminidase. Mouse N1 antibodies isolated by 2 different groups showed homologous and heterologous protection against lethal challenge with H1N1 and H5N1 viruses (*136, 137*). There is not much evidence supporting NA-based heterosubtypic (different subtypes) protection against IAVs. In a recent study, mice immunized with either N1 or N2 NA were completely protected against challenge with homologous strains and were partially protected against heterologous virus challenge, but no protection was observed against heterosubtypic challenge (*138*).

## CHAPTER II

### RECOGNITION OF INFLUENZA H3N2<sub>v</sub> VIRUS BY HUMAN NEUTRALIZING ANTIBODIES

*“Ebola is a zoonosis. So is bubonic plague. So was the so-called Spanish influenza of 1918–1919, which had its ultimate source in a wild aquatic bird and, after passing through some combination of domesticated animals (a duck in southern China, a sow in Iowa?) emerged to kill as many as 50 million people before receding into obscurity.”*

*David Quammen, Spillover: Animal Infections and the Next Human Pandemic*

#### Introduction

Novel influenza A viruses emerging from birds spill over and infect other mammalian species including humans. The ability of IAVs to cross into humans causing pandemics or sporadic outbreaks has been documented throughout last century. However, direct transmission of IAVs from birds to humans is rare due to several reasons; the most important being the differences in sialic acid receptors found in the upper respiratory tract of both species. Most often, other intermediate hosts facilitate this transmission by allowing antigenic drift and shift to generate novel IAV viruses that are better adapted for human transmission. In particular, swine have been shown to act as ideal intermediate hosts for IAV reassortment and transmission due to the ability of both human and avian influenza viruses to replicate effectively in their respiratory tract (139). Several reassortment events between avian, swine and human IAVs have been recorded in pigs, and some of these novel viruses have been transmitted to the human population.

In the recent past, swine-origin H3N2 variant viruses containing the matrix gene from the 2009 H1N1 pandemic virus are being increasingly detected in humans (82, 140, 141). Most cases

of H3N2v-associated disease have been linked with exposure to swine with very limited human-human transmission (82). Since July 2011, there have been at least 414 reported cases of human infections with H3N2v viruses, with a high prevalence in children under the age of 12. Lack of pre-existing immunity to the variant virus, especially in children, may be a major concern if a highly transmissible H3N2v outbreak occurs (84, 85, 142). A recent study showed that all children <5 years old and >80% up to 14 years old lack protective serum antibody titers against H3N2v (85) while the adults seem to have a certain level of preexisting immunity to this virus. The basis for this lack of immunity to H3N2v infections seen in children is not well understood.

Moreover, it has also been shown that H3N2v is antigenically distinct from the H3N2 seasonal strains circulating in humans, and that vaccination with 2010-11 annual trivalent inactivated virus vaccination does not induce neutralizing antibodies against the variant H3N2 virus (85). The HA of H3N2v A/Minnesota/11/2010 virus has 52 polymorphisms as compared to the seasonal H3N2 strain A/Victoria/361/2011, which allows enough variation to escape protection from sera induced by recent TIV vaccines. The residues on H3v HA that play a major role in the immune escape of H3N2v virus is the key to designing effective vaccines against swine H3N2 variant viruses. However, the sites/residues on HA that make the variant antigenically distinct from the seasonal strains are currently undefined.

In this chapter, I have described the isolation and characterization of human monoclonal antibodies (mAbs) to H3N2v HA isolated from individuals vaccinated with an experimental monovalent inactivated H3N2v vaccine candidate. I used these mAbs to define the molecular basis of strain-specificity or cross-reactivity for human neutralizing antibodies recognizing the HA of H3 seasonal or emerging H3 variant viruses. My results indicate that polymorphisms in 2 antigenic elements, the 150 helix and the 190 loop, located near the RBS on HA, play a major

role in escape of H3N2v virus from immunity induced by seasonal H3N2 vaccines. Furthermore, my results reveal that the HA protein of H3N2v strains is antigenically similar to the human H3N2 IAV strains that circulated during the late 1990s, during which several H3N2 spillover events have been suggested to occur from humans into U.S. swine (143-145).

I acknowledge Emory Vaccine and Treatment Evaluation Unit (VTEU) for processing and cryopreserving PBMCs used for my study, Dr. Andrew Ward's group for examining H3N2v antibodies in complex with HA by negative-stain single-particle electron microscopy (EM), Dr. Juergen Richt's group for performing neutralization assays against swine viruses, and past members of the Crowe laboratory for developing and optimizing the hybridoma technique that allowed me to isolate large panels of influenza-reactive human mAbs.

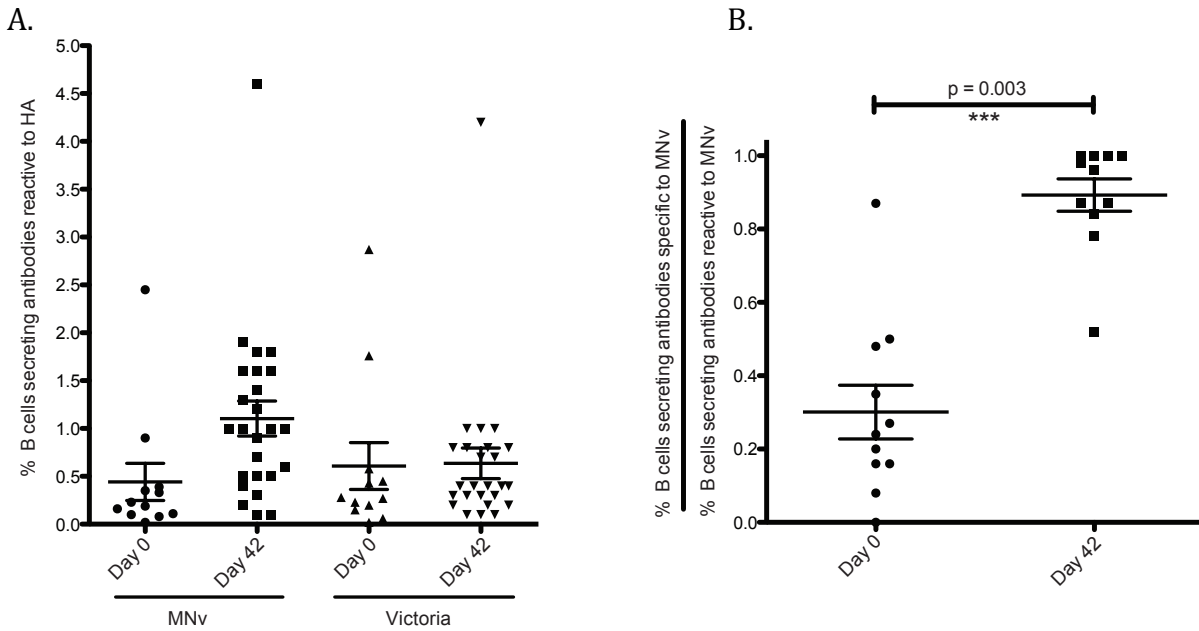
### **Study of B cell response before and after vaccination with H3N2v vaccine**

All samples used for this study were obtained from a phase II open-label clinical trial to assess the safety and immunogenicity of H3N2v vaccine. The study was conducted in healthy males and non-pregnant females aged  $\geq 18$ , who received two doses of subvirion H3N2v [15  $\mu$ g of HA/dose] 21 days apart. The vaccine was derived from H3N2v A/Minnesota/11/2010 strain. We obtained cryopreserved peripheral blood mononuclear cells (PBMC) collected on day 0 before vaccination and day 42 post vaccination from 25 subjects. Although H3N2v is antigenically distinct from the current seasonal strains, studies have shown that adults have some degree of preexisting antibody titers to H3N2v (146). To examine the frequency of H3N2v-reactive B cells before and after vaccination, I transformed day 0 (12 donors) and day 42 (25 donors) PBMCs with Epstein-Barr virus (EBV) in the presence of Chk2 inhibitor, cyclosporin A, and CpG10103. I plated the transformed cells on 384 well plates, and collected supernatants

from the resulting lymphoblastoid cell lines (LCL) on day 8. Supernatants were screened by ELISA for binding to recombinant HA protein from the H3N2v vaccine strain A/Minnesota/11/2010 (designated here MNv strain) or one of two representative H3N2 seasonal strains, A/Victoria/361/2011 (designated here Victoria strain) or A/Wisconsin/67/2005. Based on the ELISA binding data and the number of transformed B cell colonies in each well of a 384 well plate, I was able to calculate the frequency of B cells expressing antibodies reactive to each HA. Indeed, we observed that most adults had comparable B cell frequencies against MNv HA (Mean frequency = 0.4%) and the seasonal Victoria HA (Mean frequency = 0.6%) before vaccination (Figure 2-1A). Following vaccination (day 42), there was a significant rise in the frequency of MNv-reactive B cells, the mean frequency increasing to 1.1% (Figure 2-1A). Subjects did not show a significant change in the frequency of B cells to Victoria HA following vaccination, which was anticipated due to the antigenic differences between the MNv vaccine strain, and the circulating seasonal strains. There was little reactivity detected for the second seasonal strain A/Wisconsin/57/2005 HA both pre- and post-vaccination.

To examine the cross-reactive nature of antibodies secreted by B cells pre- and post-vaccination, I determined the frequency of B cells specific to MNv HA with no cross-reactivity to both seasonal strains tested. While the fraction of MNv-specific to MNv-reactive B cells was low on day 0 for most adults (mean = 0.3), the majority of the B cells secreting antibodies to variant on day 42 recognized the variant HA specifically (mean = 0.89), with limited cross-reactivity to seasonal HAs (Figure 2-1B).





**Figure 2-1. H3N2v specific and cross-reactive B cell response** (A) Frequency of HA-reactive B cells from day 0 (12 donors) and day 42 (25 donors). PBMCs from day 0 or day 42 post-vaccination were transformed with EBV in 384-well plates and supernatants were screened by ELISA for the presence of antibodies to H3N2v A/Minnesota/11/2010 HA or HAs from two seasonal strains: A/Victoria/361/2011 or A/Wisconsin/67/2005 (not shown). The graph represents frequency of B cells reactive to each HA (B) Frequency of influenza A H3N2v HA-specific B cells from 11 vaccinated donors. The graph represents data from 11 donors, showing the ratio of B cells secreting antibodies specific to H3N2v HA that did not cross-react with HA from seasonal strains to the total B cells secreting antibody reactive to H3N2v. The percentage of H3N2v specific or reactive B cells were calculated by the number of wells with ODs greater than 2 times standard deviation above background divided by total number of transformed B cells  $\times$  100. The error bars represent standard error of means and the p value was calculated by Wilcoxon test.

## **Isolation and functional characterization of H3N2v-reactive human mAbs**

Transformed B cell lines with supernatants that showed reactivity against the MNv HA in ELISA were selected for fusion with HMMA2.5 myeloma cells to generate human hybridoma cell lines secreting mAbs. I utilized PBMCs collected on study day 42 from a total of 12 subjects to isolate a panel of 36 cloned hybridomas secreting MNv-reactive mAbs. I determined the neutralization potential of these 36 MNv-reactive mAbs by microneutralization assay, using the MNv virus. 17 of 36 mAbs exhibited neutralizing activity against the variant virus, when tested at concentrations as high as 10  $\mu\text{g/mL}$  (Figure 2-2). The  $\text{IC}_{50}$  values are shown as a heat map with increased color intensity corresponding to an increase in neutralizing potency. Six mAbs (found at top of Figure 2-2, and designated H3v-126, H3v-71, H3v-47, H3v-104, H3v-98, and H3v-81) showed very potent neutralization against the virus, with  $\text{IC}_{50}$  values of less than 100  $\text{ng/mL}$ . In collaboration with Dr. Jürgen Richt's group, we also determined the ability of four mAbs (H3v-98, H3v-104, H3v-71 and H3v-45) to neutralize four H3N2 strains representing each antigenic cluster circulating in swine, A/Swine/Texas/4199-2/98 (cluster I), A/Swine/Colorado/23619/99 (cluster II), A/Swine/Oklahoma/18089/99 (cluster III) and A/Ohio/13/2012 (cluster IV) (Figure 2-3). H3v-98 and H3v-104 showed potent inhibiting activity against three out of four strains. H3v-71 and H3v-45 exhibited activity against two strains at low concentrations. We determined the nucleotide sequence of the antibody heavy chain variable gene regions. The seventeen neutralizing antibodies had unique HCDR3 sequences, indicating that the mAbs represented independent clones.

I assayed the binding of 17 neutralizing mAbs to HAs derived from MNv and three seasonal strains A/Perth/16/2009, A/Victoria/361/2011 and A/Texas/50/2012. All of the antibodies had half maximal effective concentrations ( $\text{EC}_{50}$ ) for binding below 100  $\text{ng/mL}$  to

MNV HA (Figure 2-2). Increasing intensity of the orange cell fill color in the EC<sub>50</sub> column corresponds to increasing binding for the indicated HA. The antibodies displayed a differential binding pattern - nine mAbs bound specifically to the MNv HA while the other eight bound to both the variant HA and a combination of seasonal HAs (Figure 2-2). Interestingly, all but one (H3v-47) of the potentially neutralizing mAbs exhibited a variant-specific binding phenotype without detectable cross-reactivity for the HA of H3 seasonal strains or other HA subtypes tested (H1, H3, H5, H7).

Due to the limited cross-reactivity demonstrated by these mAbs, I anticipated that the majority of the potentially neutralizing mAbs mediated neutralization by binding to the less conserved head domain of HA. To test this, I performed hemagglutination inhibition (HAI) assay, which only identifies mAbs that neutralize by interfering with the receptor-binding function of HA. A total of 9 of the 17 neutralizing mAbs exhibited HAI activity against the MNv virus, suggesting that these mAbs function by blocking virus binding to the sialic acid receptor (Figure 2-2). The most potent mAbs that displayed variant-specific binding phenotype also exhibited HAI activity, suggesting that the variant-specific polymorphisms around the RBS in the head domain region on MNv HA play a major role in determining the unique antigenic profile of the variant virus.

Monoclonal antibody	Subject number	IgG subclass	Light chain	EC <sub>50</sub> (ng/mL) for indicated strain				H3N2v IC <sub>50</sub> (ng/mL)	H3N2v HAI (µg/mL)
				H3N2v Minnesota 2010	H3N2 Perth 2009	H3N2 Victoria 2011	H3N2 Texas 2012		
H3v-126	27	1	λ	3	>	>	>	3	0.16
H3v-71	37	1	λ	10	>	>	>	7	0.31
H3v-47	10	1	κ	4	18	26	38	8	>5.0
H3v-104	41	1	κ	14	>	>	>	9	0.16
H3v-98	37	1	κ	19	>	>	>	14	0.32
H3v-81	37	1	λ	29	>	>	>	59	1.25
H3v-141	54	1	κ	25	>	>	>	137	1.25
H3v-45	9	3	λ	14	>	>	>	257	1.25
H3v-95	37	3	λ	9	159	1	239	402	2.5
H3v-62	37	1	κ	4	>	1,625	>	438	>5.0
H3v-84	37	1	κ	2	88	5	135	482	>5.0
H3v-11	1	1	κ	32	>	144	>	564	5.0
H3v-21	1	1	κ	11	>	352	>	697	>5.0
H3v-86	37	1	κ	27	357	13	368	956	>5.0
H3v-7	1	1	κ	34	>	>	>	1,226	>5.0
H3v-9	2	1	κ	38	>	>	>	1,301	>5.0
H3v-79	37	1	λ	86	353	>	219	1,602	>5.0

**Figure 2-2. Characterization of 17 neutralizing monoclonal antibodies.** The antibodies are arranged in the order of neutralization potency (column 9) with the most potent antibodies on the top. 17 mAbs isolated by human B cell hybridoma generation exhibited neutralization potential (shown as half maximal inhibitory concentration, IC<sub>50</sub>) at <5 µg/mL against the H3N2v virus by microneutralization assay. Nine antibodies exhibited hemagglutinin inhibition (HAI) activity, indicating that they disrupt receptor-binding function of the virus. The mAbs were tested for binding against HA from H3N2v or three seasonal strains (shown as half maximal effective concentration, EC<sub>50</sub>). The > symbol indicates binding was not detected at the maximum concentration tested (2 µg/mL). The experiments for determining EC<sub>50</sub> (n=4), IC<sub>50</sub> (n=3) and HAI (n=3) were conducted twice independently.

Monoclonal antibody	Lowest concentration of the mAb that can neutralize the virus (µg/mL)			
	Cluster I A/Swine/Texas/ 4199-2/98	Cluster II A/Swine/Colorado/ 23619/99	Cluster III A/Swine/Oklahoma/ 18089/99	Cluster IV A/Ohio/13/2012
H3v-71	>	0.12	>	0.12
H3v-98	>	0.31	0.16	0.16
H3v-104	>	0.08	0.03	0.01
H3v-45	>	0.63	10.0	1.25

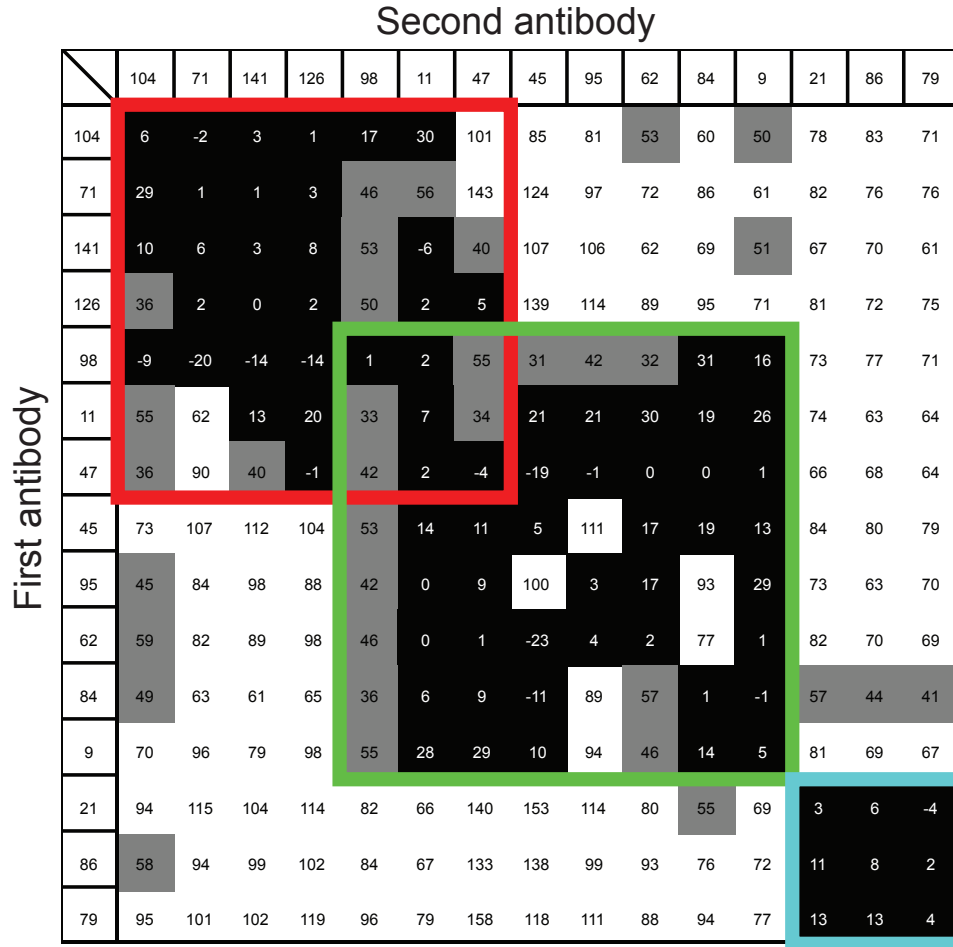
**Figure 2-3. Neutralization titers for four H3v-reactive human mAbs against swine IAVs.** H3v mAbs were tested for neutralizing activity against four H3N2 strains representing each antigenic cluster circulating in swine, A/Swine/Texas/4199-2/98 (cluster I), A/Swine/Colorado/23619/99 (cluster II), A/Swine/Oklahoma/18089/99 (cluster III) and A/Ohio/13/2012 (cluster IV). The table shows the lowest concentration of the antibody (µg/mL) that exhibited neutralizing activity against each strain. The > symbol indicates neutralization was not detected at the maximum concentration tested (10 µg/mL).

## **Competition-binding studies**

In order to determine if the neutralizing mAbs bound to common or diverse epitopes on HA, I performed competition-binding assays using biolayer interferometry with all of the neutralizing antibodies. Fifteen of the 17 neutralizing mAbs were classified into competition-binding groups based on their ability to block other mAbs from binding to the HA. I was unable to detect good binding signal for H3v-81 or H3v-7 with biolayer interferometry. The 15 neutralizing mAbs tested fell into three major competition-binding groups, with some overlap between the groups designated Group 1 and 2 and a distinct Group 3 (Figure 2-4). Antibodies belonging to group 3 were further identified to target the HA stem domain by performing competition studies with other known stem antibodies. Notably, four of the most potent neutralizing clones (H3v-98, H3v-104, H3v-126, and H3v-71) that also exhibited HAI activity and variant-specificity fell into the same competition-binding group, Group 1.

## **Epitope mapping by mutagenesis experiments and electron microscopy**

The six most potently neutralizing mAbs that displayed a variant-specific phenotype (*i.e.*, mAbs that bound specifically to the MNv HA and not to the seasonal HAs) were chosen for fine epitope mapping. I sought to determine the residues important for immune escape of the H3N2v virus from antibodies induced by seasonal vaccines. We considered that the HA of MNv has 52 polymorphisms as compared to the Victoria seasonal strain. I initially performed a mutagenesis screen by introducing variant-specific polymorphisms into a cDNA encoding the Victoria HA protein to identify mutations that would enhance binding to the variant-specific mAbs. 17 variant-specific polymorphisms were introduced into Victoria HA as single or double mutations.



Color	Interpretation	Percentage of max un-competed signal
	First antibody blocks the binding of second antibody	<30%
	First antibody might block the binding of second antibody	31-60%
	First antibody does not block the binding of second antibody	>60%

**Figure 2-4. Competition binding of neutralizing antibodies to H3N2v A/Minnesota/11/2010 hemagglutinin (HA) protein.** Biolayer interferometry was used to perform competition-binding assays. The HA was loaded onto Ni-NTA tips, and binding to two successive antibodies was tested. The binding signal for each antibody was obtained from a single association step of the mAb onto HA. If binding of the first antibody blocked the binding of the second antibody by reducing its binding signal by more than 70%, it was defined as a competitor, indicated in black. The values in the table indicate the percentage of the maximum un-competed binding signal. The red box indicates group 1, the binding group comprising the potently neutralizing mAbs. The green box and the blue box represent group 2 (partially overlaps with group 1) or group 3, respectively. The experiment was conducted twice independently.

Three double mutant HA molecules, Victoria I202V/T203I, A163E/L164Q or R142G/N144V, enhanced binding to mAbs H3v-98 and H3v-104 in comparison to wild-type Victoria HA.

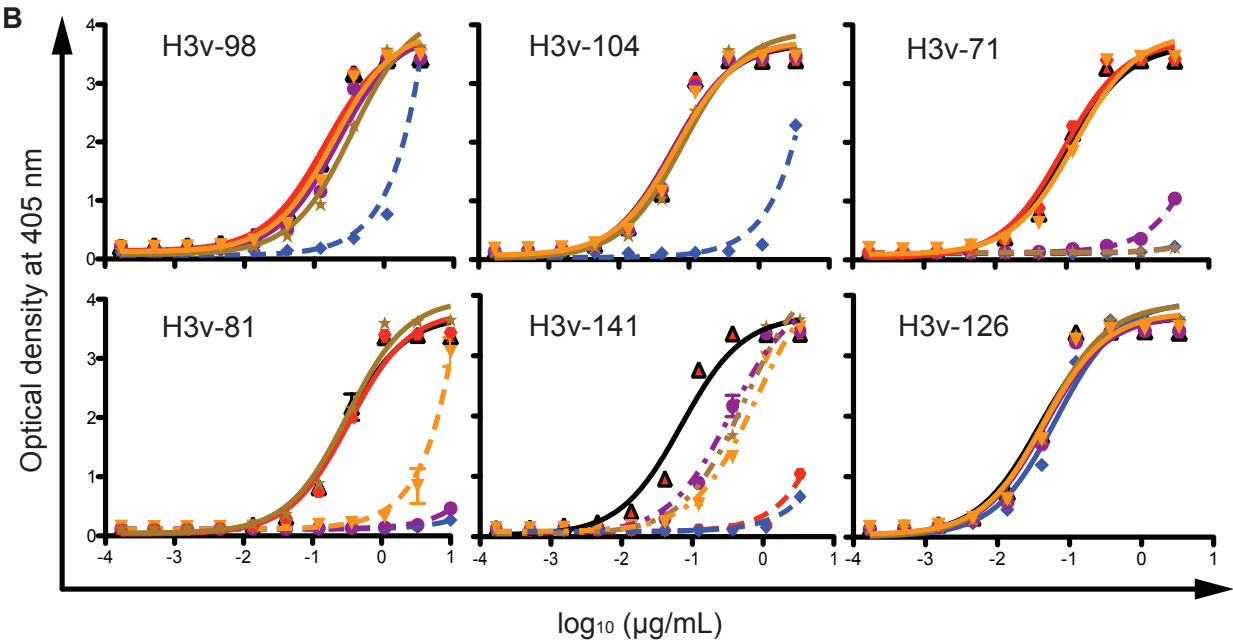
Based on the results of the initial mutagenesis screen, I targeted the region around the RBS and introduced residues from seasonal strains into the H3N2v HA to identify residues that disrupted binding to wild-type MNv. The half maximal effective concentration ( $EC_{50}$ ) values for MNv HA mutants that disrupt binding to each antibody are shown with representative binding curves (Figure 2-5A and 2-5B). Mutation of Y155T/N156K/L157S disrupted binding to both mAbs H3v-71 and H3v-81, whereas mutant MNv N158G/Y159S/K160T did not bind to mAb H3v-71 and MNv K189N/T192I/N193R did not bind to H3v-81. A single mutation Y137S disrupted binding to H3v-141. In addition, a triple alanine mutant MNv L194A/Y195A/V196A did not bind to mAbs H3v-98, H3v-104, H3v-71, H3v-81 and H3v-104.

In collaboration with Dr. Andrew Ward's group, we also performed electron microscopy of MNv HA in complex with Fab portions of the three most potent variant-specific antibodies H3v-126, H3v-71 and H3v-104 (Figure 2-6A, 2-6B, 2-6C) along with the Fab of a stem-binding antibody CR9114 (used as reference in each complex). The EM reconstructions revealed all three antibodies bound to the receptor-binding site on HA, with overlapping footprints (Figure 2-6D). This finding was consistent with the competition-binding data and demonstrated that H3v-126, H3v-71 and H3v-104 all fall under the same competition-binding group (Group 1). The H3v-104 mAb displayed a comparatively broader footprint on HA, extending below the RBS, supporting our previous observation that the Victoria R142G/N144V mutant enhanced binding to mAb H3v-104 but not to H3v-126 or H3v-71. H3v-71 bound similarly to H3v-126 but appeared to interact more with the upper rim of the RBS (Figure 2-6D). This finding could explain why mutations in the 190 helix and 150 loop impacted binding of H3v-71 but not of H3v-126.

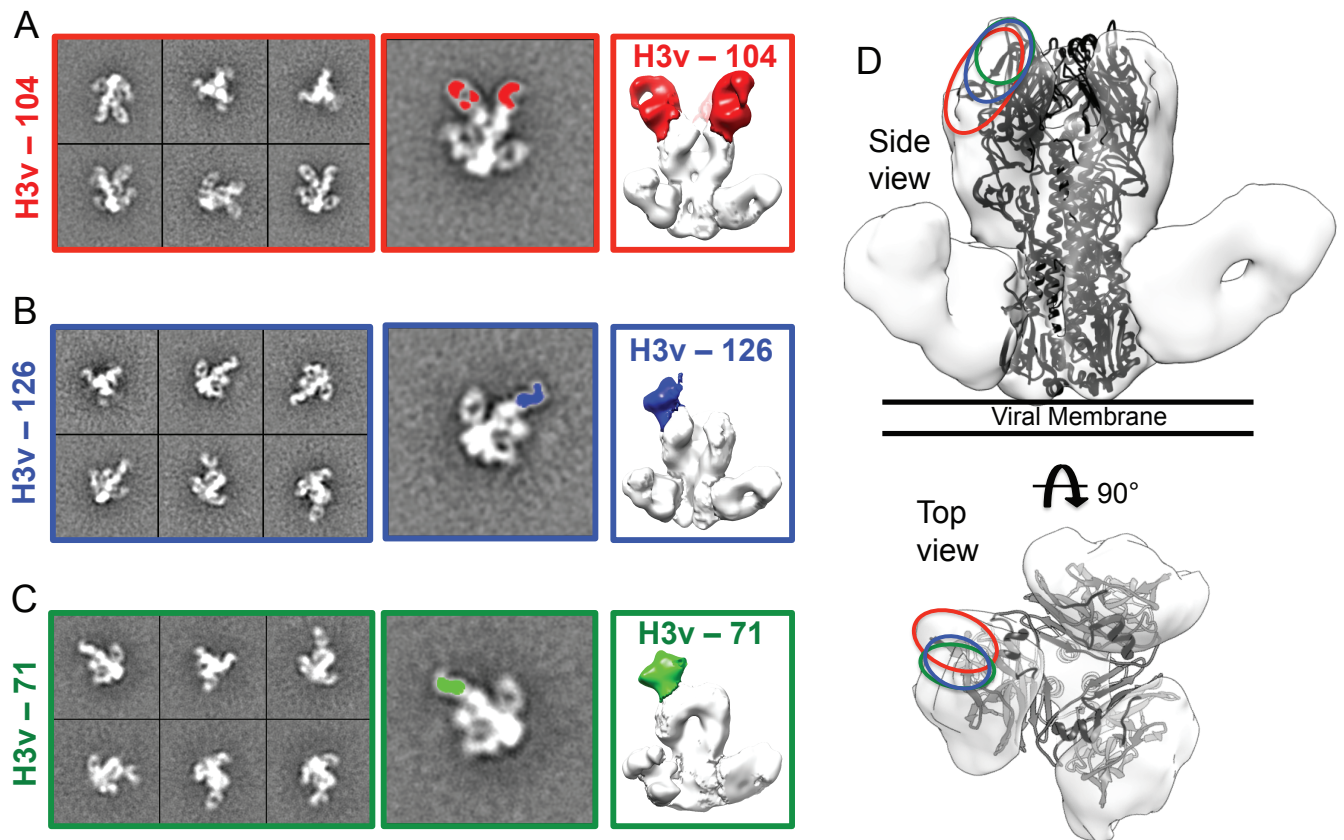


A

Graph Legend	H3N2v MN mutants	EC <sub>50</sub> for the indicated antibody (µg/mL)					
		H3v-98	H3v-104	H3v-71	H3v-81	H3v-141	H3v-126
▲	MN wild-type	0.13	0.05	0.09	0.29	0.07	0.04
●	MN Y137S	0.13	0.06	0.09	0.34	>	0.04
●	MN Y155T/N156K/L157S	0.19	0.06	>	>	0.30	0.04
★	MN N158G/Y159S/K160T	0.30	0.08	>	0.32	0.45	0.04
▼	MN K189N/T192I/N193R	0.18	0.06	0.12	>	0.61	0.04
◆	MN L194A/Y195A/V196A	2.89	9.00	>	>	>	0.06



**Figure 2-5. Binding of H3 variant specific-antibodies to mutated Minnesota hemagglutinin (HA) proteins.** Mutagenesis of MNv HA was performed to determine antigenic residues important for recognition by variant-specific mAbs. Mutants of H3N2v A/Minnesota/11/2010 (MN) HA were generated by site-directed mutagenesis, and the half maximal effective concentration (EC<sub>50</sub>) values were determined by performing ELISA with serial dilutions of each antibody against the mutant HAs. The table (A) shows EC<sub>50</sub> values and the graph (B) shows binding curves. The mutants that disrupted binding completely or decreased the EC<sub>50</sub> by greater than 5-fold are represented as dashed or dotted lines, respectively, and are indicated by red EC<sub>50</sub> values in the table. The > symbol indicates binding was not detected at the maximum concentration tested (10 µg/mL). The experiments for determining the EC<sub>50</sub> (n=4) values were performed twice independently.



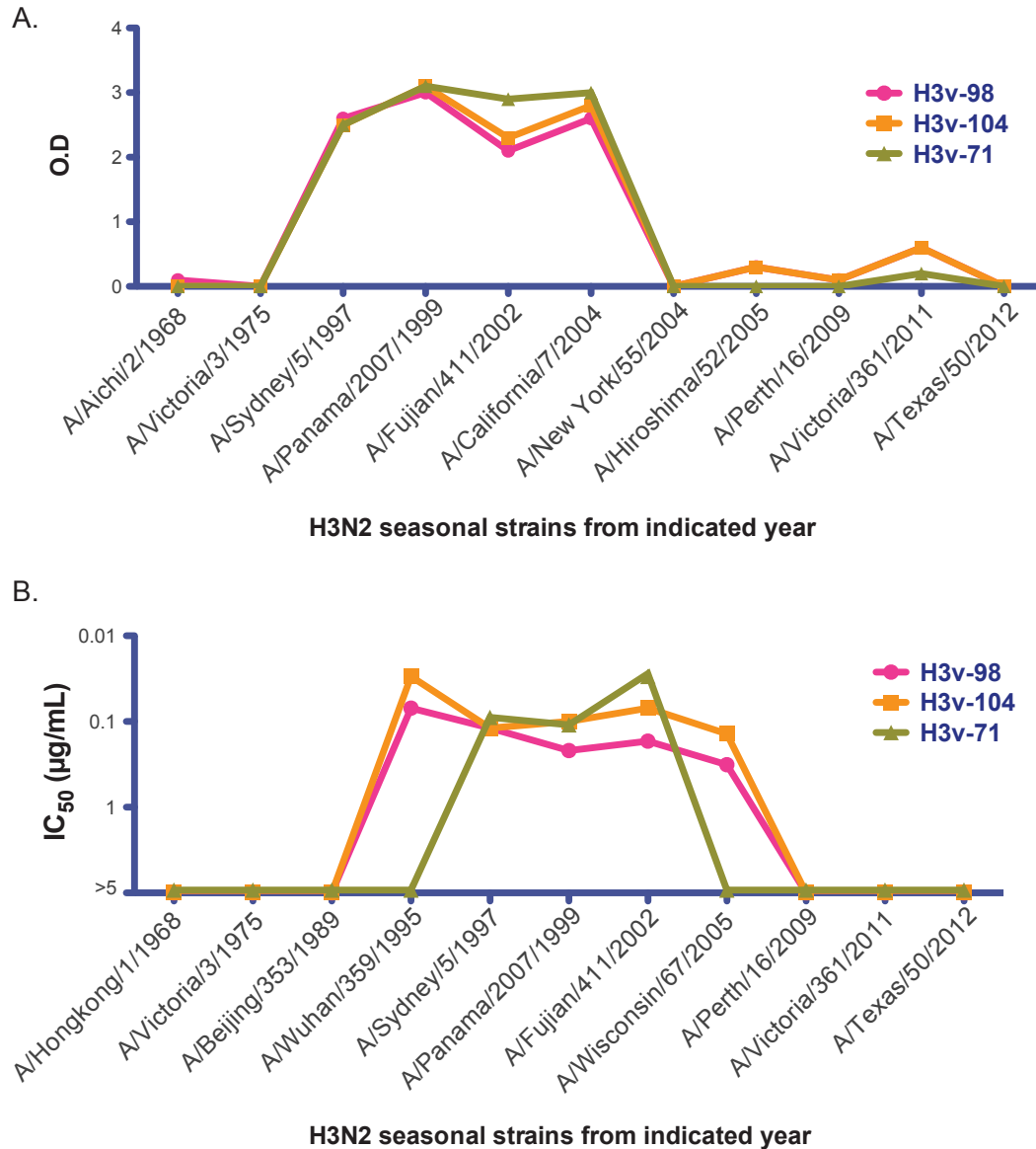
**Figure 2-6. Negative stain EM images of Hemagglutinin-Fab complexes.** In each case the stem-binding antibody CR9114 was added to the complex in order to improve 3D reconstructions. (A) Reference free 2D class averages of complex containing Fab 104 (left), single class average with Fab colored in red (middle), and 3D reconstruction (right). (B) Reference free 2D class averages of complex containing Fab 126 (left), single class average with Fab colored in blue (middle), and 3D reconstruction (right). (C) Reference free 2D class averages of complex containing Fab 71 (left), single class average with Fab colored in green (middle), and 3D reconstruction (right). (D) Side and top views of HA-Fab 126-CR9114 with Fab 126 removed and crystal structure of H3V (4FNK) fitted. Binding sites of the three antibodies described in A-C are highlighted using colors corresponding to Fabs. Figure credit: Travis Nieuwsma (Ward laboratory)

Collectively, the results from mutagenesis and EM structural studies indicated that variant-specific HA residues residing in two major structural features surrounding the RBS, the 150 loop and the 190 helix, principally account for antigenic distinction of the variant virus from current seasonal strains.

### **The HA of H3N2v virus is antigenically related to that of older human seasonal H3N2 IAVs**

The majority of the severe cases of influenza infection caused by H3N2v viruses to date in the U.S. have occurred in children, suggesting partial immunity in adults. I sought to identify the nature of preexisting immunity to the variant virus in the adult population that might provide partial protection against severe disease. Previous studies have shown that several H3N2 spillover events from human to swine population occurred during the late 1990s. Accordingly, I hypothesized that the swine-origin H3N2v viruses are antigenically similar to these older seasonal strains and therefore the variant-specific antibodies that do not recognize the current seasonal strains might recognize the seasonal H3N2 strains that circulated in the late 1990s. To examine this, I cloned, expressed, and assayed soluble HA proteins belonging to 12 different seasonal H3N2 strains that circulated in humans from 1968 to 2013 for binding to six potentially neutralizing mAbs with variant-specific binding and neutralizing phenotypes. Interestingly, three mAbs, H3v-98, H3v-104 and H3v-71, showed strong binding to H3N2 viruses that circulated between years 1997 to 2004, but not to the HA of H3 subtype strains that circulated before or after that period (Figure 2-7A). To determine if these mAbs had the potential to neutralize these older seasonal strains, I performed microneutralization assays to test activity against 12 viruses that circulated between years 1968 to 2013. Indeed, H3v-98 and H3v-104 neutralized all of the

strains tested between years 1995 to 2005 whereas H3v-71 neutralized all of the viruses between 1997 and 2002 (Figure 2-7B). Collectively, my data indicate that HA from H3N2v viruses retain antigenic features of their ancestral strains that circulated in humans. Children born after 2005 are the most susceptible subset to H3N2v infections due to the lack of pre-existing immunity.



**Figure 2-7. H3N2v is antigenically similar to older seasonal strains** (A) Binding to HA from H3N2 seasonal strains. The mAbs were tested for binding against HAs derived from 10 seasonal strains that circulated between 1968 to 2012 by ELISA at a single concentration of the antibody (0.3  $\mu\text{g/mL}$ ). The O.D. values for H3v-98 (pink), H3v-104 (orange) or H3v-71 (green) are indicated on the y-axis and the HA from H3N2 strains used for binding are indicated on the x-axis. (B) Neutralization of H3N2 seasonal strains. The monoclonal antibodies were tested for neutralization activity by microneutralization assay against 11 seasonal strains isolated between 1968 to 2012. The half maximal inhibitory concentration ( $\text{IC}_{50}$ ) values for H3v-98 (pink), H3v-104 (orange) or H3v-71 (green) are indicated on the y-axis, and the H3N2 strains used for neutralization are indicated on the x-axis. The  $\text{IC}_{50}$  values are represented as baseline if neutralization was not detected at any concentration less than 5  $\mu\text{g/mL}$ . The microneutralization assay for determining the  $\text{IC}_{50}$  (n=3) values were performed twice independently.

## Discussion

I report here the isolation of the first human mAbs against H3N2v virus and the use of them to determine the molecular basis for the antigenic distinction between H3 seasonal strains and the H3N2v viruses. 17 antibodies neutralized A/Minnesota/11/2010 H3N2v at concentrations less than 10  $\mu\text{g/mL}$ . Four of the 17 neutralizing mAbs exhibited ultra-potent neutralizing activity ( $\text{IC}_{50} < 10 \text{ ng/mL}$ ). Three of these four ultra-potent neutralizing H3N2v mAbs also displayed potent inhibiting activity against swine H3N2 strains belonging to different antigenic clusters. Collectively, these results suggest that some of these H3N2v mAbs could be used in humans as therapeutics against many H3N2 strains circulating in swine in the case of zoonotic transmission event.

The H3 HA-binding breadth of IgG secreted by memory B cells from individuals vaccinated with monovalent inactivated H3N2v revealed that there is limited cross-reactivity between antibodies secreted by variant-reactive B cells and H3 seasonal virus-reactive B cells. About half of the H3v-reactive clones that were isolated displayed specific binding to the MNv HA, with no detectable cross-reactivity for HAs from three recent seasonal H3N2 strains. The potentially neutralizing variant-specific antibodies clustered into the same competition-binding group and used the same virus neutralization mechanism by blocking the receptor-binding site on HA. This finding suggested that common antibodies induced by seasonal trivalent inactivated influenza virus (TIV) vaccination that recognize immunodominant epitopes adjacent to the RBS on HA fail to contribute to cross-protection against variant virus. A recent study showed that the molecular basis for antigenic drift in human H3N2 seasonal strains from 1968-2006 was attributed to seven single amino acid substitutions at positions 145, 155, 156, 158, 159, 189 and 193 in HA (147). Six of these residues are located in the antigenic site B (upper rim of RBS).

Fine-epitope mapping of five potentially neutralizing H3N2v-specific mAbs revealed a similar pattern in context to H3N2v antigenicity. The residues important for variant-specificity of these mAbs were located primarily in the 150 loop and 190 helix antigenic elements near the RBS.

Historically, swine influenza A viruses have caused sporadic human infections, but these outbreaks had been mostly self-limiting. The 2009 H1N1 pandemic was an example of a swine IAV variant, containing the same subtype of HA and NA as that of the circulating human strain, which caused a human pandemic. A recent rise in swine origin H3N2v human infections has raised concerns about the potential for another swine-origin influenza virus pandemic (*140, 141*). Surveillance of IAVs in Minnesota live animal markets that included human, swine and environmental samples provided evidence of interspecies transmission of IAVs from swine to human signifying a potential risk to persons attending live markets (*148*). Moreover, H3N2 was identified as the predominant subtype circulating in the swine population; a majority of these swine H3N2 isolates had the same genomic constellation as the H3N2v viruses isolated previously from humans (*148*). Vaccination with seasonal TIV does not provide protection against H3N2v viruses, indicating these swine origin viruses have the potential to spread within unprotected human populations (*85*).

The HA from swine-origin 2009 pandemic H1N1 strain is antigenically similar to human H1N1 viruses that circulated between 1918-1943 (*149*). It is hypothesized that IAV classical swine H1N1 was introduced into the domestic swine population sometime during the 1918 human pandemic and remained relatively static in swine for greater than 80 years until the end of the 20th century (*150, 151*). In light of the 2009 pandemic, swine have been thought to act as a potential reservoir of human IAVs, which can result in pandemics through reintroduction of the human-origin virus into a then susceptible human population at a remote time decades later

(149). The reactivity of the human mAbs we isolated from H3N2v vaccines revealed that the same phenomenon may be occurring now with H3 viruses, as human H3 seasonal strains from the past may be harbored in an antigenically static manner in farm swine in the U.S.

During late 1990s, there were several spillovers of H3N2 virus from humans to pigs resulting in the introduction of H3N2 viruses into the U.S swine population (143-145). The H3N2 variant viruses that were isolated from humans in 2011 were phylogenetically closer to seasonal strains that circulated during late 1990s than to current H3 human strains (145, 152). We hypothesized that the swine-origin H3N2v viruses might be antigenically related to the seasonal H3N2 viruses from late 1990s and thus the H3N2v-specific antibodies that showed no reactivity against the current seasonal strains might recognize the older seasonal viruses. Indeed, we found that three potently neutralizing variant-specific mAbs (H3v-98, H3v-104, and H3v-71) had the ability to neutralize seasonal strains that circulated between years 1997 and 2002. Additionally, H3v-98 and H3v-104 also neutralized strains from 1995 and 2005. These results indicate that the H3N2v viruses that caused human infections during 2011-13 are antigenically related to the human ancestral H3N2 strains that circulated during 1995-2005. Taken together, the data suggest that children who were born after 2005 do not have any pre-existing cross-reactive immunity against H3N2v virus because they were not exposed to the earlier H3 seasonal strains. Therefore, these children should be the priority target population for vaccination to prevent an H3N2v outbreak.

The phenomenon of antigenic similarity between swine IAVs and ancestral human strains might be explained by several mechanisms. First, swine may act as a static reservoir of human IAVs. Second, differences in the location of the immunodominant antibody epitopes on HA for swine and humans might allow preservation of antigenic epitopes targeted by humans. We



compared the HA1 sequences from H3N2v Minnesota virus and the seasonal Victoria 2011 virus with that of the Sydney 1997 strain (a possible ancestor to the H3N2v Minnesota virus). The HA1 subunit of H3N2v Minnesota and H3N2 Victoria strains has 37 or 32 polymorphisms, respectively, when compared to the HA1 sequence of H3N2 Sydney 1997, suggesting that these strains have drifted at a relatively similar rate in swine compared to the drift in humans. 13 of these positions that are situated primarily in the upper or lower rim of the RBS (antigenic sites A and B) showed variation in both Minnesota and Victoria HA. In contrast, there were comparatively more polymorphisms in the H3N2v Minnesota HA sequence in antigenic sites C and E, whereas polymorphisms in the 220-loop (antigenic site D) were seen predominantly in the Victoria 2011 strain. These host-based differences in the observed immunodominance pattern provide a possible explanation for why H3N2 viruses in the swine population retain antigenic features of their human ancestral strains. This recurring phenomenon, in which swine populations act as a static/divergent antigenic reservoir of previously circulating human IAVs, should thus be taken into serious consideration for pandemic preparedness.

### **Experimental methods**

**Influenza viruses.** The seed stock of H3N2 variant (H3N2v) strain A/Minnesota/11/2010 was obtained from Dr. Terrence Tumpey (U.S. Centers for Disease Control [CDC]). The working stocks used for microneutralization assay and hemagglutinin inhibition assays were made from the supernatant of virus-infected MDCK cell culture monolayers in plain Dulbecco's Modified Eagle Medium (Gibco DMEM, Invitrogen, 11965) with 2 µg/mL of TPCK-trypsin. The seasonal H3N2 strains A/Fujian/411/2002 (#FR-1146), A/Perth/16/2009 (#FR-370), A/Wisconsin/67/2005 (#FR-397) and A/Texas/50/2012 (#FR-1210) were provided by the

Influenza Reagent Resource ([www.influenzareagentresource.org](http://www.influenzareagentresource.org)) of the U.S. CDC. Two H3N2 seasonal strains, A/Victoria/361/2011 (NR-44022) and A/Sydney/5/1997 (NR-12278), were obtained from BEI Resources (Manassas, VA).

**Recombinant soluble HA proteins.** Sequences encoding the HA genes of interest were optimized for expression, and cDNAs were synthesized (Genscript) as soluble trimeric constructs by replacing the transmembrane and cytoplasmic domain sequences with cDNAs encoding GCN4 trimerization domain and a His-tag at the C-terminus. Synthesized genes were subcloned into the pcDNA3.1(+) mammalian expression vector (Invitrogen). HA protein was expressed by transient transfection of 293F cells with polyethylenimine (PEI) transfection reagent and grown in expression medium (Freestyle 293 Expression Medium; Invitrogen, 12338). The supernatants were harvested after 7 days, filtered sterilized with a 0.4  $\mu\text{m}$  filter and purified with HisTrap TALON FF crude columns (GE Healthcare Life Sciences).

**PBMC isolation and hybridoma generation.** A cohort of 25 donors was vaccinated twice, 21 days apart with 15  $\mu\text{g}$  of HA/0.5 mL dose of reassortant A/Minnesota/11/2010 NYMC X-203, as part of NIH sponsored clinical research trials of this experimental vaccine (DMID protocol 12-0011). The details of the clinical trial were described previously (153). PBMCs from these donors were isolated from day 0 (day of first vaccination) and protocol day 42 (three weeks after the second dose of vaccine) by density gradient separation on Ficoll and cryopreserved. The human lymphocytes from day 42 were thawed and immortalized by transformation with EBV substrain B95.8 in the presence of CpG10103, cyclosporin A and a Chk2 inhibitor (154). The cells were plated in a 384-well plate, and 8 days later the supernatants from these transformed B

cells were used to screen for the presence of antibodies that bound to soluble H3N2v A/Minnesota/11/2010 HA using capture ELISA. The positive wells containing B cells secreting anti-H3N2v antibodies were expanded onto irradiated human PBMC feeder layers for 4 days and then fused with HMMA2.5 myeloma cells using a BTX electrofusion device. After fusion, human hybridomas were selected in medium with HAT solution containing ouabain, and several rounds of limiting dilution passages were performed in 384-well culture plates to isolate cell lines of the hybridomas with the highest level of secretion of IgG (154).

**MAb production and purification.** The hybridoma cell lines with the highest level for IgG expression for each clone were selected as single cells using flow cytometric sorting to obtain clones secreting mAbs. Once hybridoma clones were obtained following sorting and growth in a 384-well plate, we expanded them first into wells of a 48-well plate and then further into a 75 cm<sup>2</sup> flask to 70% confluency in hybridoma growth medium (ClonaCell-HY medium E from STEMCELL Technologies, 03805). The cells then were washed and expanded equally to four 225 cm<sup>2</sup> flasks for antibody expression in serum-free medium (GIBCO Hybridoma-SFM, Invitrogen, 12045084). The supernatant was harvested after 3 weeks, filtered with a 0.4 µm filter, and the monoclonal IgGs were purified by affinity chromatography using protein G columns (GE Life Sciences, Protein G HP Columns).

**Half maximal effective concentration (EC<sub>50</sub>) binding analysis.** To determine EC<sub>50</sub> concentrations for each antibody, I performed ELISA using plates coated with the HA of interest at 2 µg/mL overnight at 4°C and then blocked with 5% non-fat dry milk, 2% goat serum and 0.1% Tween-20 in PBS for 1 hr. Three-fold dilutions of the mAb starting from 10 µg/mL were

added to the wells, incubated for an hour, followed by 1 hour incubation of 1:4,000 dilution of anti-human IgG alkaline phosphatase conjugate (Meridian Life Science, W99008A). The plates were washed 3 times between each step with PBS containing 0.1% Tween-20. Phosphatase substrate solution (1 mg/mL p-nitrophenol phosphate in 1 M Tris aminomethane) was added to the plates, incubated for 1 hour and the optical density values were measured at 405 nm wavelength on a BioTek plate reader. Each dilution was done in triplicate, and the EC<sub>50</sub> values were calculated in Prism software (GraphPad) using non-linear regression analysis.

### **Hemagglutinin inhibition (HAI) and neutralization assays to determine IC<sub>50</sub> values.**

Neutralization potential of all of the mAbs was determined by microneutralization assay and HAI assay. For microneutralization, 50 µL of two-fold serial dilutions of each antibody starting at 20 µg/mL was incubated with 50 µL of 100 TCID<sub>50</sub> of the virus in viral growth medium (VGM) for 1 hr at RT. VGM consists of plain DMEM with 2 µg/mL of TPCK-trypsin and 50 µg/mL gentamicin. The MDCK cell monolayer cultures were washed 2 times with 100 µL PBS containing 0.1% Tween-20, and the virus-antibody mixture then was added to cells and incubated for 32 hours at 37°C. The cells were washed again and fixed with 100 µL of 80% methanol/20% PBS. The presence of influenza nucleoprotein in the fixed cells was determined by ELISA using a 1:8,000 dilution of mouse anti-NP antibody (BEI Resources, NR 4282) as the primary antibody and a 1:4,000 dilution of goat anti-mouse alkaline phosphatase conjugate as the secondary antibody (ThermoFisher Scientific, 31320). Each dilution was tested in duplicate and the half-maximal inhibitory concentration (IC<sub>50</sub>) was determined by non-linear regression analysis of log<sub>10</sub> (inhibitor) vs. response function, using Prism software (GraphPad). An IC<sub>50</sub> value of 2 µg/mL was used as the threshold to determine the presence of functional

neutralization. For performing the HAI assay, we used turkey red blood cells (Rockland) that were diluted to 0.5% in Alsever's solution (Sigma, A3551). 25  $\mu$ L of four hemagglutination units of virus were incubated with 25  $\mu$ L of two-fold dilutions of the mAb, starting at 10  $\mu$ g/mL in PBS for 1 hr at 37°C. 50  $\mu$ L of the virus-antibody mixture was incubated with turkey red blood cells for 1 hr at RT. The HAI titer was defined as the highest dilution of antibody that inhibited hemagglutination of red blood cells. Each dilution was performed in duplicate.

**Competition-binding groups.** Biolayer interferometry using an Octet Red instrument (ForteBio) was used to confirm mAb-HA binding and to perform competition-binding assays. The HA was loaded onto ForteBio Ni-NTA tips at a concentration of 25  $\mu$ g/mL, and binding to two successively applied mAbs at 100  $\mu$ g/mL was tested. All of the dilutions were made in 1X kinetic buffer (ForteBio, 18-5032). The *actual binding signal* for each mAb was obtained after 300 seconds of a single association step of the mAb on to HA. If binding of the first antibody blocked the binding of the second antibody by reducing its actual binding signal by more than 70%, it was defined as a competitor. If binding of the first antibody did not block the binding of the second antibody by reducing its actual binding signal by less than 30%, it was defined as a non-competitor. A signal reduction between 30 and 70% was defined as partial blocking.

**Site-directed mutagenesis of genes encoding HA proteins.** Primers for site-directed mutagenesis were designed using the Agilent QuikChange Primer Design program (Agilent Technologies). The Quickchange Lightning Multi-site Mutagenesis kit (Agilent, 210515-5) was used to introduce multiple mutations into cDNAs encoding the HA genes of H3N2v A/Minnesota/11/2010 or H3N2 A/Victoria/361/2011, according to the manufacturer's

instructions. These mutant HAs were tested for antibody binding in ELISAs, as above, to determine EC<sub>50</sub> values for binding and to identify amino acids that comprise the epitope.

**Electron microscopy.** SEC-purified MNv complexed with Fab H3v-104 and Fab CR9114 was diluted to 14.7 µg/mL, applied to freshly glow discharged 400 mesh carbon coated copper grids and negatively stained with 2% uranyl formate. Similar complexes containing MNv and Fab CR9114 were then prepared separately with both Fab H3v-126 and Fab H3v-71 at 7.2 µg/mL and 5.8 µg/mL, respectively. The complexes containing Fab H3v-104 or Fab H3v-126 were imaged at 92K times magnification on an FEI Talos at 200keV resulting in a pixel size of 1.57 Å/pixel (calibrated using catalase crystal diffraction) with a dose of 23.96 e/Å<sup>2</sup>. The complex containing Fab H3v-71 was imaged at 52K times magnification on an FEI Tecnai T12 at 120kV TEM resulting in a pixel size of 2.05 Å /pixel with a dose of 25.41 e/Å<sup>2</sup>. All data was collected using Legion Multi-Scale Imaging (MSI-raster 3.1) software (155). The Talos is equipped with an FEI Ceta 4k x 4k CMOS and the T12 TEM is equipped with a Teitz F416 4k x 4k CMOS.

**EM data processing.** For the complex containing Fab H3v-104 DoGpicker was used to automatically select particles from 450 raw micrographs that were then binned by 2 resulting in a 3.14 Å /pixel size and placed into 128 x 128 pixel boxes (156). Particles were aligned with Iterative MRA-MSA and ISAC resulting in a final stack of 3,618 raw particles (157, 158). Class averages from ISAC were used to create a common lines initial model in EMAN2 (159). Model refinement was conducted in EMAN resulting in a 21.3 Å resolution reconstruction based on a 0.5 FSC cutoff value (160). The same processing pipeline was used to prepare a reconstruction

of the complex containing Fab H3v-126 from 306 raw micrographs and a final stack of 3,202 particles. Because of variable occupancy of the Fab several rounds of MRA-MSA were conducted to isolate particles containing a single bound Fab H3v-126. A model of HA bound with Fab CR9114 only was used as an initial model for refinement resulting in a resolution of 19.8 Å. The complex containing Fab H3v-71 also had variable Fab occupancy. Five rounds of MRA-MSA and one round of ISAC were conducted to isolate particles with only one Fab H3v-71 bound resulting in a final stack of 3,931 particles in 192 pixel boxes. A model of HA bound with Fab CR9114 only was used as an initial model for refinement resulting in a resolution of 27.2 Å.

**Antibody heavy and light chain variable gene sequence analysis.** Antibody heavy and light chain genes for each of the neutralizing mAbs were cloned from the hybridoma lines after single cell flow cytometric sorting to biologically clone the cell lines. RNA was extracted from these hybridoma clones using the RNeasy mini kit (Qiagen, 74106), followed by RT-PCR amplification of antibody gene cDNAs. PCR products encoding antibody heavy or light chain genes were cloned individually into the pGEM-T vector, and Sanger nucleotide sequence analysis was used to determine the antibody cDNA sequences. Analysis of variable gene sequences was performed using the international ImMunoGeneTics (IMGT) information system ([imgt.org](http://imgt.org)).

**Statistics.** The IC<sub>50</sub> values were calculated after log-transformation of antibody concentrations using a three parameter non-linear fit analysis of antibody log<sub>10</sub> concentration vs. response with R<sup>2</sup> values > 0.85. The EC<sub>50</sub> values were calculated after log-transformation of antibody

concentrations using sigmoidal dose-response non-linear fit analysis with  $R^2$  values of  $> 0.85$ . All statistics were analyzed using Prism software version 5 (GraphPad). A p value less than 0.05 was considered significant.

**Study approval.** PBMCs were collected at the Emory University Vaccine Treatment and Evaluation Unit after informed consent from otherwise healthy subjects with prior history of experimental H3N2v subunit vaccination, as described in Materials and Methods. The protocol and consent form were approved prior to study by the Emory University Institutional Review Board Committee, Atlanta, GA. The animal protocol covering the H3N2v influenza virus challenge infections of passively immunized mice was reviewed and approved by the Institutional Animal Care and Use Committee at St Jude Children's Research Hospital.



## CHAPTER III

### A BROAD H3 HUMAN MONOCLONAL ANTIBODY THAT TARGETS INFLUENZA HA HEAD EXPLOITS MULTIPLE ANTIVIRAL STRATEGIES

*“In many ways, it is hard for modern people living in First World countries to conceive of a pandemic sweeping around the world and killing millions of people, and it is even harder to believe that something as common as influenza could cause such widespread illness and death.”*

*Charles River Editors, The 1918 Spanish Flu Pandemic: The History and Legacy of the World's Deadliest Influenza Outbreak (2014)*

#### Introduction

Since H3N2 viruses began circulating in the human population in 1968, they have caused higher morbidity and mortality rates during their dominant seasons than H1N1 or influenza B viruses, and therefore present a substantial health challenge (161-163). Due to the high rate of antigenic drift and rapid evolution of human H3 viruses (164, 165), H3 vaccine strains need to be changed frequently to remain effective (166, 167). During the global 2014-2015 influenza season, H3N2 viruses predominated, accounting for more than 90% of all subtyped influenza A viruses (168, 169). In addition to seasonal infections, influenza A H3N2 variant (H3N2v) viruses of swine-origin have caused sporadic influenza infection in humans following direct exposure to swine (170). Due to the significant health threat posed by H3N2 strains, it would be beneficial to develop a vaccine that targets a conserved epitope on HA and induces breadth of response against both human and swine H3 strains. Although several human monoclonal antibodies that neutralize H3N2 viruses have been previously isolated, very few exhibit broad activity against all

human H3N2 strains.

Antibodies targeting HA typically function by blocking viral attachment to host cells or fusion with the host cell membrane. More recently, a broad influenza B antibody CR8071 that binds the vestigial esterase domain on HA head was shown to function primarily by inhibiting viral egress, similar to the function exhibited by NA inhibitors (107, 115). However, the molecular mechanism by which CR8071 inhibits viral egress is not completely understood. Another study demonstrated that HA antibodies possess some level of egress inhibition activity, possibly facilitated by Fc-mediated steric hindrance of NA active site (171). In addition to the neutralization mechanisms, antibodies to influenza proteins are capable of mediating additional effector functions through their Fc region by ADCC (58, 172) or antibody-dependent phagocytosis (ADP) (173). In recent years, ADCC elicited by influenza antibodies has emerged as a factor that may contribute to the protective immunity afforded by stem antibodies *in vivo* (61). However, neutralizing antibodies to the head domain that block receptor-binding sites typically are not thought to possess ADCC activity (61, 174).

In this chapter, I report the characterization of a *V<sub>H</sub>I-69* gene-encoded mAb designated H3v-47 that possesses broadly neutralizing activity against both human and swine H3N2 viruses. The details of the isolation of mAb H3v-47 (selected after immunization with H3N2v experimental vaccine) are reported in chapter II. Here, I describe the analysis of the epitope, breadth and function of the H3v-47 monoclonal antibody. Crystal structure and electron microscopy reconstruction of H3v-47 Fab with the H3N2v hemagglutinin (HA), revealed a unique epitope spanning the vestigial esterase and receptor-binding subdomains that is distinct from that of any known neutralizing antibody for influenza A H3 viruses. Functional assays to determine the mechanism of neutralization revealed that H3v-47 does not block receptor binding

or pH-induced conformational changes in HA. Rather, it functions by inhibiting viral egress at concentrations comparable to the neuraminidase inhibitor Zanamivir. Surprisingly, mAb H3v-47 that targets the HA head domain was also shown to possess ADCC activity by engaging Fc $\gamma$  receptor. *In vivo* studies with mice that were treated prophylactically with H3v-47 displayed reduction in viral loads in lungs following virus challenge. Collectively, these findings identify a novel conserved epitope on H3 HA that can aid in development of a broad H3N2 vaccine and provide insights into unique antiviral approaches exploited by a vestigial esterase domain-binding antibody.

I acknowledge Dr. Ian Wilson's group for resolving the co-crystal structure of Fab H3v-47 complexed with MNv HA and for their detailed analysis of the H3v-47 epitope, Dr. Stephen Kent's group for performing ADCC analysis on mAb H3v-47, Dr. Randy Albrecht for determining the *in vivo* prophylactic efficacy of mAb H3v-47 and Dr. Janice Williams from the Vanderbilt Cell Imaging Shared Resource (CISR) for teaching me everything I know about transmission electron microscopy (TEM)

### **MAb H3v-47 exhibits broad neutralizing activity against human and swine H3N2 strains**

I have previously reported the isolation of H3v-reactive human monoclonal antibodies (mAbs) from donors vaccinated with an experimental H3N2v vaccine containing the A/Minnesota/11/2010 strain (153, 175). To further investigate the breadth of one of these mAbs (H3v-47), I assayed binding by ELISA against a panel of recombinant HA molecules expressed from the HA genes of seasonal H3N2 strains that circulated during 1968 to 2014. MAb H3v-47 showed strong binding to H3N2 strains that circulated after 1989 ( $EC_{50}$  from 19 to 169 ng/mL) (Table 3-1). Heng Zhang from Dr. Wilson's laboratory also compared relative binding of H3v-47

Fab or IgG to a panel of seasonal H3 HAs by bio-layer interferometry. Consistent with the ELISA data, H3v-47 IgG exhibited high affinity to HA from seasonal H3 strains that occurred between 1989 and 2011 ( $K_d < 1$  pM) whereas H3v-47 Fab displayed moderate-high affinity of binding to HA from H3 strains that circulated after 1989 ( $K_d$  from 224 nM to  $< 1$  pM). Thus, H3v-47 can recognize HA molecules representing the diversity present in a 25-year time period from 1989 to 2014, during which significant antigenic drift occurred in human seasonal H3N2 viruses. H3v-47 did not show any binding to HA proteins from the four other influenza A subtypes tested (H1, H2, H5 or H7).

In the previous chapter, I showed that H3v-47 neutralizes H3N2v A/Minnesota/11/2010 strain at 8 ng/mL. To examine the neutralization potency of H3v-47 against human seasonal strains, I propagated 20 different H3N2 viruses that circulated in the human population since 1968. I determined their half-maximal tissue culture infectious dose ( $TCID_{50}$ ) titers and performed neutralization assays with 100  $TCID_{50}$  of each virus. The *in vitro* neutralization activity for this mAb was largely consistent with the binding data. H3v-47 showed strong neutralization against all tested H3 strains isolated after 1989, but had considerably lower neutralizing activity against H3 strains isolated before 1989 (Table 3-1). I also compared relative neutralizing activity exhibited by H3v-47 Fab,  $F(ab')_2$  or IgG against H3N2v A/Minnesota/11/2010 virus. While the  $F(ab')_2$  form of H3v-47 neutralized at a similar potency to the IgG, H3v-47 Fab displayed a greater than 190-fold reduction in the  $IC_{50}$  value in comparison to IgG ( $< 1$  pM) (Figure 3-1). Thus, H3v-47 requires the bivalency of IgG to potently neutralize the virus.

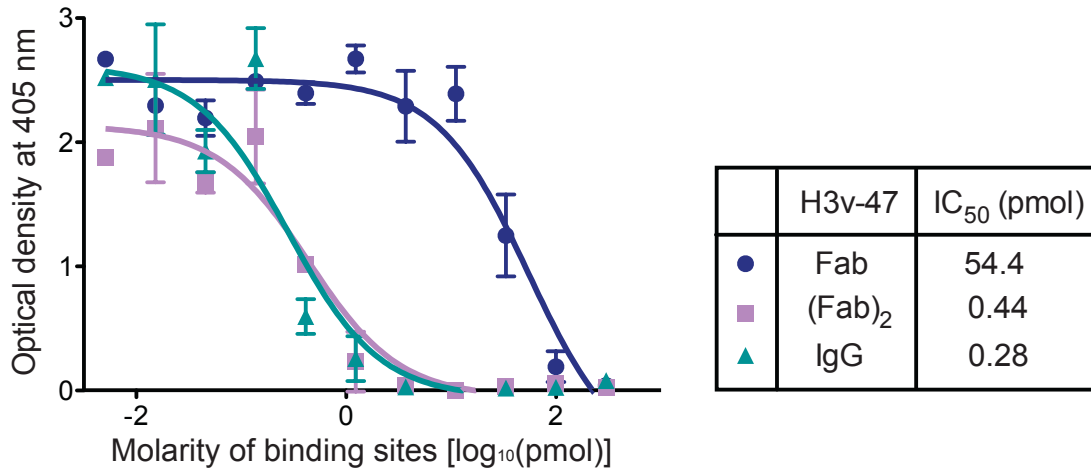
**Table 3-1. H3v-47 IgG breadth of HA binding and virus neutralization for human or swine H3N2 viruses**

<b>Virus</b>	<b>Strain</b>	<b>Binding EC<sub>50</sub> (ng/mL)</b>	<b>Neutralization IC<sub>50</sub> (ng/mL)</b>
<b>H3N2v</b>	A/Minnesota/11/2010	4	8
<b>Human H3N2 strains</b>	A/Hong Kong/1/1968	>	>
	A/Victoria/3/1975*	>	>
	A/Bangkok/1/1979*	NT	>
	A/Leningrad/360/1986*	NT	>
	A/Beijing/353/1989*	NT	158
	A/Shandong/9/1993*	NT	223
	A/Wuhan/359/1995*	NT	127
	A/Sydney/5/1997*	24	385
	A/Panama/2007/1999*	20	2,217
	A/Fujian/411/2002*	27	578
	A/New York/55/2004*	22	210
	A/California/7/2004*	35	NT
	A/Hiroshima/52/2005*	25	NT
	A/Wisconsin/67/2005*	NT	2,741
	A/Brisbane/10/2007*	NT	1,632
	A/Perth/16/2009*	19	711
	A/Victoria/361/2011*	19	1,170
	A/Texas/50/2012*	31	598
A/Switzerland/9715293/2013*	169	718	
A/Hong Kong/4801/2014*	NT	167	
<b>Swine H3N2 strains (Cluster I-IV)</b>	A/Swine/Texas/4199-2/98	NT	1,220
	A/Swine/Colorado/23619/99	NT	200
	A/Swine/Oklahoma/18089/99	NT	340
	A/Ohio/13/2012	NT	670

NT: not tested

\*WHO H3N2 vaccine strain for indicated year.

> symbol indicates values >10,000



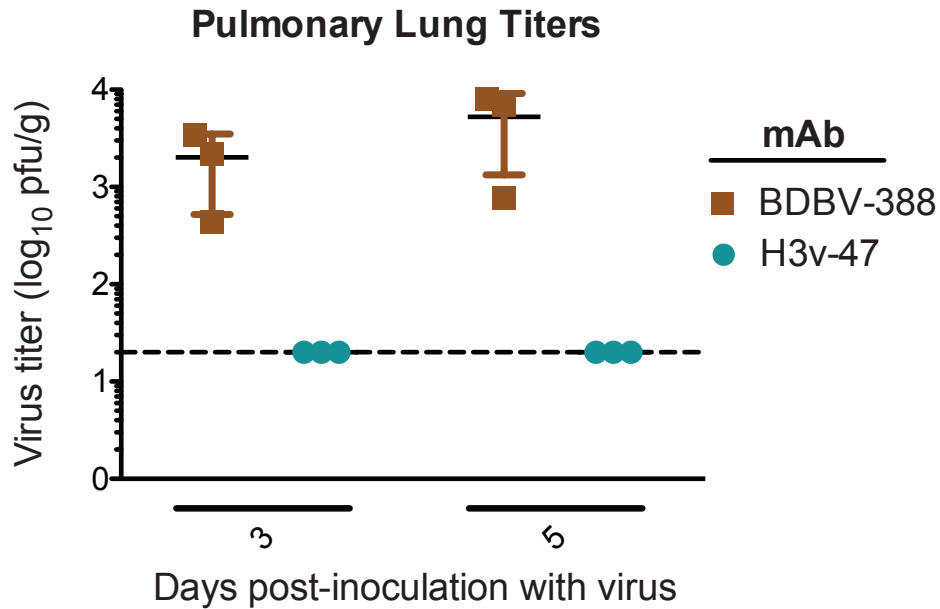
**Figure 3-1. Comparison of neutralizing activity exhibited by H3v-47 Fab, F(ab')<sub>2</sub> or IgG against A/Minnesota/11/2010 H3N2v virus.** The amounts of H3v-47 Fab, F(ab')<sub>2</sub> or IgG used for the neutralization assay were normalized for the number of binding sites present on each molecule, with a starting concentration of 15 µg/mL of the Fab, 16.5 µg/mL of F(ab')<sub>2</sub> and 22.5 µg/mL of IgG. The antibody was diluted three-fold across the plate. The IC<sub>50</sub> values were determined by non-linear regression analysis of log<sub>10</sub> [inhibitor] vs. response function, using Prism software (GraphPad)

Since most healthy adult donors were partially immune to H3 seasonal viruses prior to experimental vaccination with the H3N2v-based subunit vaccine candidate, we cannot be sure that this antibody arose as a component of the primary response to the H3N2v antigen from a naïve B cell. However, when tested for neutralization against swine viruses representing each antigenic cluster circulating in swine, A/Swine/Texas/4199-2/98 (cluster I), A/Swine/Colorado/23619/99 (cluster II), A/Swine/Oklahoma/18089/99 (cluster III) or A/Ohio/13/2012 (cluster IV), it was of interest that H3v-47 efficiently neutralized all four swine H3N2 strains (Table 3-1), which has not been reported previously for human H3 antibodies (60, 112, 113, 176). These data suggest that H3v-47 possesses broad-spectrum neutralizing activity for viruses of the H3 subtype and can efficiently inhibit both human and swine H3N2 viruses.

#### **Prophylactic administration of H3v-47 reduced pulmonary viral load in mice**

To determine the prophylactic efficacy of H3v-47 *in vivo*, prophylactic studies were performed in collaboration with Dr. Randy Albrecht. For passive immunization experiments, groups of 6 BALB/c mice were injected intravenously with 15 mg/kg of either human mAb H3v-47 or a similarly prepared human mAb to an unrelated antigen (mAb BDBV-388 reactive with Bundibugyo virus glycoprotein) on day -1. At 24 hours post-immunization, animals were inoculated with  $1 \times 10^4$  PFU of H3N2v A/Minnesota/11/2010 virus. Lung samples were collected on day 3 (n=3) or day 5 (n=3) post-inoculation and viral titers were quantified using immunostaining plaque assay. The virus titer in H3v-47 treated mice was at the lower limit of detection. An approximate 100-fold reduction of pulmonary viral titers was observed in H3v-47 treated mice compared to control-antibody treated mice on day 3, and the effect was more pronounced on day 5 (~ 260-fold reduction) than on day 3 (Figure 3-2). Significantly, none of

the mice treated with mAb H3v-47 had detectable viral loads in their lungs at both the time points tested.



**Figure 3-2. Prophylactic efficacy of H3v-47 in mice.** 12-week old BALB/c mice (n=6) were immunized passively with 15 mg/kg of either H3v-47 IgG or a similarly prepared control human antibody to a heterologous target (BDBV) and challenged 24 hours post-immunization with  $1 \times 10^4$  pfu of the A/Minnesota/11/2010 H3N2v virus. Lung samples were collected from 3 mice per antibody group on both day 3 and day 5 after virus inoculation. Pulmonary titers of influenza virus were quantified by immunostaining virus plaques on MDCK cells. The dotted line represents the limit of virus detection.



## **Epitope mapping and structural characterization of the H3v-47-HA complex reveals a unique neutralizing epitope on H3 head domain**

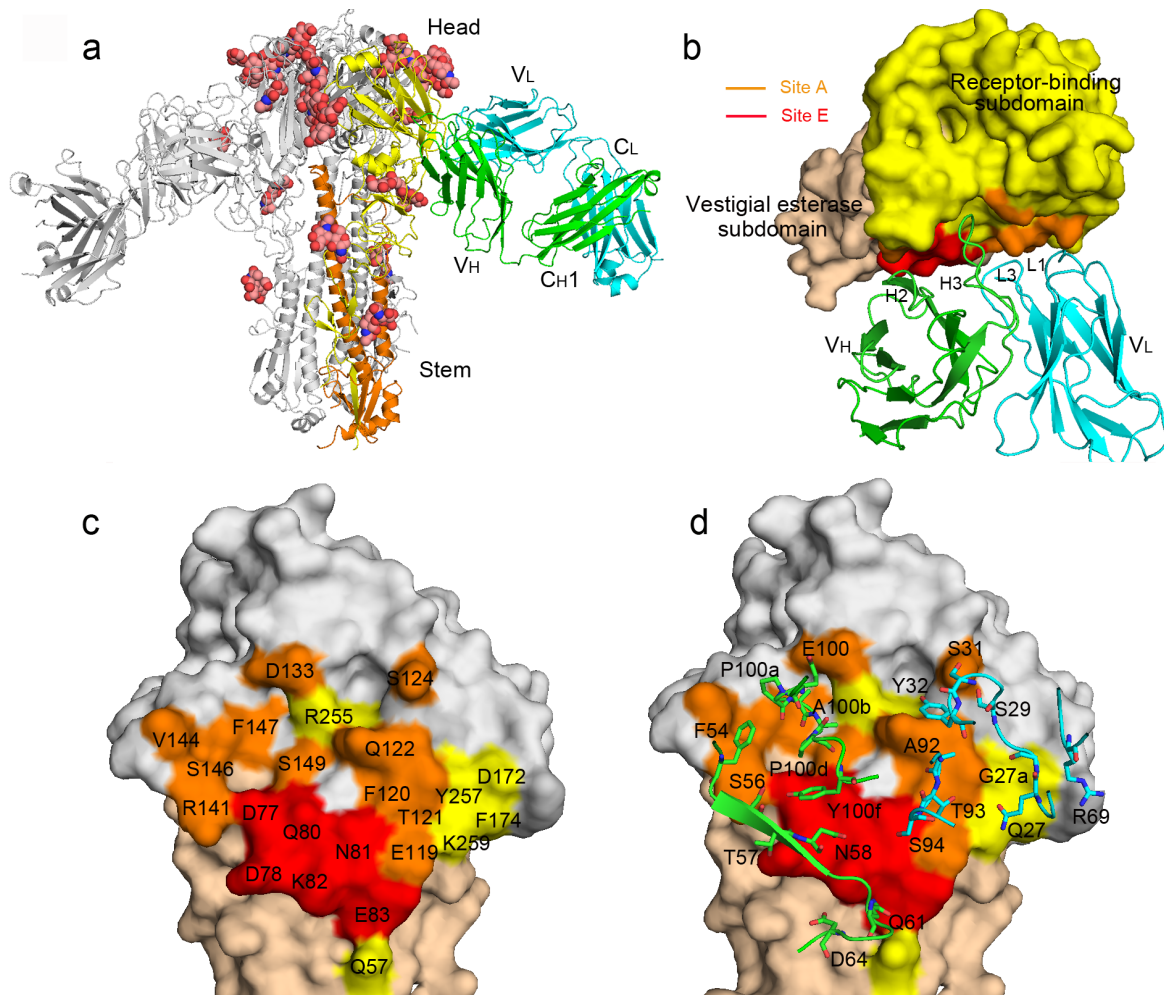
In my original study of H3v-reactive antibodies, it was apparent that H3v-47 does not bind to the RBS on HA head in a conventional manner due to its lack of hemagglutination inhibition (HAI) activity (175). To examine if the antibody binds to the stem region, I used bio-layer interferometry to compete H3v-47 for binding against other known broad stem-binding antibodies CR8020, CR9114, FI6v3 and 39.29 as well as the control RBS-binding antibody, CO5. Surprisingly, I observed partial competition between H3v-47 and the RBS mAb CO5, but did not detect competition with the stem-binding antibodies, indicating that H3v-47 does not bind to the HA stem region (Figure 3-3).

To further investigate the antibody epitope, I collaborated with Dr. Ian Wilson's group to determine the crystal structure of H3v-47 Fab in complex with H3N2 A/Minnesota/11/2010 (Minn2010/H3v) HA (Figure 3-4). Structural data (3.57 Å resolution) revealed the Fab binding to the globular head of HA below the RBS, in a region near the vestigial esterase subdomain (Figures 3-4A and 3-4B). The position of the binding region suggested that H3v-47 cannot block the sialic acid-binding pocket, which is consistent with the observation that H3v-47 does not exhibit HAI activity. H3v-47 targets a unique conformational epitope spanning the RBS and vestigial esterase region in the HA head (Figure 3-4B and 3-4C). The epitope and paratope residues are depicted in Figures 3-4C and 3-4D, respectively. The H3v-47 footprint residues in H3 subtype viruses are distinct from the residues at the same position in other virus subtypes, revealing why H3v-47 does not show cross-neutralization against other virus subtypes.

		Second antibody					
		H3v-47	C05	CR8020	CR9114	FI6v3	39-29
First antibody	H3v-47	4	49	100	94	108	78
	C05	46	0	94	114	91	91
	CR8020	94	99	0	0	0	0
	CR9114	71	89	3	5	21	24
	FI6v3	94	98	11	42	0	37
	39-29	55	86	2	27	24	0

Color	Interpretation	Percentage of max un-competed signal
Black	First antibody blocks the binding of second antibody	<30%
Grey	First antibody partially blocks the binding of second antibody	31-60%
White	First antibody does not block the binding of second antibody	>60%

**Figure 3-3. Competition binding of H3v-47 with other influenza head- or stem-binding antibodies.** Competition-binding assays were performed using biolayer interferometry. The His-tagged A/Minnesota/11/2010 H3N2v HA was loaded onto Ni-NTA tips, and binding of two successively applied antibodies (IgG) was tested. MAb H3v-47 was competed against mAb C05, a receptor binding site mAb or each of four stem-binding antibodies: CR8020, CR9114, 39.29 or FI6v3. Numbers indicate normalized percent level of association to HA, compared to uncompleted control (100%). The colored boxes indicate each competition-binding group. There was partial overlap between group 1 and 2, shown in cyan and blue, respectively. Competition was not detected between H3v-47 and the stem antibodies indicated in the red competition-binding group box. The experiment was conducted twice independently.



**Figure 3-4. Crystal structure of antibody H3v-47 Fab in complex with H3N2v HA (A/Minnesota/11/2010) and identification of the epitope.** (A) Overall structure of the H3v-47 Fab- H3N2v HA complex. One HA/Fab protomer of the trimeric complex is colored with HA1 in yellow, HA2 in orange, Fab heavy chain in green, and Fab light chain in cyan. N-linked glycans are depicted as colored balls representing their atom types (carbon in pink, oxygen in red and nitrogen in blue). The other two protomers are in gray, but the third Fab molecule is hidden behind the HA trimer. (B) Zoomed-in view of the interaction between H3N2v HA and H3v-47 Fab with color coding as in (A). H3v-47 Fab binds to the region spanning the receptor-binding and vestigial esterase sub-domains (shown as a solid surface in yellow and wheat, respectively) mainly using CDRs H2, H3, L1 and L3. The contact regions ascribed to antigenic sites A and E are highlighted in orange or red, respectively. (C) H3v-47 epitope mapped onto the H3N2v HA surface. The footprint of antibody H3v-47 on the HA shows the central role of antigenic E site residues for H3v-47 binding. The interacting surface contributed by residues from antigenic sites A or E is colored in red or orange, respectively, whereas residues that contribute to the epitope outside of these two antigenic sites, are colored in yellow. (D) Antibody contact residues (sticks) that interact with the HA with CDRs H2, H3, L1, L3 and FR3 in the light chain. Figure credit: Heng Zhang (Wilson laboratory).

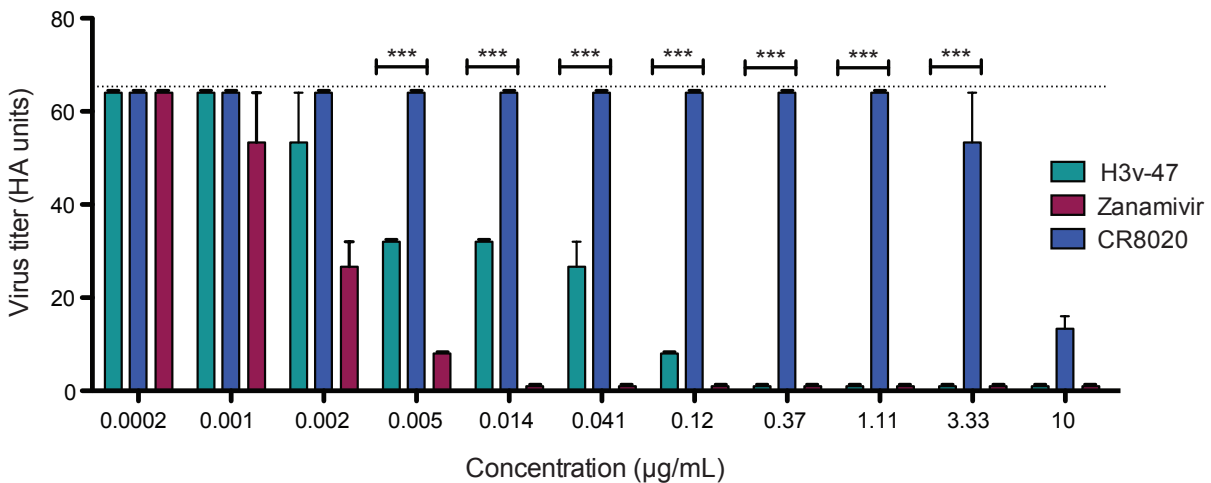
### **Mechanism of neutralization by mAb H3v-47**

Although mAb H3v-47 binds to the HA head region, it does not neutralize by blocking the RBS unlike most other head domain-reactive neutralizing antibodies. To further explore the mechanism of neutralization mediated by H3v-47 recognition of this unusual epitope, trypsin digestion of Minn2010/H3v HA was performed in which the HA protein was exposed to a low pH (pH 5.0) to trigger the pH-induced conformational changes and acquire sensitivity to trypsin cleavage. As expected, the low-pH-treated HA could be completely digested by trypsin in the absence of H3v-47 Fab. Binding of H3v-47 Fab to the HA did not protect the HA from degradation by trypsin when treated at pH 5.0, suggesting binding of H3v-47 does not prevent the low-pH induced conformational changes in HA as do stem-binding antibodies (107).

I next tested whether H3v-47 functions through an alternative mechanism by blocking virus budding. I performed virus egress inhibition assays using MDCK cells inoculated with Minn2010/H3v virus that were treated with H3v-47 IgG at 3 h post inoculation to allow for unhindered virus attachment and fusion. The neuraminidase inhibitor zanamivir or the stem-specific neutralizing mAb CR8020 IgG were used in parallel as positive or negative control reagents, respectively, for egress inhibition. The assay was performed in the absence of trypsin to restrict viral replication to a single cycle. Infected cell supernatants were collected after 12 hours, and the virus titers were determined by hemagglutination assay as HA units. A 50% reduction in the HA titer of virus compared to the untreated control was observed at concentrations of 4-10 ng/mL of the H3v-47 antibody (Figure 3-5). This concentration correlates well with the  $IC_{50}$  of 8 ng/mL seen for H3v-47 against the Minn2010/H3v virus, suggesting that the main mechanism of neutralization by H3v-47 is inhibition of viral egress. As expected, zanamivir that blocks NA activity also showed potent inhibition of viral egress at similar molar concentrations as H3v-47,

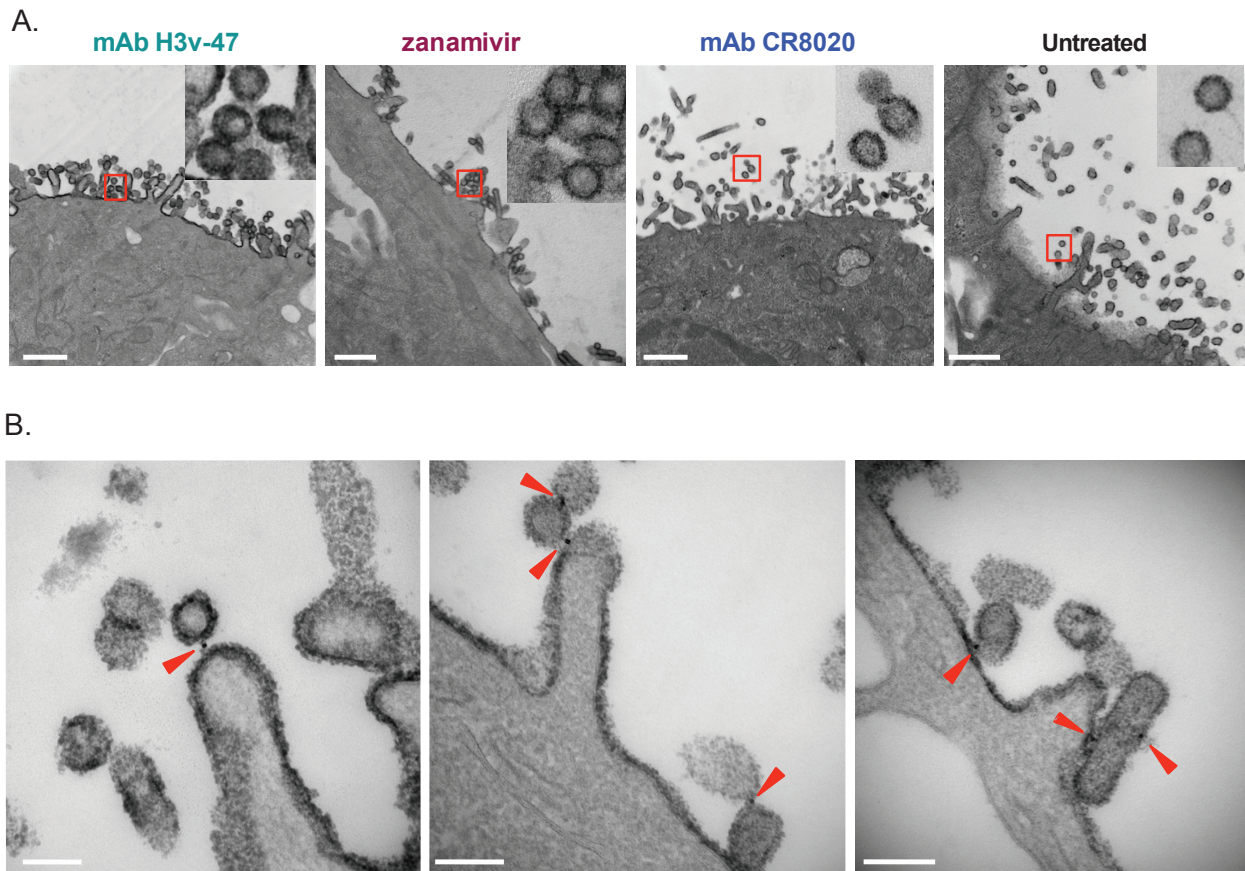
whereas the stem-binding antibody CR8020 did not mediate significant reduction in HA titer at concentrations as high as 3.3  $\mu\text{g}/\text{mL}$  (Figure 3-5). I did observe, however, some activity for CR8020 at the highest concentration tested (10  $\mu\text{g}/\text{mL}$ ). The cause for this activity is uncertain. This reduction in HA titer at higher antibody concentrations could be a result of minor inhibition of NA enzymatic activity exhibited by HA stem antibodies (171). Alternatively, we also have observed that stem antibody CR8020 can exhibit HAI activity at 10  $\mu\text{g}/\text{mL}$  (not shown).

To confirm that H3v-47 was acting at the step of virus egress from infected cells, I performed transmission electron microscopy (TEM) of MDCK cells inoculated with Minn2010/H3v virus and either untreated or treated with H3v-47 IgG, CR8020 IgG or zanamivir at 3 h post-inoculation. As expected, the major phenotype observed in zanamivir-treated cells was cell surface aggregation of fully formed virus particles, in contrast to the prevalence of released virus particles in the untreated cells (Figure 3-6A). H3v-47 mAb-treated cells also revealed virus aggregations on the cell surface, similar to those in the zanamivir-treated samples (Figure 3-6A). In contrast, cells treated with stem mAb CR8020 showed individually budded particles resembling the pattern in untreated virus-infected cells (3-6A). CR8020-treated cells also had considerably more virus particles inside the cells compared to zanamivir- or H3v-47-treated cells. Zanamivir-treated cells displayed more filamentous influenza particles on the cell surface compared to H3v-47-treated cells. Taken together, the data indicates that H3v-47 mAb functions by preventing viral egress in a manner comparable to zanamivir.



**Figure 3-5. Inhibition of egress of A/Minnesota/11/2010 H3N2v virus by IgG of mAbs H3v-47 or CR8020 or by the small molecule neuraminidase inhibitor zanamivir.** Twenty-hours prior to the experiment, MDCK cells were seeded on 6-well plates in DMEM + 5% FBS. The cells were washed twice with PBS and inoculated with a previously optimized amount of A/Minnesota/11/2010 H3N2v virus that is required to achieve 90-100% infection. After 1 h incubation at 37 °C, the cells were washed twice with PBS and replenished with 1.5 mL plain Opti-MEM I medium. After 3 h, the cells were washed again and replenished with 1.5 mL of Opti-MEM I containing serial dilutions of the antibodies or zanamivir. The cells were incubated at 37 °C for 12 h, and the supernatants were harvested. The supernatants were diluted serially 11 times and added to an equal volume of 0.5% turkey RBCs in v-bottom plates to determine the virus titer by hemagglutination assay. Dotted line represents virus titer in supernatant in the absence of antibody treatment. The experiment was conducted three times independently. The hemagglutination assay to determine virus titer was also conducted three times independently (n=3). The significance in the reduction of HA titer between H3v-47 and CR8020 was calculated at each concentration using 2-way ANOVA and displayed on the graph as \*\*\* (P<0.001).

The molecular mechanism of egress inhibition by an HA antibody is not well understood, as HA does not participate in the release of viral particles from cell surface. Antibodies to HA have been hypothesized to inhibit viral egress either by blocking NA enzymatic activity by Fc-mediated steric hindrance or by cross-linking newly formed virions or HA trimers on the cell surface (107). To further elucidate the molecular mechanism by which H3v-47 inhibits egress, I performed TEM with gold labeling to determine the localization of H3v-47 during egress. The infected MDCK cell samples were prepared for TEM as before, but with the addition of anti-human IgG conjugated to gold particles 1 hour before fixing cells. We observed that H3v-47 was predominantly present at the interface between the MDCK cells and newly budded virus particles or at virus-virus interfaces in comparison to CR8020 (Figure 3-6B). The ratio of the number of gold particles present at the interfaces (I) (virus-virus and surface-virus) to the total number of gold particles on the surface (S) was higher for H3v-47 (I/S=5/8) compared to CR8020 (I/S=2/8). Also, there was significantly less gold particle labeling of IgG on the cell surface of CR8020-treated cells. Trace amounts of gold particles were present in zanamivir-treated and untreated cells. Collectively, these results along with our previous observation that the (Fab)<sub>2</sub> form of H3v-47 had similar neutralization potency as the IgG (Figure S2), we suggest that H3v-47 may primarily function by tethering newly formed virions to the cell surface or to other viral particles rather than Fc-mediated steric hindrance of NA. However, it is possible that H3v-47 also possesses some level of neuraminidase enzymatic inhibition activity that contributes to its overall potency.

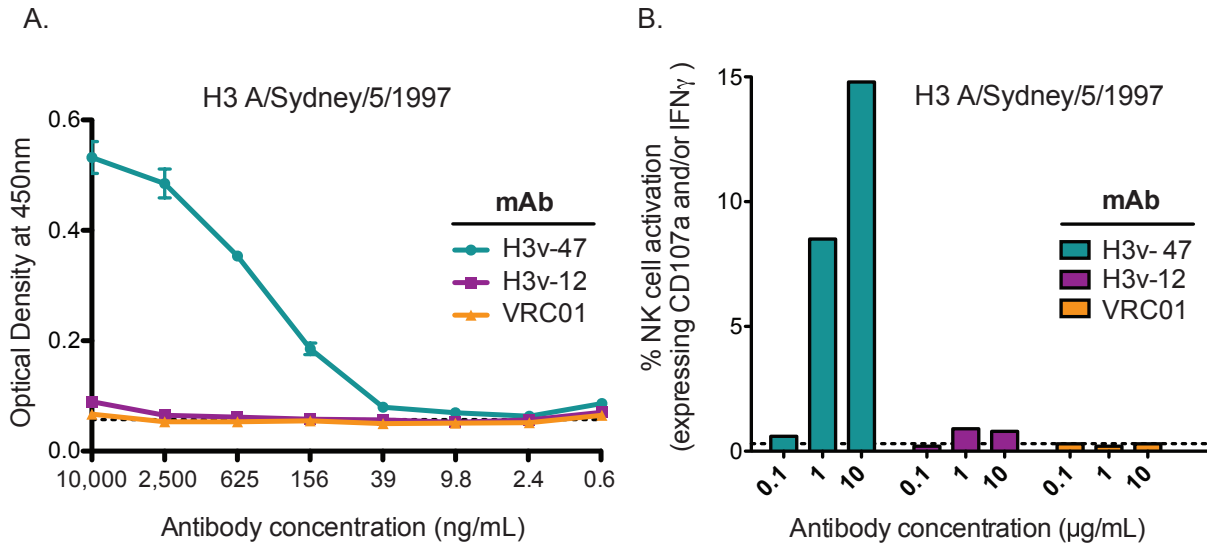


**Figure 3-6. H3v-47 localizes to interfaces between virus and cell surface or between viral particles (A)** Representative TEM images of the surface of MDCK cells inoculated with A/Minnesota/11/2010 H3N2v virus and infected cells were incubated with mAb H3v-47, zanamivir, mAb CR8020 or plain Opti-MEM at 3 h post-inoculation and fixed for imaging at 14 h. For each image, the virus particles in the red squares are shown at higher magnification, below. Representative images of 2 independent experiments are shown. The white scale in each image represents 500 nm. **(B)** Representative TEM images are shown of the surface of MDCK cells that were inoculated with virus and subsequently incubated with H3v-47 mAb similar to (A), with addition at 13 h post-inoculation of anti-human IgG conjugated to 10 nm gold particles. The black opaque dots indicated by the red triangles represent the gold particles. The white scale in each image represents 100 nm. The experiment was conducted twice independently.



### **H3v-47 mAb exhibits ADCC activity**

HA stem-reactive antibodies frequently possess ADCC activity and depend on Fc receptor engagement to confer protection *in vivo* (61, 177). Recent work suggested that while stem-binding antibodies potently elicit ADCC activity, the receptor-binding site antibodies seem to lack the ability to induce ADCC (177, 178). We collaborated with Dr. Stephen Kent's group to examine if H3v-47, which targets the vestigial esterase subdomain on the HA head, could mediate ADCC activity. As an initial screen, we performed an ELISA using recombinant soluble (rs), dimeric, low-affinity ectodomains (rsFcγR) of FcγRIIIa as described (179). These dimers require simultaneous engagement of two Fc domains to achieve stable binding detected by ELISA. We tested the ability of three mAbs [H3v-47, H3v-12 (HA-reactive) or VRC01 (an HIV-reactive control mAb)] bound to A/Sydney5/1997 HA to simultaneously engage both binding sites on rsFcγR. Only H3v-47 bound to FcγR in this assay (Figure 3-7A), suggesting its potential to mediate ADCC activity. Next, we examined the ability of these antibodies to mediate functional ADCC activity as measured by activation of primary CD3<sup>-</sup> CD56<sup>+</sup> NK cells following incubation with HA from A/Sydney5/1997. NK cell activation was measured by intracellular IFN-γ expression and degranulation (CD107a expression). A concentration-dependent increase in the percentage of NK cell activation was observed for H3v-47 (14.8% NK cell activation at 10 μg/mL), while activation was not observed for H3v-12 or VRC01 at the highest concentration tested (10 μg/mL) (Figure 3-7B). Collectively, these data show that mAb H3v-47 engages FcγRIIIa and induces ADCC activity, even though it binds to the head domain.



**Figure 3-7. H3v-47 mAb exhibits ADCC activity. (A)** Cross-linking of Fc $\gamma$ RIIIa. Binding curves were obtained by performing ELISA with serial dilutions of each antibody (H3v-47, H3v-12 or control mAb VRC01 [to HIV]) onto HA-coated plates and assessing the ability of HA-bound mAbs to engage both Fc-binding sites on the soluble Fc $\gamma$ RIIIa dimer. **(B)** Primary NK cell activation. Antibody (H3v-47, H3v-12 or VRC01) at 0.1, 1 or 10  $\mu$ g/mL each were added independently on 96-well plates coated with purified A/Sydney/05/1997 H3 HA and incubated for 2 h. The plates were washed, and  $5 \times 10^5$  purified NK cells were added to each well. The cells were stained with anti-human CD107a allophycocyanin-H7 Ab, anti-human CD3 PerCP, anti-human CD56 allophycocyanin and anti-IFN $\gamma$  AF700. The data for 20,000 to 50,000 events were acquired using an LSRFortessa flow cytometer. The percentage of NK cell activation was calculated as the percentage of NK cells that expressed CD107a and/or IFN $\gamma$ . The dotted lines in both (A) and (B) indicate the limit of detection. The results are representative of three independent experiments.

## Discussion

Recent research on influenza vaccinology has focused on the idea of identifying components of a broadly protective or universal vaccine that would protect better against seasonal drift virus strains or newly emerging pandemic strains. The most obvious conserved antigenic site for inclusion in such a vaccine studied to date is the stem region, which possesses highly conserved residues that can be recognized by human antibodies. In this chapter, I describe the unique human mAb H3v-47 that mediates very broad neutralization of H3 influenza viruses by binding to an unusual conserved epitope on the side of the H3 HA head domain. This antibody mediates inhibition of virus replication using multiple molecular mechanisms including inhibition of virus egress and mediation of ADCC activity. Animals injected prophylactically with H3v-47 IgG before virus challenge displayed a significant reduction in pulmonary viral loads, indicating that H3v-47 has promising potential for influenza treatment. The detailed structural and functional data presented here suggest that engineered HA head domain antigens that focus the antibody response on the H3v-47 epitope could be an important component of a broadly protective H3 vaccine.

Most neutralizing antibodies (mAbs C05, F045-092, S139/1, HC19 and HC63) that bind to the HA head of H3N2 viruses recognize epitopes in or surrounding the RBS (180). Three structurally characterized H3-neutralizing antibodies, HC45, BH151 and F005-126, bind to a region more distant from the RBS. Although HC45 and BH151 target the vestigial esterase subdomain, both are A/Aichi/2/1968 strain-specific H3 antibodies with narrow breadth of neutralization activity (181, 182) while F005-126 spans a cleft formed by two HA monomers in the head domain, and neutralizes certain H3 viruses isolated during the period from 1968 to 2004. On the other hand, H3v-47 recognizes a distinct epitope that spans the RBS and vestigial

esterase subdomain and exhibits broad activity against H3 strains. H3v-47 antibody exhibits inhibitory activity for human seasonal and swine H3 viruses isolated after ~1989, but variability in the epitope does occur. E82 or K82 residues are highly conserved (~100% conservation) across human and swine-origin H3N2 strains isolated before or after 1989. The occurrence of the natural antigenic drift mutation E82K is consistent with the cross-neutralization activities of H3v47 for human and swine H3 viruses isolated after ~1989. Moreover, the K82E variant disrupts binding of H3v-47 Fab to the HA, indicating that the substitution may play a major role in H3v-47 recognition and specificity, but the antibody retains binding to such variants in the IgG form by avidity effects.

HC45 neutralizes viral infectivity by blocking receptor binding, as it has HAI activity (182) and prevents the low-pH induced conformational changes of the HA required for membrane fusion (183). H3v-47 functions in a distinct manner, because it does not prevent the low-pH induced conformational changes in the HA, nor does it have detectable HAI activity. Instead, H3v-47 functions primarily by interfering with progeny release similarly to the action of neuraminidase inhibitors like zanamivir. Egress inhibition activity has been recorded previously for an influenza type B antibody CR8071 that binds to HA head domain and is oriented perpendicular to the long axis of the HA (115) (Figure 8a). It appears that H3v-47 functions in a similar manner as CR8071 despite binding to diverse epitopes (107). Detailed analysis of H3v-47-mediated egress inhibition by TEM indicates that H3v-47 might aggregate newly formed virions by cross-linking HA molecules.

In conclusion, a novel human mAb H3v-47 showed broad neutralization of human and swine H3N2 viruses by targeting a unique conserved epitope that has not previously been characterized as immunogenic on H3 viruses. MAb H3v-47 functions uniquely by inhibiting

viral egress and also by facilitating ADCC activity by engaging FcγRIIIa on NK cells. This epitope may induce production of broadly neutralizing antibodies against human and swine H3 viruses and enable design of more broadly protective H3 vaccines.

### **Experimental methods**

**Culture of influenza virus.** The original seed stocks for all the viruses were obtained from varying sources as recorded in the previous chapter. All of the working stocks were obtained by virus inoculation of MDCK cell culture monolayers in plain Dulbecco's Modified Eagle Medium (Gibco DMEM, Invitrogen, 11965) with 2 μg/mL of TPCK-trypsin.

**Production of recombinant soluble HA proteins.** The design and expression of recombinant HA proteins for binding studies are described in chapter II. HA proteins expressed in mammalian system were used for EC<sub>50</sub> studies, competition binning and functional studies. Soluble HA proteins for crystallization were produced using a baculovirus expression system, as described previously (*184*).

**Production of H3v-47 IgG.** Purified H3v-47 IgG from hybridoma cell expression was used for all EC<sub>50</sub> and IC<sub>50</sub> studies, egress assays, TEM and ADCC assays.

**Half maximal effective concentration (EC<sub>50</sub>) and half maximal inhibitory concentration (IC<sub>50</sub>) analysis.** The experiments to determine EC<sub>50</sub> and IC<sub>50</sub> values were performed as described previously. The experiments for determining EC<sub>50</sub> ( $n = 4$ ) and IC<sub>50</sub> ( $n = 3$ ) were conducted twice independently. Plaque reduction assay was used to determine IC<sub>50</sub> values for H3v-47 against swine H3N2 strains. MDCK cells were seeded onto the 12-well tissue culture plates the day

before inoculation. On the next day, 50 pfu of each H3N2 virus in 100  $\mu$ L was first incubated with two-fold serially diluted antibodies for 1 hour at 37 °C. The mixture was then added onto MDCK cells after removing their culture medium and incubated for one hour at 37 °C. Plaque formation was assessed after a 2-3 day incubation at 37 °C. The inhibition mediated by H3v-47 antibody against each H3N2 virus was calculated as the percentage of the plaque reduction, and  $IC_{50}$  values were determined as the concentration at which 50% of plaque reduction was observed.

**Expression of recombinant H3v-47 Fab.** The heavy and light chain variable regions of H3v-47 were cloned into the vector phCMV containing the  $C_{H1}$  region of an IgG1 appended to myc- and His-tags, respectively. The Fab fragment was expressed by transient co-transfection of the expression vector containing heavy chain and light chain into FreeStyle 293-F cells. Recombinant Fab was purified from culture supernatant using a nickel column followed by size exclusion chromatography using a Superdex 75 column (GE Healthcare). Purified Fab was measured by optical absorbance at 280 nm, and purity and integrity were analyzed by reducing and nonreducing SDS-PAGE. The purified H3v-47 Fab was concentrated to  $\sim$ 10 mg/mL for crystallization and  $K_d$  determination.

***In vivo* efficacy of H3v-47.** Experimental groups of 6 BALB/c mice (purchased from Jackson Labs) aged 12 weeks were immunized passively with 15 mg/kg of either H3v-47 or a similarly prepared control human antibody (to Bundibugyo virus; BDBV) and challenged the next day with  $1 \times 10^4$  PFU of H3N2v A/Minnesota/11/2010 virus. Lung samples were collected from 3 mice per group on day 3 and on day 5. Pulmonary titers of influenza virus were quantified by plaque assays on MDCK cell culture monolayers. The formalin-fixed MDCK cell cultures then

were labeled with convalescent serum from mice infected with A/California/4/2009 (swine-origin H1N1) followed by sheep anti-mouse IgG conjugated with horseradish peroxidase (GE Healthcare Life Sciences, RPN4201). Immunostained influenza virus plaques then were visualized by addition of TrueBlue™.

**Protease susceptibility assay.** Experiments to test for trypsin susceptibility of the HA were performed as previously described (113). For A/Minnesota/11/2010 (H3N2) HA, each reaction mixture contained 2.5 µg of the HA or 2.5 µg of the HA and a two-fold molar excess of H3v-47 Fab (two Fabs per HA protomer). Reaction mixtures were incubated at 37 °C for 1 h at pH 5.0 and at 8.0. After incubation, the reaction mixture was neutralized to pH 8.4. Trypsin then was added to all samples except controls at a final ratio of 1:20 (wt/wt) of trypsin to HA, and reaction mixtures were incubated overnight at 22 °C. Samples then were analyzed by non-reducing SDS-PAGE.

**Egress inhibition assay.** MDCK cells were seeded in plain Dulbecco's Modified Eagle Medium (Gibco DMEM, Invitrogen, 11965) containing 10% FBS on six-well plates overnight. The cells were washed three times with PBS and 200 µL of previously optimized virus titer required to achieve 90-100% infection was added to the cells and incubated for 1 hr at 37 °C degrees with periodic shaking. One hour after inoculation, the cells were washed once and replenished with 2 mL Opti-MEM I with glutamax medium (Gibco, Life Technologies, 51985) per well and incubated for 2 more hours at 37 °C degrees. After a total of 3 h after inoculation, the cells were washed again and replenished with medium containing three-fold serial dilutions of H3v-47 antibody, CR8020 antibody or zanamivir (Relenza, NDC0713068101), starting at the highest

concentration of 10  $\mu\text{g}/\text{mL}$ . Trypsin was not added to the cells, in order to restrict the infection to a single cycle. The plates were incubated for 12 hours at 37 °C degrees and the supernatants were collected for performing hemagglutination assay (HA). For HA assay, we used turkey red blood cells (Rockland Immunochemicals, R313) that were washed and diluted to 0.5% in 2.5% sodium citrate. 50  $\mu\text{L}$  of the supernatants that were serially diluted two-fold in medium were incubated with 50  $\mu\text{L}$  of the 0.5% turkey red blood cells in v-bottom plates for 1 hr at 4 °C. The HA titers in the supernatants were calculated based on the lowest supernatant dilution at which hemagglutination was observed. The HA titers were performed in triplicate, and results shown are an average of three wells.

**Transmission electron microscopy (TEM).** MDCK cells were inoculated with A/Minnesota/11/2010 H3N2v virus and subsequently incubated with H3v-47 IgG (5  $\mu\text{g}/\text{mL}$ ), CR8020 IgG (10  $\mu\text{g}/\text{mL}$ ), Zanamivir or plain Opti-MEM I medium at 3 h post-inoculation using the same conditions as the egress assay. Trypsin was not added to cells to capture the phenotype of egress inhibition. For gold labeling, the samples were treated identically except for the addition of goat-anti-human IgG conjugated to 10nm gold particles (EMS, 25208) at 13 h post-inoculation. At 14 h after virus inoculation, samples were washed with 0.1 M cacodylate buffer and fixed in 2.5% gluteraldehyde in 0.1 M cacodylate buffer, pH 7.4 at room temperature (RT) for 1 h then transferred to 4 °C, overnight. The samples were washed in 0.1 M cacodylate buffer, then incubated 1 h in 1% osmium tetroxide at RT, then washed with 0.1 M cacodylate buffer. Subsequently, the samples were dehydrated through a graded ethanol series and then three exchanges of 100% ethanol. Next, the samples were incubated for 5 minutes in 100% ethanol and propylene oxide (PO) followed by two exchanges of pure PO. Samples then were infiltrated



with 25% Epon 812 resin and 75% PO for 30 minutes at RT. Next, they were infiltrated with Epon 812 resin and PO [1:1] for 1 h at RT, then overnight at RT. The next day, the samples underwent a 3:1 (resin: PO) exchange for 3-4 hours, then were incubated with pure epoxy resin overnight. Samples then were incubated in two more changes of pure epoxy resin and allowed to polymerize at 60 °C for 48 h. For imaging, 70-80 nm ultra-thin sections were cut and collected on 300-mesh copper grids and post-stained with 2% uranyl acetate, and then with Reynold's lead citrate. Samples subsequently were imaged on a Philips/FEI Tecnai T12 electron microscope at varying magnifications. Specimens were processed for TEM and imaged in the Vanderbilt Cell Imaging Shared Resource - Research Electron Microscopy facility.

**Dimeric recombinant soluble FcγRIIIa (CD16a) binding ELISA.** A dimeric recombinant soluble FcγRIIIa (rsFcγRIIIa) ELISA was used to model the need for ADCC-inducing Abs to cross link FcγRIIIa (179). A 96-well ELISA plate was coated with 50 ng of purified influenza HA protein from H3N2 A/Sydney/5/1997 (Sino Biological Inc., 40149-V08B) protein overnight at 4 °C in PBS. The plate was washed twice with PBST and blocked with 140 μL of PBS 1 mM EDTA, 1% BSA (PBSE/BSA) for 1 h at 37 °C. The plate then was washed twice with PBST and 50 μL of H3v-47 diluted in PBSE/BSA was added into duplicate wells, with concentrations ranging from 40 μg/mL to 2.4 ng/mL. Negative control wells with HA protein and PBS alone also were included (“no antibody control”). Following addition of H3v-47 or PBS, the plate was incubated at 37 °C for 1 h. The ELISA plate was washed five times with PBST and 50 μL of 0.1 μg/mL rsFcγRIIIa (V176) dimer was added to the wells, then the plate was incubated for 1 h at 37 °C. Pierce High Sensitivity Streptavidin-HRP (Thermo Fisher Scientific, 21130) was diluted 1:10,000 in PBSE/BSA, added to all wells, and the plate was incubated at 37 °C for 1 h. The

plate was washed eight times with PBST and blotted dry. 50  $\mu$ L of TMB substrate was added to each well and the plate was developed for 4-8 min in the dark. The reaction was stopped with 1 M HCl and the plate read at an absorbance of 450 nm.

**NK cell activation assay.** 96-well ELISA plates were coated with 600 ng of purified influenza H3N2 A/Sydney/5/1997 HA protein (Sino Biological Inc., 40149-V08B) overnight at 4 °C in PBS. The wells were washed five times with PBS and incubated with 10  $\mu$ g/mL, 1  $\mu$ g/mL or 0.1  $\mu$ g/mL of H3v-47 diluted in PBS for 2 h at 37°C. Negative control wells with HA protein and PBS alone also were included (“no antibody control”). Plates were washed seven times with PBS, and  $5 \times 10^5$  purified NK cells were added to each well. Healthy donor PBMCs were isolated with Ficoll-Paque PLUS (GE Healthcare Life Sciences, 171440). NK cells were purified from freshly isolated PBMCs using the EasySep human NK cell enrichment kit (STEMCELL Technologies, 19055) and resuspended in RF10 medium (RPMI 1640 supplemented with 10% FCS, penicillin, streptomycin, and l-glutamine. Mouse anti-human CD107a allophycocyanin-H7 antibody (clone H4A3; BD Biosciences, 561343), 5  $\mu$ g/mL brefeldin A (Sigma-Aldrich, B6542), and 5  $\mu$ g/mL monensin (BD GolgiStop; BD Biosciences, 554724) were added to the cells and incubated for 5 h at 37 °C in 5% CO<sub>2</sub>. Purified NK cells then were incubated with 1 mM EDTA to minimize cell adherence to the plates, anti-human CD3 PerCP (clone SP34-2; BD Biosciences, 552851) and anti-human CD56 allophycocyanin (clone B159; BD Biosciences, 555518) for 30 min at room temperature in the dark. Cells were fixed with 1% formaldehyde for 10 min and permeabilized with FACS permeabilizing solution 2 (BD Biosciences, 347692) for 10 min. PBMCs then were incubated at room temperature for 1 h with anti-human IFN $\gamma$  AF700 (clone B27; BD Biosciences, 561024) in the dark. Finally, cells were again fixed with 1%

formaldehyde and data for 20,000 – 50,000 events was acquired using an LSRFortessa flow cytometer (BD Biosciences). The experiment was performed twice independently.

**Crystallization and x-ray structure determination.** Apo H3v-47 Fab and apo Minn2010/H3v HA crystals were grown using our automated Rigaku CrystalMation robotic system at The Scripps Research Institute by sitting drop vapor diffusion. Crystals of H3v-47 Fab (10 mg/mL) grew at 20 °C using 20% (w/v) polyethylene glycol (PEG) 6000, 0.1 M sodium citrate (pH 5.0) as precipitant. Crystals were cryo-protected in mother liquor supplemented with 15% (w/v) glycerol, flash cooled, and stored in liquid nitrogen until data collection. Crystals of Minn2010/H3v HA (10 mg/ml) grew at 20 °C with 0.2 M calcium acetate, 18% (w/v) polyethylene glycol PEG 8000, 0.1 M sodium cacodylate (pH 6.5) as precipitant. Complexes of the HA with human receptor analog LSTc were obtained by soaking HA crystals in precipitant solution that contained glycan ligands in a final concentration of 5 mM. Crystals were cryo-protected in mother liquor supplemented with 15% (w/v) glycerol, flash cooled, and stored in liquid nitrogen until data collection. X-ray diffraction data for the H3v-47 Fab apo, Minn2010/H3v HA apo, and HA-LSTc complex were collected to 2.57 Å, 3.15 Å and 2.90 Å resolutions at beamline 23ID-D at the Advanced Photon Source (APS), respectively. The diffraction data from H3v-47 Fab and Minn2010/H3v HA were processed using HKL2000 in spacegroups  $P3_1$  and  $I2_13$ , respectively (185). The crystal structure of H3v-47 Fab was determined by molecular replacement with Phaser (186) using the variable and constant domains of an Fab in the PDB (4Q9Q) as a search model; two Fabs were found in the asymmetric unit. The model was iteratively rebuilt using Coot (187) and refined in Phenix (188). Refinement parameters included rigid body refinement (for each Ig domain), simulated annealing, and

restrained refinement including TLS refinement (for each Ig domain). The initial Minn2010/H3v HA apo structure was solved by molecular replacement method using Phaser (186) with an H3 HA structure (PDB code 2YP2) as a search model. The H3v HA apo structure was used as the starting model for structure determination of the H3v HA-LSTc complex structure. Structure refinement was carried out in Phenix (188) and model building with COOT (187).

The H3v-47-Minn2010/H3v HA complex was prepared by adding recombinant H3v-47 Fab to HA in a 1.2:1 molar ratio and the saturated complex was purified by gel filtration. Crystals of the complex (~ 8 mg/mL) were grown by sitting drop vapor diffusion at 20°C with 10% (v/v) 2-methyl-2,4-pentenediol (MPD), 0.1 M MES (pH 5.0) as precipitant. Crystals were cryo-protected in mother liquor supplemented with 10% MPD, flash cooled, and stored in liquid nitrogen until data collection. X-ray diffraction data for the H3v-47-Minn2010/H3v HA complex were collected to 3.57 Å resolution at APS beamline 23ID-D and processed in spacegroup  $P2_13$  using HKL2000 (185). The structure was determined by molecular replacement with Phaser (186) using H3v-47 Fab *apo* and Minn2010/H3v HA-LSTc complex (instead of *apo* form) as the search model. The model was iteratively rebuilt using Coot (187) and refined in Phenix (188). Refinement parameters included rigid body refinement (for the HA and for the variable and constant domains of each Fab), restrained refinement including TLS refinement (for the HA and for the variable and constant domains of Fab), using the high-resolution HA and Fab as reference models. Final refinement statistics are summarized in Table S2.

**Structural analyses.** Hydrogen bonds and van der Waals contacts were calculated using HBPLUS (189) and CONTACTSYM (190), respectively. The surface area buried upon Fab binding was calculated using MS (191). MacPyMOL (DeLano Scientific) was used to render

figures. Kabat numbering was applied to the coordinate files using the AbNum server (192). The final coordinates were validated using the JCSG quality control server (v2.8), which includes MolProbity (193).

**Sequence analysis of the antibody epitopes.** The full-length and non-redundant influenza A HA sequences were downloaded from the Influenza Virus Resource at the National Center for Biotechnology Information (NCBI) database (194). At the time of download (December 31, 2015), the dataset includes 4,859 human H3 HA sequences. The sequences were aligned using MUSCLE(195) with default parameters.

**Accession codes:** Atomic coordinates and structure factors for the crystal structures of H3v-47 Fab, A/Minnesota/11/2010 (H3N2) HA in *apo* form, the HA in complex with LSTc and the HA in complex with H3v-47 Fab have been deposited in the Protein Data Bank with the accession codes 5XRQ, 5XRT, 5XRS and 5W42, respectively.

## CHAPTER IV

### **A BROADLY PROTECTIVE HUMAN ANTIBODY FOR INFLUENZA TYPE A VIRUSES RECOGNIZES A HIDDEN EPITOPE ON THE HA HEAD DOMAIN**

*'You might be asking too much if you're looking for one vaccine for every conceivable influenza. If you have one or two that cover the vast majority of isolates, I wouldn't be ashamed to call that a 'universal vaccine.'*

*Anthony Fauci, NIAID director, Nature news (2009)*

#### **Introduction**

The potential emergence of novel IAVs in the human population as pandemics poses a major public health threat. Although vaccination is the most effective intervention against influenza disease, current seasonal vaccines typically induce protection only against strains that are closely related to the antigens included in the vaccine. Due to the lack of cross-protective vaccines and the rise of drug-resistant IAV strains, there is a need for new therapeutics and vaccines that can provide broad protection against IAV infections. Broadly protective antibodies for human influenza virus are of interest for development as therapeutic molecules and for guiding rational development of improved influenza vaccines.

The majority of neutralizing antibodies elicited by IAV vaccination or natural infection target the HA head domain. However, the high level of sequence and antigenic diversity occurring in the HA head domain of naturally occurring strains along with the incorporation of glycans in this region to evade immune recognition usually results in induction of narrow strain-specific antibody responses to the HA head. Although the majority of heterosubtypic HA monoclonal antibodies (mAbs) target the stem-domain, a few mAbs have been isolated against

the HA head domain that can provide protection against viruses of more than one subtype (196, 197). The broad HA head domain reactive antibodies described to date directly interact with the RBS, which has a high level of sequence conservation across several subtypes compared to the rest of the HA head. Recognition of the conserved residues in the recessed RBS is associated with breadth, but interaction with highly variable residues along the rim of the RBS reduces breadth. RBS antibodies must navigate a tricky balance between achieving a minimal footprint of interaction only with residues that are conserved, while preserving enough area of interaction to achieve high-affinity binding. It likely is not possible to find a single RBS-specific antibody that binds to all IAVs with high affinity. Furthermore, interactions between HA and the sialic acid receptors on the effector cells have been shown to be critical for Fc-mediated effector functions (198). Consequently, antibodies that target the RBS and block these sialic acid interactions in turn may have reduced capacity to mediate ADCC activity.

In this chapter, I present the identification of a major new site of vulnerability on the HA head domain, discovered by isolation and study of a broadly reactive naturally occurring human mAb, designated FluA-20, which was isolated from a donor with a vaccination history including not only seasonal inactivated vaccines containing H1N1 and H3N2 subtypes but also with experimental H5N1 and H7N9 antigens. MAb FluA-20 recognizes HA proteins from nearly all IAV subtypes. Remarkably, structural studies revealed that FluA-20 achieves broad cross reactivity by recognizing a novel conserved epitope on the HA head domain near the protomer interface, which is partially buried in the HA trimer. The ability of FluA-20 to recognize this hidden epitope on a HA trimer also provides insight into previously unrecognized HA dynamic features of the three HA head domains in the HA trimer that allow access to this epitope. FluA-20 provided *in vivo* protection in mice challenged with IAVs of the H1N1, H3N2, H5N1 or

H7N9 subtypes. Interestingly, the observed prophylactic efficacy of FluA-20 appeared to be facilitated principally by its ability to mediate ADCC responses rather than by mediating classical neutralizing activity. Recognition of this previously unrecognized epitope in the trimer interface of the HA head domain provides a new antigenic site for incorporation into design of broadly protective or universal IAV vaccine candidates.

I acknowledge Dr. Ian Wilson's group for resolving the structure of FluA-20 Fab in complex to HA and detailed analysis of FluA-20 epitope, Dr. Adolfo Garcia-Sastre's group for testing the prophylactic efficacy of FluA-20 in mice, Dr. Stephen Kent's group for ADCC studies, Dr. Sheng Li for providing hydrogen deuterium exchange mass spectrometry (HDX-MS) data and Dr. Pavlo Gilchuk for training me on flow cytometry.

### **Donor vaccination history**

We identified a donor who had received annual licensed inactivated seasonal vaccines for over 2 decades. The donor also had participated previously in clinical trials of experimental H5N1 and H7N9 subunit vaccines in the NIH Vaccine Treatment and Evaluation Unit (Figure 4-1A). The first H5 vaccine was a monovalent inactivated subvirion vaccine incorporating the HA from A/Vietnam/1203/2004 (VN/1203) H5N1 clade 1 influenza virus (batch 04-067) consisting of 90 µg of hemagglutinin in each dose (DMID study 04-062). After 22 months, the individual was boosted with a monovalent inactivated surface antigen influenza A (H5N1) vaccine made from the modified HA and NA of A/Anhui/01/2005(H5N1)-PR8-IBCDC-RG6 virus (DMID study 07-0022). The volunteer subsequently received an H7 subunit vaccine [in DMID 13-0033; a phase II human clinical trial with monovalent inactivated influenza A/Shanghai/02/2013 H7N9]). For the current study, the donor was vaccinated with a 2014-15 seasonal influenza



vaccine on day 0. Peripheral blood samples were obtained using heparin anticoagulation on days 0, 3, 4, 5, 6, 7, 10, 11, 14 and 31 following immunization.

### **Isolation and characterization of human mAb FluA-20**

To generate human hybridoma cell lines secreting mAbs to influenza, I screened supernatants from EBV-transformed B cell lines derived from the vaccinee for binding to several recombinant forms of influenza HA. Cryopreserved PBMC samples from day 31 after seasonal vaccination were immortalized by EBV transformation and the supernatants were screened for the presence of antibodies that displayed heterosubtypic binding breadth to recombinant HA proteins derived from H1 (A/California/04/2009, A/Texas/36/1991), H3 (A/Hong Kong/1/1968, A/Victoria/3/1975), H7 (A/Shanghai/2/2013, A/Netherlands/219/2003) and H9 (A/Hong Kong/1073/99) subtypes by capture ELISA. The hybridoma cell line secreting the FluA-20 mAb was isolated from a B cell line that exhibited heterosubtypic breadth during the initial screen. Two additional mAbs were used in these studies for comparative purposes, designated FluA-45 and FluA-55. These mAbs are broadly reactive heterosubtypic antibodies that were isolated from individuals previously vaccinated with an experimental H7 vaccine (in the NIH Vaccine Treatment and Evaluation Unit [DMID 13-0033; a phase II human clinical trial with monovalent inactivated influenza A/Shanghai/02/2013 H7N9]).

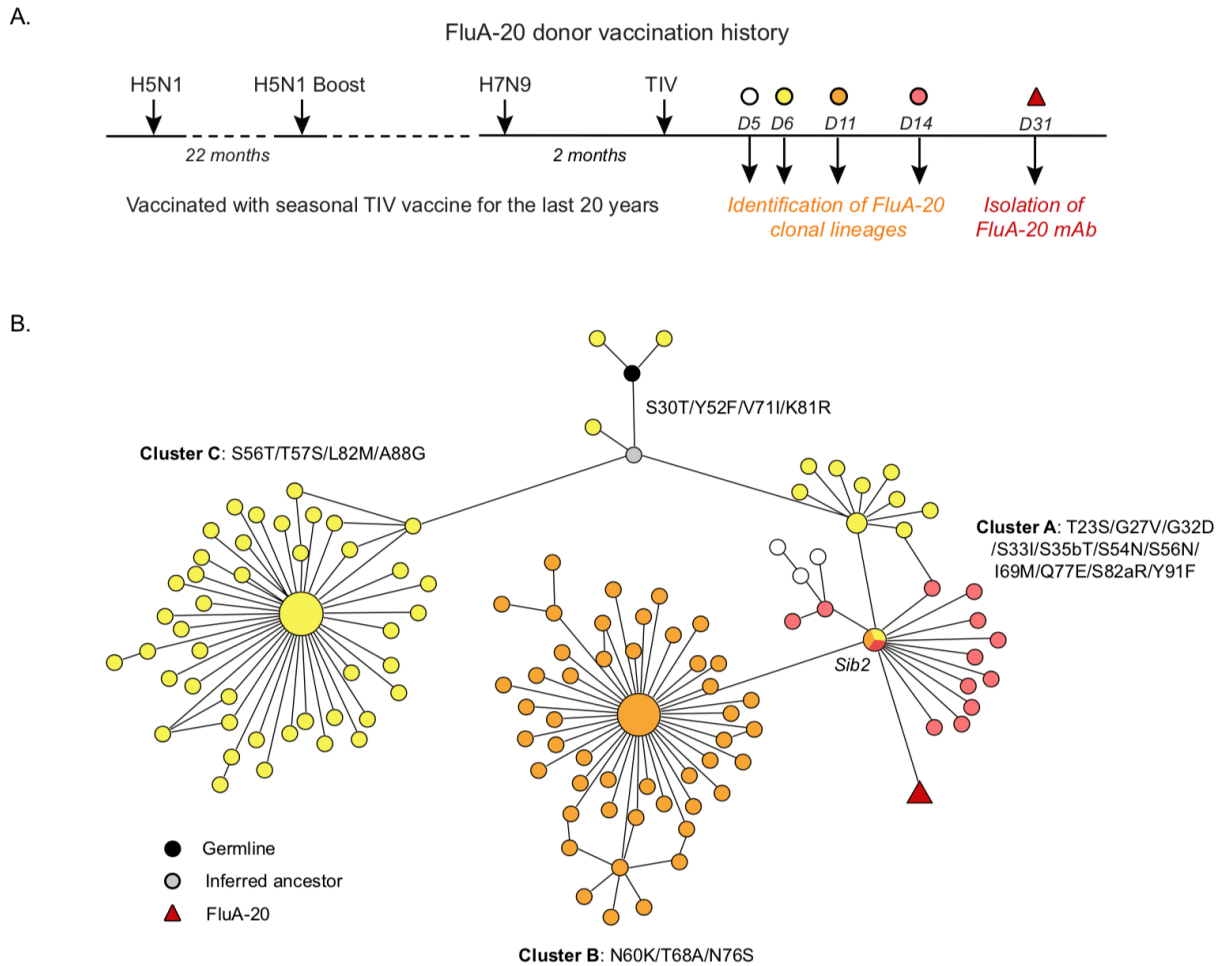
To investigate the breadth of the cloned mAb FluA-20, I tested purified IgG for binding activity to HA from different IAV subtypes by ELISA. FluA-20 exhibited extraordinary binding breadth and affinity to recombinant HA belonging to group 1 (H1, H2, H5, H6, H8, H9 and H12) and group 2 (H3, H4, H7, H10, H14 and H15) viruses, with  $EC_{50}$  values for binding ranging from 4 ng/mL to 1.7  $\mu$ g/mL (Figure 4-2).

FluA-20 belongs to the IgG1 subclass and is encoded by the V<sub>H</sub>4-61/D2-15/J<sub>H</sub>4 and V<sub>K</sub>1-39/J<sub>K</sub>1 antibody variable gene segments, a genetic configuration not previously reported for broadly reactive human influenza antibodies. The analysis of the FluA-20 cDNA sequence revealed that FluA-20 shares 93% identity with both the V<sub>H</sub>4-61\*01 and V<sub>K</sub>1-39\*01 germline genes. Compared to the inferred unmutated common ancestor (UCA) sequence, FluA-20 harbored 16 somatic mutations in the heavy chain variable gene amino acid sequence and 12 in the light chain variable gene sequence. I expressed a recombinant form of the FluA-20-UCA IgG to determine the binding breadth of the germline gene-encoded sequence. A cDNA of the wild-type FluA-20 variable gene also was synthesized and expressed in recombinant form to serve as a matched control for comparison with the UCA mAb (so that both the parental and UCA antibodies were produced in the same cell type, 293F cells). The recombinant FluA-20 (rFluA-20) IgG protein showed generally lower binding affinities to varying HAs in comparison to the hybridoma-produced FluA-20 IgG protein. UCA retained similar binding breadth as rFluA-20 for binding to HA of many subtypes, but also displayed additional decrease in affinity to recent H3 seasonal strains tested. Both rFluA-20 and the UCA antibody exhibited reduced or no binding to H5 strains compared to hybridoma FluA-20 (Figure 4-2). The similarity in binding breadth between the UCA and rFluA-20 antibodies indicates that there is no significant contribution of somatic mutations in FluA-20 to its breadth.

### **Identification of clonal lineages**

We performed a search of our antibody sequence database for sequences that may have been related clonally to FluA-20 (*i.e.*, “siblings”), defining two sequences as clonally related if they share the same V and J gene use and have 3 or fewer amino acid mutations in their HCDR3

region. The analysis of these clonally related sequences was done in collaboration with Jessica Finn of Crowe lab. While FluA-20 was isolated from blood sample collected 31 days post-vaccination, we identified siblings to FluA-20 in four time points: days 5, 6, 11 and 14 post-vaccination with TIV. We inferred that the majority of these siblings arose from one common ancestor, and cluster into three major families (Cluster A, B and C) that differ by mutations across the V gene region (Figure 4-1B). Network analysis of these sequences reveals that FluA-20 arose from blasting cells present at day 6 that were also observed at day 11 and day 14 (Figure 4-1B). I expressed and tested the recombinant form of several sibling antibodies related to FluA-20 from cluster A (Sib2) and cluster B (Sib 3, Sib 28, Sib 7, Sib 33, Sib 48 and Sib 45). Three sibling antibodies, Sib 2, Sib 3, and Sib 45, exhibited very similar activity and breadth as FluA-20, suggesting that multiple variations of this FluA-20 clonotype were sustained in the repertoire that did not acquire functional differences. Also, I found that two sibling antibodies, Sib 28 and Sib 48 lost binding to some H3 and H5 HAs, and Sib 7 and Sib 33 completely lost activity to any HA tested, likely due to the introduction of additional somatic mutations.



**Figure 4-1. Network analysis of sequences clonally related to FluA-20.** (A) Timeline showing the vaccination history of FluA-20 donor and the time points from which FluA-20 (triangle) and its clonally related siblings (circles) were identified. (B) Nodes represent unique sequences observed in our database, with the size of the node correlating to the count of replicate sequences observed. The color of each node denotes the time point at which it was found; white for day (5), yellow for day (6), orange for day (11) and pink for day (14). The black node represents the  $V_{H4-61/J_H4}$  germline sequence and the gray node represents an inferred common ancestor. The maroon, triangle-shaped node represents FluA-20. Edges drawn between nodes show that those sequences are more closely related to each other than to any other sequence. Edge distances are arbitrary and used only to visually clarify the graph.

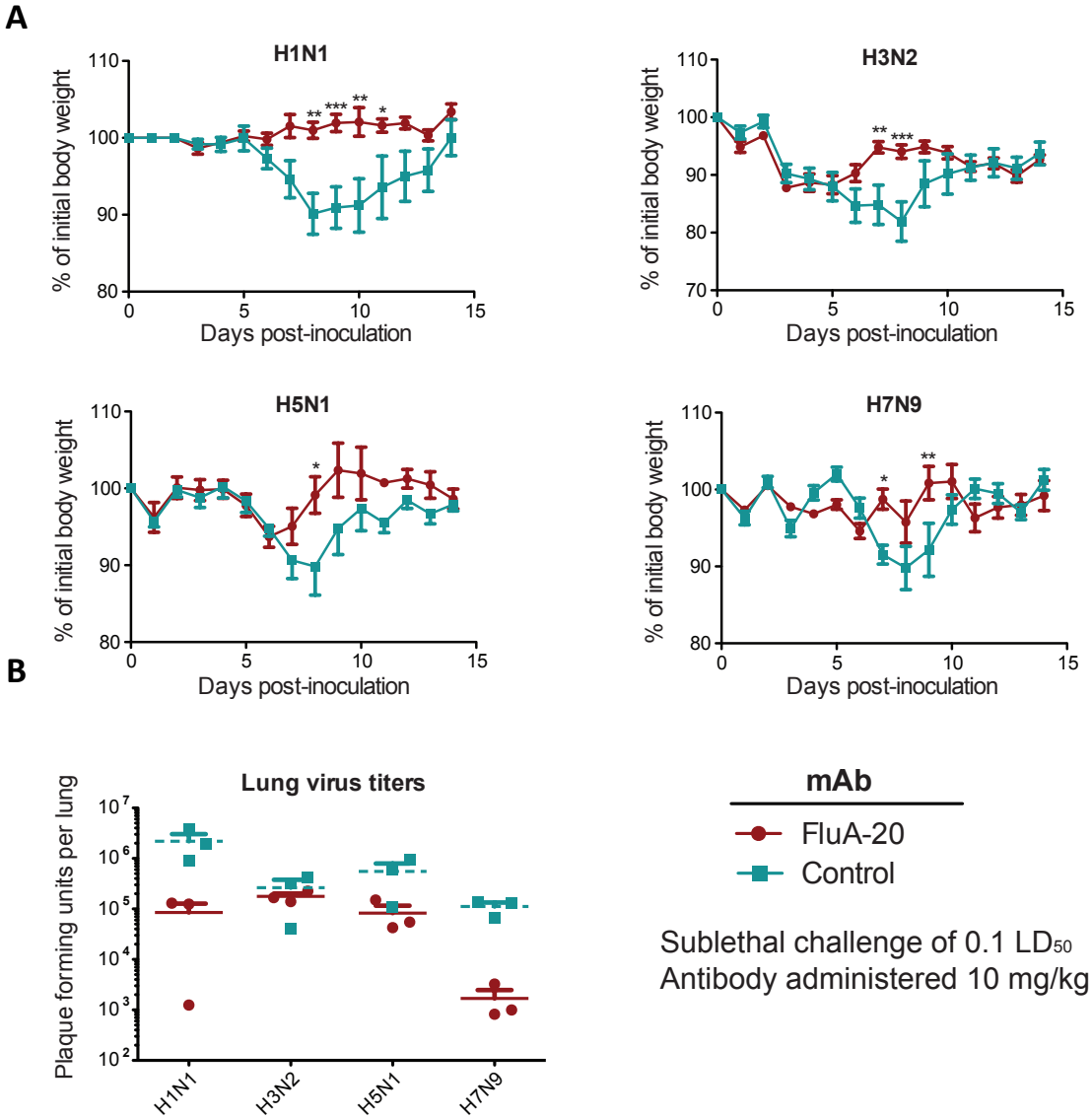
		Group 1										Group 2													
Subtype		H1				H2	H5		H6	H8	H9	H12	H13	H16	H3		H4	H7		H10	H14	H15			
HA from indicated strain		A/California/2009	A/Texas/36/1991	A/Fort Monmouth/1/1947	A/Solomon Islands/03/2006	A/Singapore/1/1957	A/Vietnam/1203/2004	A/Indonesia/05/2005	A/Taiwan/2/2013	A/Turkey/Ontario/6118/1967	A/Turkey/Wisconsin/1/1966	A/Hong Kong/1073/99	A/Duck/Alberta/60/1976	A/Gull/Maryland/704/1977	A/black-headed gull/Sweden/4/1999	A/Hong Kong/1/1968	A/Texas/50/2012	A/Switzerland/9715293/2013	A/Duck/Czechoslovakia/1956	A/New York/107/2003	A/Shanghai/2/3013	A/Netherlands/219/2003	A/chicken/Germany/N/1949	A/mallard duck/Astrakhan/263/1982	A/shearwater/WesternAustralia/2576/1979
EC <sub>50</sub> (ng/mL)	FluA-20	8	4	12	5	7	283	85	147	1740	63	9	51	70	>	6	4	19	13	808	66	29	31	13	15
	rFluA-20	31	46	20	47	178	>	6046	229	959	193	407	50	>	>	35	86	548	18	>	117	54	129	71	136
	UCA	140	48	39	36	70	>	>	831	4327	359	342	67	>	>	54	1304	2365	25	>	150	83	361	132	73

**Figure 4-2. Binding of FluA-20 to group 1 and group 2 HAs.** Binding EC<sub>50</sub> (ng/mL) for FluA-20, rFluA-20 and FluA-20-UCA to HAs derived from 24 different strains belonging to 15 HA subtypes. > indicates EC<sub>50</sub> values greater than 5 µg/ml.

### FluA-20 exhibits prophylactic efficacy *in vivo* against viruses of influenza type A

#### H1N1, H3N2, H5N1 or H7N9 subtypes

I collaborated with Dr. Adolfo Garcia-Sastre's group to examine if mAb FluA-20 could mediate protective activity *in vivo*. We chose H1N1 A/Netherlands/602/2009, H3N2 A/X-31, H5N1 A/barn swallow/Hong Kong/D10-1161/2010 and H7N9 A/Shanghai/1/2013 virus strains, representative of group 1 and group 2 IAVs, for prophylactic studies. Mice (n=8 per group) were administered 10 mg/kg of FluA-20 or a similarly prepared control antibody by the intraperitoneal route, and then challenged 24 hours later intranasally with a sub-lethal dose of virus. Mice treated with FluA-20 (n=5) showed complete protection from weight loss after H1N1 challenge (Figure 4-3A). FluA-20 treated mice challenged with H3N2, H5N1 or H7N9 strains showed significantly faster recovery from weight loss compared to control animals (Figure 4-3A). Additionally, FluA-20 treatment significantly reduced pulmonary lung titers (day 6) following H1N1 and H7N9 challenge (Figure 4-3B).

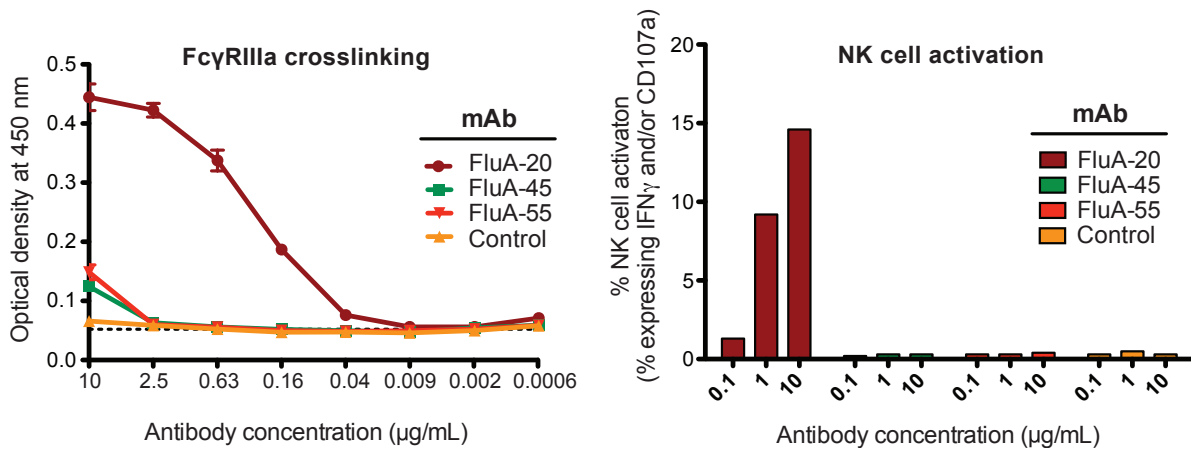


**Figure 4-3. FluA-20 antibodies prophylactically protect mice from sub-lethal challenge from pathogenic IAV for humans.** Groups of mice (n=8) were treated with 10 mg/mL of either FluA-20 or a similarly prepared control antibody to an unrelated target (MRSA) and challenged 24 h later with either H1N1 A/Netherlands/602/2009 or H3N2 A/X-31 (6:2 PR8 backbone) or H5N1 A/barn swallow/Hong Kong/D10-1161/2010 (7:1 PR8 backbone) or H7N9 A/Shanghai/1/2013 (6:2 PR8 backbone). **(A)** The weight loss of mice (n=5) was measured daily for 14 days after inoculation (Day 0). The significance in weight loss between FluA-20 and the control group was calculated for each day using 2-way ANOVA and displayed on the graph as \* (P<0.05), \*\* (P<0.01) and \*\*\*(P<0.001). **(B)** Lung samples were collected from mice (n=3) per antibody group 6 days post-inoculation. The graph shows pulmonary virus titers in FluA-20 and control treated mice.

### **FluA-20 lacks neutralizing function but possesses ADCC activity**

To determine if FluA-20 has neutralizing activity, I performed micro-neutralization assays against H1N1 A/California/04/2009, H3N2 A/Texas/50/2012 or H7N9 A/Shanghai/2/2013 (6:2 PR8 backbone) viruses. FluA-20 did not exhibit any neutralizing activity at the highest concentration tested, 20  $\mu\text{g}/\text{mL}$ . Additionally, neutralizing activity was not detected against pseudoviruses displaying the HA from H1N1, H3N2 or H5N1 subtype viruses. We collaborated with Dr. Stephen Kent's group to examine if FluA-20 could mediate ADCC activity. We performed an ELISA-based screen using recombinant soluble (rs), dimeric, low-affinity ectodomains (rsFc $\gamma$ R) of Fc $\gamma$ RIIIa, as described (179). These rsFc $\gamma$ R low-affinity dimers require simultaneous engagement of both receptors by HA-bound IgGs in order to achieve stable binding on ELISA. Four similarly prepared antibodies, FluA-20, FluA-45, FluA-55 or VRC01 (an HIV-reactive negative control mAb) were added to plates coated with H1 A/California/04/2009 HA to test for their ability to engage both binding sites on rsFc $\gamma$ R simultaneously. The FluA-20 IgG engaged the rsFc $\gamma$ R dimers, suggesting its potential to mediate ADCC activity, while neither the similarly prepared FluA-45 nor FluA-55 broadly reactive heterosubtypic mAbs nor the HIV-specific control mAb VRC-01 engaged these Fc $\gamma$ R molecules (Figure 4-4A). To test whether this Fc $\gamma$ R binding activity corresponded with functional ADCC activity, we examined the ability of these antibodies to activate primary CD3<sup>-</sup> CD56<sup>+</sup> NK cells following incubation with HA from A/California/04/2009. NK cell activation was measured as the percentage of NK cells expressing intracellular IFN- $\gamma$  and/or CD107a, a marker for degranulation. A robust concentration-dependent increase in the percentage of NK cell activation was observed for FluA-20 (1.3, 9.2% or 14.6% NK cell activation at 0.1, 1 or 10  $\mu\text{g}/\text{mL}$  respectively), while FluA-45, FluA-55 and VRC01 did not exhibit any NK cell activation at the

highest concentration tested (10  $\mu\text{g/mL}$ ) (Figure 4-4B). Taken together, these results indicated that the *in vivo* prophylactic efficacy of FluA-20 against both group 1 and group 2 IAVs mediated by the non-neutralizing mAb FluA-20 correlates with the ability to engage Fc $\gamma$ RIIIa and to induce potent ADCC activity.

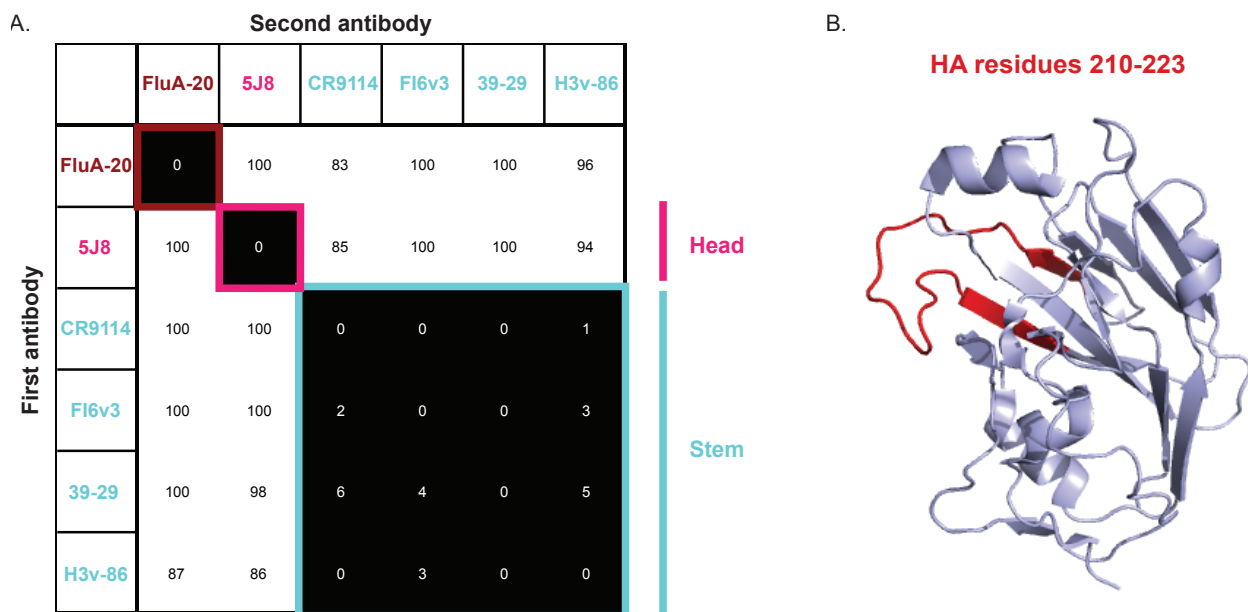


**Figure 4-4. FluA-20 likely protects by ADCC activity (A)** Cross-linking of Fc $\gamma$ RIIIa. Binding curves were obtained by performing ELISA with serial dilutions of each antibody (FluA-20 and control mAbs FluA-45, FluA-55 and VRC01) onto HA-coated plates and assessing the ability of HA-bound mAbs to engage both Fc-binding sites on the soluble Fc $\gamma$ RIIIa dimer. The dotted line indicates the limit of detection. **(B)** FluA-20 or control mAbs were each added independently on 96-well plates coated with purified A/California/07/2009 H1 HA. The percentage of NK cell activation was calculated from the number of NK cells incubated with HA-bound antibody that expressed CD107a and/or IFN $\gamma$ .



## **Epitope binning, DXMS and structural studies reveal FluA-20 epitope**

The majority of broad-spectrum influenza antibodies described to date target conserved epitopes on the HA stem domain to achieve heterosubtypic breadth. Other heterosubtypic antibodies against the HA head target the RBS, which is functionally conserved for receptor binding. To determine if FluA-20 binds to these conserved sites, I used bio-layer interferometry to compete FluA-20 for binding against other broad stem-binding antibodies (CR9114, FI6v3, 39.29 and H3v-86) or the H1N1 RBS-binding human mAb 5J8. Surprisingly, FluA-20 did not compete for binding to HA with the RBS- or stem-specific mAbs, indicating it recognizes a novel epitope on HA that is conserved across group 1 and group 2 IAVs (Figure 4-5A). Next, we sought to define where the conserved epitope for FluA-20 is located. Unexpectedly, the antibody bound to a truncated form of the HA molecule that includes the head domain but not the stem domain. In collaboration with Dr. Sheng Li's group, we conducted HDX-MS experiments with a monomeric head domain construct to identify peptides on the surface of HA that are occluded following binding of FluA-20. Recombinant HA head domain protein from H5 A/Vietnam/03/2204 was labeled with deuterated water in the presence or absence of FluA-20 antibody. The head domain protein was digested with pepsin, and deuterium labeling of resulting peptides was measured by mass spectrometry. A decrease in deuterium binding suggested that residues in a peptide were in contact with the mAb. The peptides that exhibited decreased deuterium labeling when incubated with mAb are indicated in bold (Figure 4-5B). Remarkably, the mAb blocked labeling of peptides comprising of residues 210-223, which are derived from a region of the HA head domain that is located near the interface of two HA head domain protomer.



**Figure 4-5. Epitope mapping by competition binning and HDX-MS studies.** (A) Competition-binding assays were performed using bio-layer interferometry. The His-tagged A/California/07/2009 H1 HA was loaded onto Ni-NTA tips, and binding of two successively applied antibodies (IgG) was tested. MAb FluA-20 was competed against mAb 5J8, a receptor binding site mAb, or each of four stem-binding antibodies: CR9114, Fl6v3, 39.29 or H3v-86. FluA-20 does not compete with either the RBS or the stem-antibodies indicated. (B) Deuterium exchange of the H5 head domain from A/Vietnam/1203/2004 (H5N1) with or without FluA-20 binding. Regions of HA with slower deuterium exchange after binding FluA-20 are mapped in red onto the surface of H5 A/Vietnam/1203/2004 head domain (purple).

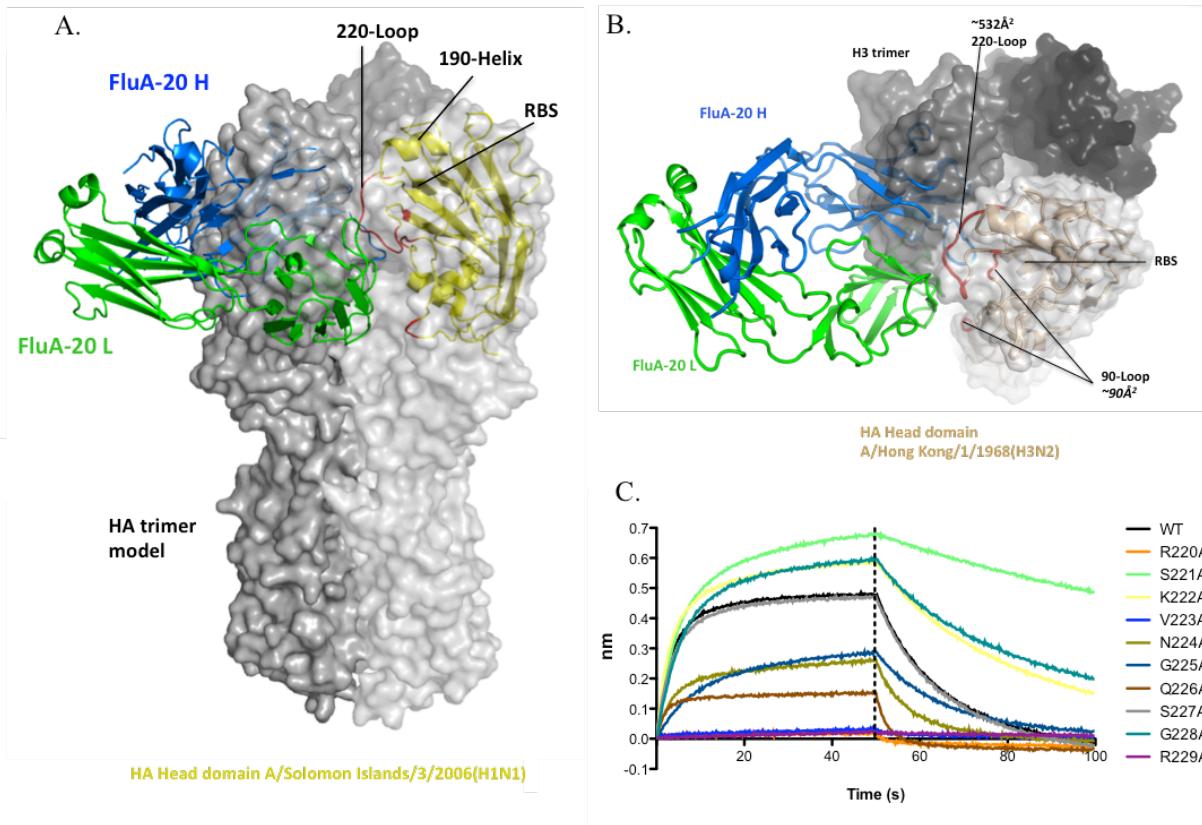
It was surprising that the HDX-MS data suggested an epitope at the interface of two HA molecules in the trimer, since this surface of the protein is not accessible in the crystal structures of trimeric HA molecules that have been determined in the past. To understand details of the specific interactions of FluA-20 with HA head domain, we collaborated with Dr. Ian Wilson's group to solve the structure of the complex of FluA-20 Fab with a recombinant HA monomeric head domain protein. Crystal structures of apo FluA-20 Fab and its complex with the HA head domain from A/Solomon Islands/3/2006 (H1N1) or HA head domain of A/Hong Kong/1/1968 (H3N2), were determined at 1.73 Å, 2.85 Å and 2.10 Å resolutions, respectively (Figure 4-6A and 4-6B). The complex structures revealed that FluA-20 interacts primarily with the 220-loop and has some contacts to the 90-loop on HA head (Figure 4-6A and 4-6B). When the HA head domain in the Fab complex was superimposed with an existing HA trimer model, it was apparent that FluA-20 recognizes an epitope hidden in the HA trimer interface that would not be accessible for antibody binding in the canonical trimer conformation. The variable domain of FluA-20 would overlap with the head domain from an adjacent protomer in the HA trimer (Figure 4-6A and 4-6B). These results suggest that FluA-20 recognizes HA in a form different from the canonical trimer.

The crystal structure suggested specific contacts between the Fab CDRs and HA residues. Next, we tested the importance of individual HA residues to the interaction. I mutated residues on the H5 Vietnam HA head domain to alanine and tested binding to mAb FluA-20. Mutagenesis revealed that single point-mutants made in the residues R220, V223, Q226, and R229 on the HA head disrupted binding to mAb FluA-20 (Figure 4-6C). Our collaborators performed similar mutagenesis studies on H1 and H3 HA. Single mutants of R220A, V223G, or R229A in both H1 and H3 HA backbones completely abolished FluA-20 binding, illustrating that the antibody

engages similar binding mechanism for H1 and H3 as that observed for H5. However, the loss of FluA-20 binding to Q226A mutant on HA was unique to H5 (Figure 4-6C).

### **Mutation experiments to identify critical residues in the FluA-20 IgG paratope**

I mutated residues in the apparent paratope of the antibody to determine which amino acids were critical to binding. I altered residues Y34, T96, E97, D98, Y100a or C101 on the heavy chain (HC) and Y49, N53 or Q55 on the light chain (LC) to alanines and determined binding of each mutant to HA from different subtypes. We compared the binding  $EC_{50}$  to HAs for each FluA-20 mutant IgG with rFluA-20 IgG. Two mutants HC D98A and LC Y49A showed complete loss of binding to all examined HA molecules, validating the importance of interaction between HC D98 and R229 on HA and the hydrophobic interaction between LC Y49 and P221 on HA (Table 4-1). Surprisingly, LC Q55A mutant showed >10-fold or complete loss of binding  $EC_{50}$  to all the HA molecules except H1 A/Texas/36/1991, H3 A/Hong Kong/1/1968 and H7 A/Netherlands/219/2003, while a HC Y100aA mutant also showed >10-fold loss of binding  $EC_{50}$  to all HAs except H3 A/Hong Kong/1/1968 (Table 4-1). In addition to the above-mentioned mutants that disrupted binding to several HAs, mutants HC C101A and LC N53A also disrupted binding to the H5 A/Indonesia/5/2005 HA. Collectively, these findings reveal that, while FluA-20 may require as many as six interactions to engage HA from H5 A/Indonesia/5/2005, it only needs two major interactions to bind other HAs like H3 A/Hong Kong/1/1968. Additionally, most of the FluA-20 residues that directly interact with HA are conserved from the UCA antibody, especially the key HA-contacting D98 (HC), Y100a (HC), Y49 (LC), and Q55 (LC). This finding is consistent with the observation that FluA-20 UCA retains substantial binding breadth compared to affinity matured FluA-20.



**Figure 4-6. FluA-20 targets the 220-loop and the 90-loop at the trimer interface of the H1 head domain.** (A) Structural overview of FluA-20 Fab in complex with the head domain of H1 HA (A/Solomon Islands/3/2006). FluA-20 Fab is shown as a backbone trace in blue heavy chain (H) and green light chain (L). The backbone of the HA head domain is shown as a yellow trace and residues contacted by FluA-20 are colored in red. The H1 head domain is superimposed with one protomer colored in light grey surface from an HA trimer model (PDB 4M4Y). The adjacent HA protomers are shown with dark grey solid surface. The variable domain of FluA-20 would clash with a large volume of the head domain from an adjacent protomer in the HA trimer model. (B) The structure of FluA-20 in complex with the H3 head domain (A/Hong Kong/1/1968) is presented similarly as (A), with the H3 head domain is colored in wheat. The H3 residues interacting with FluA-20 are colored in red and the antibody footprint size on HA is analyzed. The H3 head domain is superimposed with one protomer in H3 trimer model (PDB 4FNK) (C) Mutations of the 220-loop residues on H5 A/Vietnam/1203/2004 head domain substantially influence binding of FluA-20 IgG. The R220A, V223A, and R229A mutants of H5 completely eliminate FluA-20 binding, whereas N224A, G225A, and Q226A mutants decrease FluA-20 binding. Figure credit for panel (A) and (B): Shanshan Lang (Wilson lab)

Subtype	Strain	Binding EC <sub>50</sub> (µg/mL) for mutant for indicated chain												
		Wild type	Heavy chain						Light chain					
		FluA-20	Y34A	T96A	E97A	D98A	Y100aA	C101A	Y49A	N53A	Q55A			
H1	A/Solomon Islands/03/2006	0.07	0.04	0.03	0.07	<b>NB</b>	>	0.20	<b>NB</b>	0.05	>			
	A/Texas/36/1991	0.05	0.05	0.04	0.05	<b>NB</b>	>	0.15	<b>NB</b>	0.04	0.23			
H2	A/Singapore/1/1957	0.15	0.11	0.07	0.13	<b>NB</b>	>	0.44	<b>NB</b>	0.16	<b>NB</b>			
	A/Hong Kong/1/1968	0.05	0.07	0.10	0.07	<b>NB</b>	0.07	0.13	<b>NB</b>	0.06	0.08			
H3	A/Texas/50/2012	0.11	0.16	0.07	0.18	<b>NB</b>	>	0.39	<b>NB</b>	0.09	<b>NB</b>			
	A/Switzerland/9715293/2013	0.52	0.80	0.36	0.93	<b>NB</b>	>	2.43	<b>NB</b>	0.39	<b>NB</b>			
H5	A/Indonesia/5/2005	0.69	2.12	0.11	4.96	<b>NB</b>	>	>	<b>NB</b>	>	<b>NB</b>			
	A/Netherlands/219/2003	0.06	0.07	0.04	0.08	>	>	0.17	>	0.05	0.17			
H7	A/Shanghai/2/2013	0.94	0.44	0.37	1.00	<b>NB</b>	>	3.44	<b>NB</b>	0.87	<b>NB</b>			
	A/HongKong/1073/99	0.32	0.21	0.10	0.36	<b>NB</b>	>	0.77	<b>NB</b>	0.17	<b>NB</b>			
H12	A/duck/Alberta/60/1976	0.04	0.05	0.04	0.06	<b>NB</b>	>	0.09	<b>NB</b>	0.03	>			
	A/mallard duck/Astrakhan/263/1982	0.70	0.54	0.23	0.64	<b>NB</b>	>	1.08	<b>NB</b>	>	<b>NB</b>			
H15	A/shearwater/Western Australia/2576/1979	0.08	0.10	0.07	0.12	<b>NB</b>	>	0.11	<b>NB</b>	0.06	>			

> indicates EC<sub>50</sub> values 10 fold higher than Wild type FluA-20  
NB indicates no binding was observed at antibody concentrations below 10 µg/mL

### **FluA-20 binding to HA is substantially reduced after HA cleavage**

During viral replication, HA is synthesized as a single polypeptide precursor protein (HA0), which assembles into a trimer in the endoplasmic reticulum (ER), before its transportation to the cell surface. HA0 gets cleaved post-translationally into the mature form of HA that consists of 2 subunits, HA1 and HA2. Upon cleavage, the N-terminal of the newly generated HA2 subunit, also known as the fusion loop, is relocated to the trimer interior forming a metastable conformation that is primed for fusion. Except for this minor rearrangement in the stem domain, the trimeric HA0 molecule and cleaved HA trimer are structurally identical.

Despite the FluA-20 epitope being occluded in the trimer interface, FluA-20 showed significant binding to trimeric recombinant soluble HA molecules in screening assays,  $EC_{50}$  analysis and competition binding studies. To facilitate this binding event, HA protomers in the trimer conformation must undergo significant dynamic motions. Notably, all of these studies were performed with recombinant uncleaved HA (HA0) protein. Interestingly, we observed that trypsin cleavage of HA substantially decreased binding of FluA-20 to soluble HA, while antibodies binding to RBS showed no difference in binding to cleaved and uncleaved forms of HA. We next sought to determine if FluA-20 binds preferentially to uncleaved HA compared to cleaved HA expressed on the cell surface. I performed flow cytometric analysis to measure binding of two mAbs, CR9114 (broad stem antibody) or FluA-20, to H3 A/Hong Kong/1/1968 HA expressed on HEK293F cells that were either untreated or treated with trypsin. Consistent with our observations with recombinant HA protein, FluA-20 displayed significantly better binding to HA on untreated cells compared to trypsin-treated cells (2.6-fold) (Figure 4-7). Surprisingly, mAb CR9114 that was used as a control displayed better binding to HA on trypsin-treated cells than untreated cells (Figure 4-7). This reduction in binding observed for FluA-20 to

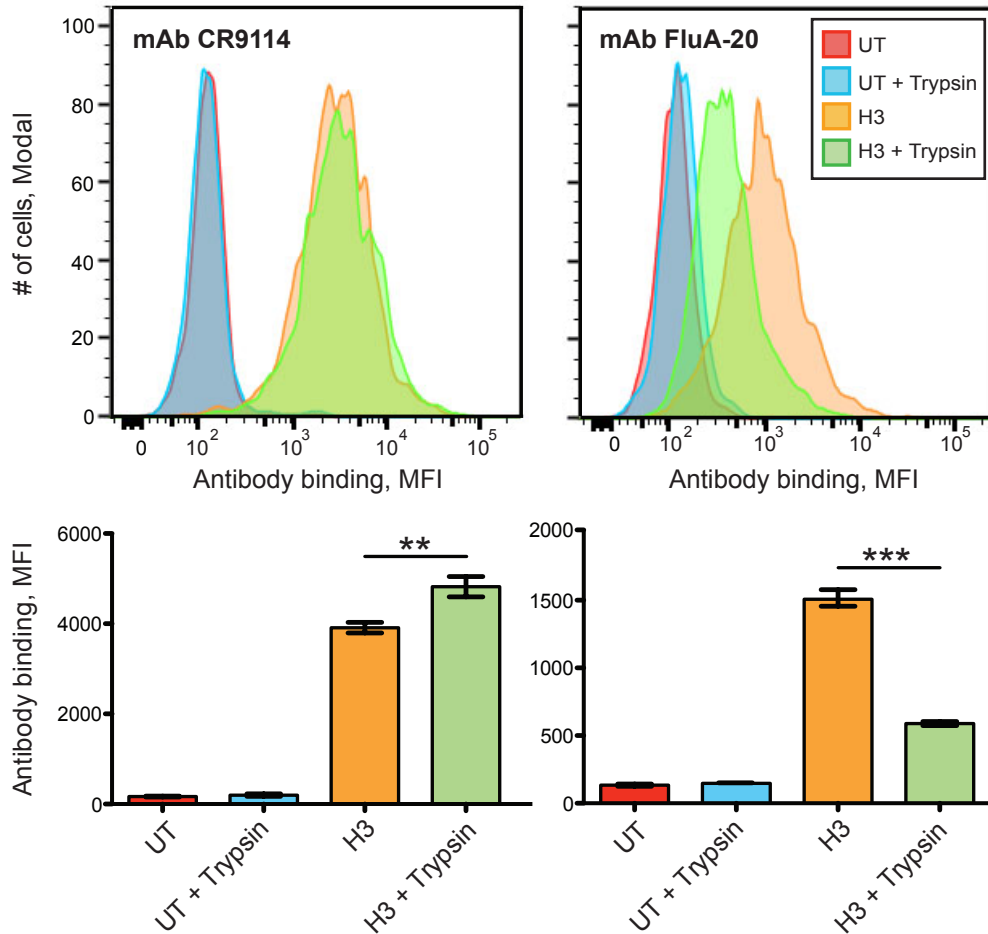
the cleaved form of HA suggests a potential decrease of dynamics of HA monomers in the trimer conformation following trypsin treatment. Additionally, mAb CR9114 exhibited significantly higher binding (2.6 fold) to H3 HA on the cell surface compared to mAb FluA-20, even though FluA-20 IgG has a better binding affinity ( $K_d < 1$  nM) to recombinant H3 A/Hong Kong/1/1968 HA trimer compared to CR9114 ( $K_d = 2.2$  nM). This suggests that the FluA-20 epitope in the trimer interface may be less frequently or less proportionally exposed than the CR9114 epitope.

To investigate the dynamic changes occurring in the uncleaved and cleaved forms of HA trimer, we performed HDX-MS experiments, in collaboration with Dr. Sheng Li's group, with either HA0 or trypsin-treated HA trimers that were deuterium labeled for different lengths of time between 10 to 100,000 seconds. Interestingly, we observed an overall reduction of deuterium exchange in the cleaved HA molecules compared to HA0 proteins, except for few residues near the vestigial esterase subdomain of HA head. These results indicate that the HA0 trimer is indeed more dynamic in comparison to cleaved trimer thus allowing for better epitope accessibility for FluA-20 binding.

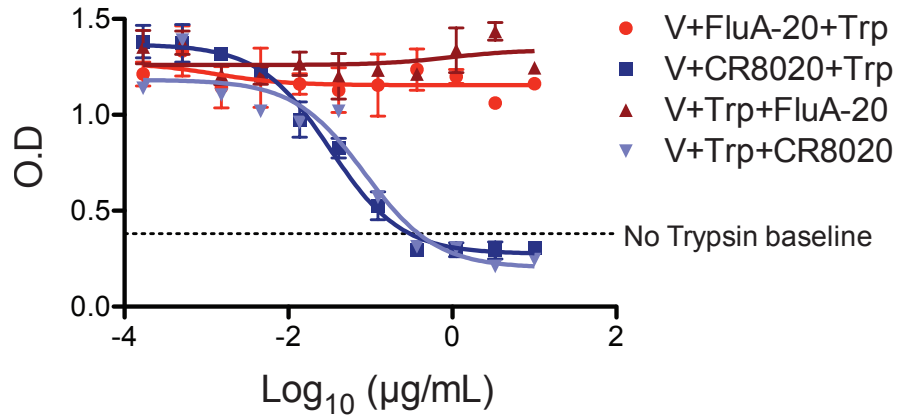
Since the HA cleavage status was shown to be a major determinant for FluA-20 binding, I tested the effect of HA cleavage on susceptibility to neutralization by FluA-20. I prepared a stock of HA0 virus (H3 A/Hong Kong/1/1968) that was generated in the absence of trypsin. I tested for neutralization of HA0 virus by mAb FluA-20 and control mAb CR8020 that was previously reported to neutralize both HA0 and trypsin-treated virus. Even though FluA-20 bound uncleaved HA to a higher degree, it still did not neutralize virus with uncleaved HA (Figure 4-8). In summary, these data suggest that HA cleavage into its functional form reduces HA trimer dynamics, which may inhibit exposure of the FluA-20 epitope in the matured, functional form of HA on virions. This model would explain why the antibody could facilitate



ADCC through recognition of uncleaved HA on infected cells, but not neutralize budding infectious virion particles that have cleaved HA on the surface.



**Figure 4-7. Flow cytometric analysis of antibody binding to cell-surface expressed HA.** Untransfected (UT) or H3 A/Hong Kong/1/1968 HA cDNA-transfected HEK293F cells were either untreated or treated with TPCK trypsin for 15 min at 37°C. The cells were incubated with 10 µg/mL of mAb CR9114 or mAb FluA-20, followed by incubation with secondary goat anti-human IgG PE-conjugated antibodies. Antibody binding to cleaved or uncleaved HA on the cell surface was determined by flow cytometric analysis. Top panel, representative overlay histograms; bottom panel, mean ± SD of technical replicates. Statistical significance was calculated using the unpaired two-tailed t-test with GraphPad software.



**Figure 4-8. FluA-20 does not neutralize HA0 virus.** HA0 A/Hong Kong/1/1968 (H3N2) virus was incubated with serial dilutions of mAbs (FluA-20 or CR8020) either before or after treatment with 1 µg/mL of trypsin (Trp) at 37 degrees for 45 minutes. The samples were trypsin-inactivated with 10% FBS before adding to MDCK monolayers. The dotted line indicates the baseline infection with HA0 virus (untreated).

## Discussion

There is a high medical need for broad immunity to diverse IAV infections. Infection of humans with highly pathogenic avian or swine influenza strains has been detected with increasing frequency, and current seasonal IAV vaccines often exhibit poor immunogenicity against antigenically drifted H1 or H3 strains. Isolation of naturally occurring broad-spectrum human mAbs to IAV addresses this need by identifying candidate therapeutic molecules and by identifying critical epitopes for incorporation into new rationally designed structure-based broadly protective (or “universal”) influenza vaccine candidates. Identification of broadly neutralizing antibodies to the conserved stem domain in the recent years has led to the development of numerous stem-based immunogens, with the goal of boosting the immune response to the conserved HA stem domain rather than to the immunodominant but variable regions in the head domain (121, 122, 199-201). Although broadly neutralizing antibodies that target the head domain have been isolated in the recent years (196, 197), none of them display extensive heterosubtypic breadth comparable to that of the best HA stem antibodies. In this work, I report for the first time the isolation and characterization of a broad-spectrum HA head antibody FluA-20 that recognizes with high affinity nearly all IAV HA subtypes. When administered prophylactically, FluA-20 protected mice from weight loss against H1N1, H3N2, H5N1 or H7N9 challenge, and thus could serve as a potential antiviral drug against infections with diverse IAV strains.

Typically, the protective ability of mAbs against influenza have been evaluated by the HAI assay, which detects antibodies that block the RBS, or by a neutralization assay that detects not only RBS antibodies but also stem binding antibodies that block fusion. Although a rough correlation has been made with certain serum HAI titers and partial protection *in vivo*, a true

correlate of protection has not been defined fully. Recent studies in murine models of IAV infection have revealed the importance of antibody Fc-mediated effector functions in clearing influenza infection *in vivo*. For example, the broadly neutralizing stem mAb FI6 that functions by inhibiting viral fusion showed substantially reduced *in vivo* protection when its ability to engage Fc $\gamma$ R was eliminated (60). A recent study reported that broadly neutralizing stem antibodies, but not RBS-specific antibodies, require Fc-mediated interactions to provide protection *in vivo* (61). RBS-specific antibodies may not be able to mediate Fc-mediated activity efficiently, since optimal activation of Fc effector function may require interaction between the RBS and its sialic acid receptor on effector cells (198). Although FluA-20 binds to the HA head domain, it binds a unique epitope in the head and does not block the RBS, and consequently it is able to mediate Fc-dependent ADCC activity and provide *in vivo* protection. Unlike most antibodies reported in the literature that mediate enhanced inhibitory activity by combining Fc-mediated effector functions with neutralizing activity, the non-neutralizing mAb FluA-20 apparently mediates protection entirely by its ability to engage Fc $\gamma$ R.

Recently, Lee *et al.* reported the identification of three protective antibodies to H1 and H3 that bound to the monomeric but not trimeric form of HA (119). They were isolated from donors vaccinated with trivalent inactivated vaccine. The low-resolution negative-stain EM map of the Fab molecules complexed with the HA protomer indicated that these antibodies bound to a region on RBS that is inaccessible in the intact HA trimer. In the current study, we have reported the detailed characterization of a novel conserved epitope on HA head domain targeted by mAb FluA-20 which is also present in the occluded interface between adjacent HA protomers. Collectively, these studies show that broad-spectrum antibodies targeting such occluded sites are

indeed present in individuals vaccinated with trivalent seasonal influenza vaccine, and they provide a new avenue for universal influenza vaccine design.

It is striking that FluA-20, which recognizes an epitope occluded in the HA trimer interface, is able to provide *in vivo* protection against IAV challenge. The HA molecules on the cellular or viral surface generally have been considered to be stable trimers, with the trimer interface regarded as inaccessible and thus not targetable by the immune response or therapeutics. Our identification of FluA-20 epitope and analysis of HA trimer dynamics changes this notion and demonstrates for the first time the extensive dynamics occurring in the trimer interface allowing accessibility to previously unrecognized epitopes. An early study from Yewdell *et al.* reported the characterization of murine mAb Y8-10C2 that binds to influenza HA monomers but not native trimers (202). The mAb epitope, also indicated to be present between adjacent protomers in the globular head domain, was only accessible at elevated temperatures, suggesting increased conformational flexibility between the three head domains of the HA trimer at higher temperatures. Yewdell's study also implied that changes made near the fusion loop could indirectly affect the flexibility of the globular head domain. Nevertheless, the effect of trypsin-mediated cleavage on the conformational dynamics and flexibility of the globular head domain in HA trimer conformation is poorly understood. Interestingly, FluA-20 displayed binding to both uncleaved recombinant HA trimers and to native HA trimers on the virus particle, but not to cleaved HA trimers, suggesting that there is higher conformational flexibility or "breathing" occurring between adjacent HA protomers in the head domain of uncleaved than cleaved HA trimers. Taken together, these data offer insight into previously unrecognized dynamics of the globular head domain of HA and identify an important new conserved site of vulnerability on the influenza HA molecule.

## **Experimental methods**

**PBMC isolation and hybridoma generation.** The study was approved by the Vanderbilt University Medical Center Institutional Review Board. Peripheral blood was collected with heparin anticoagulation from a healthy donor with prior history of many seasonal influenza vaccinations and participation in clinical trials of experimental H5N1 and H7N9 subunit vaccinations. Generation of human hybridoma cell lines secreting human monoclonal antibodies was performed as described previously. Briefly, human B cells in the PBMC suspension were immortalized by transformation with EBV in the presence of CpG10103, cyclosporin A and a Chk2 inhibitor and plated in 384-well culture plates. On day 8, the supernatants from transformed B cells were used to screen for the presence of heterosubtypic antibodies that bound broadly to HA antigens from H1, H3, H7 or H9 subtypes using a capture ELISA. The recombinant HA antigens used for screening were based on the sequence of HAs from the following influenza strains: H1 A/California/04/2009, H1 A/Texas/36/1991, H3 A/Hong Kong/1/1968, H3 A/Victoria/3/1975, H7 A/Shanghai/2/2013, H7 A/Netherlands/219/2003 or H9 A/Hong Kong/1073/99. Cells from the wells containing B cells secreting heterosubtypic HA-reactive antibodies were fused with HMMA2.5 myeloma cells using a BTX ECM 2001 electro cell manipulator. The hybridomas were cloned by flow cytometric sorting of single cells into 384 well plates and then expanded in culture. Particular clones for downstream studies were selected by choosing the clone for each independently derived hybridoma line that exhibited the highest level of IgG secretion.

**Next-generation DNA sequence analysis of expressed antibody variable genes.** Total RNA was extracted from 10 million PBMCs. A one-step RT-PCR was performed for 25 cycles using

heavy-chain BIOMED-2 variable antibody gene-specific primers (203) and the OneStep SuperScript III with Platinum® Taq High Fidelity kit (Invitrogen, 11304011). The Illumina-specific adapters were added using the Illumina TruSeq Library Preparation Kit (Illumina, FC-121-3001) according to the manufacturer's recommendations. The final amplicon libraries were sequenced on an Illumina MiSeq instrument using the MiSeq PE-300 v3 reagent kit (Illumina, MS-102-3001). Sequence analysis was performed using IG-BLAST v1.4, and results were parsed to MongoDB for further study.

**Identifying Clonally Related Sequences.** From a database of annotated antibody sequences obtained from this donor, we queried HCDR3s with  $V_{H4-61}/J_{H4}$  lineage. These HCDR3 sequences were pairwise aligned to the HCDR3 of FluA20 using a PAM30 matrix, with penalties for gap opening and gap extension of -14 and -3, respectively. HCDR3 sequences with a Hamming distance of  $\leq 3$  to FluA20 were selected as siblings and the 'full length' nucleotide and amino acid sequence was queried from our database for further analysis.

**Visualizing Clonally Related Sequences.** A network graph was built from the aligned, full-length sequences queried as described previously. Identical sequences were clustered into single nodes, and edges were drawn between two nodes if their Hamming distance was the lowest compared to all other nodes. Nodes denoting the inferred common ancestor and the germline  $V_{H4-61}/J_{H4}$  sequence were manually added. This network was visualized using Cytoscape and manually adjusted for visual clarity (to prevent nodes from overlapping edges to which they are not connected, and to shorten distances between nodes that are closely related).

**Production of IgG for mAb FluA-20 from hybridoma cells.** The selected cloned cell line secreting mAb FluA-20 was grown initially in hybridoma growth medium (ClonaCell-HY medium E from STEMCELL Technologies, 03805) and then switched to serum-free medium (GIBCO Hybridoma-SFM, Invitrogen, 12045084) for antibody expression and purification. IgG from the hybridoma cell line supernatants was purified by affinity chromatography using protein G columns (GE Life Sciences, Protein G HP Columns). Purified FluA-20 IgG generated from hybridomas was used for all EC<sub>50</sub> and IC<sub>50</sub> studies, competition-binding studies, DXMS, and ADCC assays and mouse studies.

**Influenza viruses.** The virus stocks were made from the supernatant of virus-infected MDCK cell culture monolayers in plain Dulbecco's Modified Eagle Medium (Gibco DMEM, Invitrogen, 11965) with 2 µg/mL of TPCK-trypsin. To obtain virus with uncleaved HA0 on the surface, the stocks were made by inoculating MDCK cells with virus for 1 hr. The cells were washed thoroughly and replenished with plain DMEM without TPCK-trypsin. The supernatant containing the virus was harvested at 48 hours post inoculation.

**Dimeric recombinant soluble FcγRIIIa (CD16a) binding ELISA.** A dimeric recombinant soluble FcγRIIIa (rsFcγRIIIa) ELISA was used to model the need for ADCC-inducing Abs to cross link FcγRIIIa (179). A 96-well ELISA plate was coated with 50 ng of purified influenza HA protein from H1N1 A/California/07/2009 (Sino Biological Inc., 11085-V08B) protein overnight at 4 °C in PBS. The plates were treated as described (179). Briefly, the plates were blocked for 1 h and 50 µL of antibodies (FluA-20, FluA-45, FluA-55 or an unrelated negative control mAb [HIV-specific VRC01]) at various concentrations (40 µg/mL to 2.4 ng/mL) were



added to the plates. The plates were washed with PBST and 50  $\mu$ L of 0.1  $\mu$ g/mL rsFc $\gamma$ RIIIa (V176) dimer was added to the wells and incubated for 1 h at 37 °C. Pierce High Sensitivity Streptavidin-HRP (ThermoFisher Scientific, 21130) was diluted 1:10,000 in PBSE/BSA and added to wells. The plates were developed with TMB substrate solution and the reaction was stopped with 1 M HCl. The plates were read at an absorbance of 450 nm.

**NK cell activation assay.** 96-well ELISA plates were coated with 600 ng of purified influenza HA protein from H1N1 A/California/07/2009 (Sino Biological Inc., 11085-V08B) overnight at 4 °C in PBS. The plates were washed and incubated with 10  $\mu$ g/mL, 1  $\mu$ g/mL or 0.1  $\mu$ g/mL of antibodies (FluA-20, FluA-45, FluA-55 or VRC01) diluted in PBS for 2 h at 37°C. Plates were washed and 5 x 10<sup>5</sup> purified NK cells were added to each well. NK cells were purified from freshly isolated PBMCs using the EasySep human NK cell enrichment kit (STEMCELL Technologies, 19055). Mouse anti-human CD107a allophycocyanin-H7 antibody (clone H4A3; BD Biosciences, 561343), 5  $\mu$ g/mL brefeldin A (Sigma-Aldrich, B6542) and 5  $\mu$ g/mL monensin (BD GolgiStop; BD Biosciences, 554724) were added to the cells and incubated for 5 h. Purified NK cells then were incubated with anti-human CD3 PerCP (clone SP34-2; BD Biosciences, 552851) and anti-human CD56 allophycocyanin (clone B159; BD Biosciences, 555518) for 30 min at RT. Cells were fixed and permeabilized for 10 min and then incubated with anti-human IFN $\gamma$  AF700 (clone B27; BD Biosciences, 561024) in the dark. Finally, cells again were fixed with 1% formaldehyde, and data was acquired for 20,000 – 50,000 events using an LSRFortessa flow cytometer (BD Biosciences).

***In vivo* efficacy of FluA-20 IgG.** Female C57/bl 6 mice aged 6–8 weeks were obtained from Charles River Laboratories, Wilmington, MA, and housed under specified pathogen-free conditions with food and water *ad libitum*. Experimental groups of 8 mice were given i.p. with 10 mg/kg of either FluA-20 or a similarly prepared control human antibody to an unrelated target (a mAb to methicillin-resistant *Staphylococcus aureus*; MRSA). They were challenged 24 hours later with a sublethal dose (0.1 LD<sub>50</sub>) of either H1N1 A/Netherlands/602/2009 or H3N2 A/X-31 (6:2 PR8 backbone) or H5N1 A/barn swallow/Hong Kong/D10-1161/2010 (7:1 PR8 backbone) or H7N9 A/Shanghai/1/2013 (6:2 PR8 backbone). Challenge under mild ketamine/xylazine anesthesia was by intranasal administration of 50 µl virus preparation diluted in PBS. Decrease in body weight was used as a measure of morbidity after infection. Mice (n=5) were weighed every day for 14 days post-challenge. Mice that had lost >25% of their initial body weight were killed. All infections were conducted under BSL-2<sup>+</sup> containment and were authorized by the Institutional Ethics Committee on Experimental Animals.

For pulmonary titers, mice from each group (n=3) were killed at 6 days post-inoculation and lungs were removed aseptically, snap frozen on dry ice and stored at -80°C until titration. Lungs were homogenized in 1 ml PBS using a Fastprep 24 homogenizer (MP Biomedicals). The homogenates were centrifuged (5 min, 16100xg, 4°C) to remove cellular debris and used for virus titration by plaque assay. Hereto, 200 µl of tenfold dilutions of homogenized lungs in PBS were used for infecting confluent monolayers of MDCK cells. Virus was allowed to attach to MDCK cells for 1h at 37° C. Cells were washed once with warm PBS and overlaid with oxid agar (Oxoid Ltd., Basingstoke, Hampshire) prepared using NaHCO<sub>3</sub>-buffered serum-free 2x MEM/BA containing DEAE Dextran and supplemented with TPCK-treated trypsin (1µg/ml). Endpoint virus titers were determined by visualizing virus plaques 2 days after infection by

staining with H1N1 post challenge serum (1/1000 dilution), horseradish peroxidase-conjugated sheep-derived anti-mouse serum (GE Healthcare UK, NA-931) and TrueBlue substrate (KPL-Seracare, 5510-0031).

**Characterization of antibody isotype, subclass, and variable genes.** The isotype and subclass of secreted antibodies were determined by ELISA. Antibody heavy- and light-chain variable region genes were sequenced from antigen-specific hybridoma lines that had been cloned biologically from flow cytometry. Briefly, total RNA was extracted using the RNeasy Mini kit (Qiagen, 74106) and reverse-transcriptase PCR (RT-PCR) amplification of the antibody gene cDNAs was performed using the PrimeScript One Step RT-PCR kit (Clontech, RR055A) according to the manufacturer's protocols with gene-specific primers as previously described (204). PCR products were purified using Agencourt AMPure XP magnetic beads (Beckman Coulter) and sequenced directly using an ABI3700 automated DNA sequencer without cloning. The identities of gene segments and mutations from germlines were determined by alignment using ImMunoGeneTics database (205, 206).

**Molecular engineering of antibody variable gene domains and generation of Fc mutants.**

For the expression of recombinant forms of antibody clones, nucleotide sequences of antibody variable domains were optimized for mammalian expression and synthesized on the BioXP 3200 System (SGI-DNA). These inserts were then joined with a 6.8-kb EcoR1/HindIII digested backbone of pML-huCG1 for expression of  $\gamma$ 1 or BgIII/NotI digested backbone of pML-huCk or pML-huCL vectors for  $\kappa$  or  $\lambda$  chains (Ref), respectively, using the NEBuilder HiFi DNA Assembly master mix (NEB, E2621). For the generation of Fc mutants, 4 nucleotide sequences of antibody constant domains with single mutations (K332A, D265A, and N297A) and a double

mutant (L234A, L235A) in the constant heavy-chain region (CH2) were optimized for mammalian expression and synthesized on the BioXP 3200 (SGI-DNA). These inserts were then joined with a 6.0-kb HindIII/XbaI digested backbone of pML-huCG1 (207) for construction of 4 separate  $\gamma$ 1 mutant chains using the NEBuilder HiFi DNA Assembly master mix (NEB).

**Peptide fragmentation and deuterium exchange mass spectrometry.** To maximize peptide probe coverage, the optimized quench condition was determined prior to deuteration studies (208, 209). In short, HA head domain was diluted with H<sub>2</sub>O buffer (8.3 mM Tris, 150 mM NaCl, in H<sub>2</sub>O, pH7.15) at 0°C and then quenched with 0.8% formic acid (v/v) containing various concentration of GuHCl (0.8-6.4 M) and Tris(2-carboxyethyl)phosphine (TCEP) (0.1 or 1.0 M). After incubating on ice for 5min, the quenched samples were diluted 4-fold with 0.8% formic acid (v/v) containing 16.6% (v/v) glycerol and then were frozen at -80°C until they were transferred to the cryogenic autosampler. 6.4 M GuHCl, 1.0 M TCEP in 0.8% formic acid gave an optimal peptide coverage map.

The samples later were thawed automatically on ice and then immediately passed over an AL-20-pepsin column (16  $\mu$ L bed volume, 30 mg/mL porcine pepsin (Sigma)). The resulting peptides were collected on a C18 trap and separated using a C18 reversed phase column (Vydac) running a linear gradient of 0.046% (v/v) trifluoroacetic acid, 6.4% (v/v) acetonitrile to 0.03% (v/v) trifluoroacetic acid, 38.4% (v/v) acetonitrile over 30 min with column effluent directed into an Orbitrap Elite mass spectrometer (Thermo-Fisher Scientific). Data were acquired in both data-dependent MS:MS mode and MS1 profile mode. Proteome Discoverer software (Thermo Finnigan Inc.) was used to identify the sequence of the peptide ions. DXMS Explorer (Sierra Analytics Inc., Modesto, CA) was used for the analysis of the mass spectra as described previously (210). FluA-20 mAb bound HAs were prepared by mixing FluA-20 mAb with

monomeric H5 A/Vietnam/03/2204 HA head domain at a 1:1.1 stoichiometric ratio. The mixtures were incubated at 25 °C for 30 min. All functionally deuterated samples, with the exception of the equilibrium-deuterated control, and buffers were pre-chilled on ice and prepared in the cold room.

Functional deuterium-hydrogen exchange reaction was initiated by diluting free HA or antibody-bound HA stock solution with D2O buffer (8.3 mM Tris, 150 mM NaCl, in D2O, pDREAD 7.15) at a 1:2 vol/vol ratio. At 10 sec, 100 sec and 1,000 sec, quench was added to the respective samples, and then samples were frozen at -80°C. In addition, nondeuterated samples, equilibrium-deuterated back-exchange control samples were prepared as previously described (208, 209, 211). The centroids of the isotopic envelopes of nondeuterated, functionally deuterated, and fully deuterated peptides were measured using DXMS Explorer, and then converted to corresponding deuteration levels with corrections for back-exchange (212).

## CHAPTER V

### HUMAN ANTIBODY RESPONSES TO INFLUENZA A H7N9 VIRUS

*“It worries the flu scientists because they know that H5N1 influenza is (1) extremely virulent in people, with a high lethality though a relatively low number of cases, and yet (2) poorly transmissible, so far, from human to human. It’ll kill you if you catch it, very likely, but you’re unlikely to catch it except”*

*David Quammen, Spillover: Animal Infections and the Next Human Pandemic*

#### Introduction

Avian influenza A viruses (AIV) of H5 and H7 subtypes have caused sporadic human infections and are considered potential causes for a future influenza pandemic. Since 2013, novel avian H7N9 viruses have caused five annual epidemics in China with high morbidity and mortality rates. During the first four epidemics, 88% of subjects developed pneumonia, 68% were admitted to an intensive care unit, and 41% died (213). The number of human H7N9 cases during the fifth epidemic (764) was significantly higher than that in the first four epidemics, which resulted in 135 (first), 320 (second), 226 (third) or 119 (fourth epidemic) human infections (73, 213). Sequence analysis of HA and NA genes from H7N9 strains isolated during the fifth epidemic have identified the emergence of a) highly pathogenic avian H7N9 viruses with a four-amino acid insertion in the HA cleavage site and b) strains with drug-resistance to one or more neuraminidase inhibitors used for anti-viral treatment (73). Most of these infections occurred in individuals with direct poultry exposure, but there is evidence suggesting limited human-human transmission (74).

Due to the health concern posed by avian H7N9 viruses, numerous candidate vaccines are

being developed and evaluated currently. In the recent past, several groups including our laboratory have isolated human monoclonal antibodies (mAbs) to HA induced by H7 vaccination or natural infection (204, 214-216). The H7N9 experimental subunit vaccines induced B cells encoding both neutralizing and non-neutralizing H7 antibodies that displayed *in vivo* protection in mice challenge studies (214). Typically, the neutralizing antibodies were specific to the H7 HA and functioned by blocking the receptor binding site (RBS), while the non-neutralizing antibodies displayed heterosubtypic breadth and provided protection by Fc-mediated mechanisms (204, 214). These observations indicate that traditional neutralization assays used to evaluate vaccine efficacy may not be a good predictor of protective responses induced by H7N9 vaccines. The epitopes targeted by these heterosubtypic mAbs may provide valuable information on antibody epitopes important for engaging Fc-mediated functions. To this end, I have isolated several broadly cross-reactive antibodies to HA from H7N9 vaccinees. I describe my analysis of these antibodies in chapter VI under future directions.

In this chapter, I will focus mainly on the human antibody response to N9 NA. NA antibodies do not block attachment or entry but reduce viral replication by inhibiting the release of nascent virions. NA antibodies are known to be a correlate of protection against disease caused by influenza viruses (217, 218). MAbs that inhibit NA enzymatic activity were shown to provide *in vivo* protection in mice that were challenged with lethal influenza infection (217). Mice immunized with adjuvanted recombinant NA protein were protected against challenge with homologous or heterologous strains within the same subtype, but were not protected against challenge with virus of a different subtype (138). Early studies published by Webster *et al.* during the 1980s demonstrated the presence of several antigenic sites on N2 and N9 NAs using murine mAbs (219, 220). The epitopes of two murine N9 mAbs, designated mAbs NC10 and

NC41, were resolved in more detail by crystallographic studies of mAb-N9 complexes (221, 222). More recently, antigenic sites on N1 NA were mapped using murine mAbs that provided either homologous (only H1N1) or heterologous (H1N1 and H5N1) protection against IAVs carrying N1 NA (137). However, all of these antigenic sites were mapped using murine antibodies, and relatively little is known about the antigenic sites targeted by human mAbs.

Avian N9 neuraminidases are particularly interesting, as they possess a second sialic acid binding site or hemadsorption site (Hb) apart from the enzymatic site (128). Although the Hb site binds to sialic acids, the sialic acid specificity and the binding properties of Hb site vary from those of the HA receptor-binding site (130). The N9 hemadsorption site was demonstrated recently to enhance viral binding to human-like SA receptors and therefore was implicated in the transmission of H7N9 virus (130). Also, N9 NA differs antigenically from N1 and N2 NAs derived from the seasonal strains. There is little information on the nature of human NA antibodies elicited by H7N9 vaccination or natural infection.

In this chapter, I have compared the human antibody responses to H7 HA and N9 NA following H7N9 vaccination or natural infection with H7N9 virus. While H7 HA induced a heterosubtypic HA response, N9 elicited a narrow subtype-specific NA response with limited cross-reactivity to other subtypes. I present here the isolation and functional characterization of the first panel of human mAbs to N9 NA. I isolated a total of 35 N9-specific mAbs; 9 mAbs displayed inhibition of function of both N9 enzymatic site and the Hb site, 3 mAbs inhibited only the enzymatic site, 3 mAbs inhibited only the Hb site and 20 mAbs displayed no inhibitory activity. The epitopes of these functional N9 mAbs were mapped by competition-binding assays, hydrogen deuterium exchange mass spectrometry (HDX-MS) experiments and negative-stain electron microscopy (EM) imaging analysis. The majority of these functional mAbs bound near



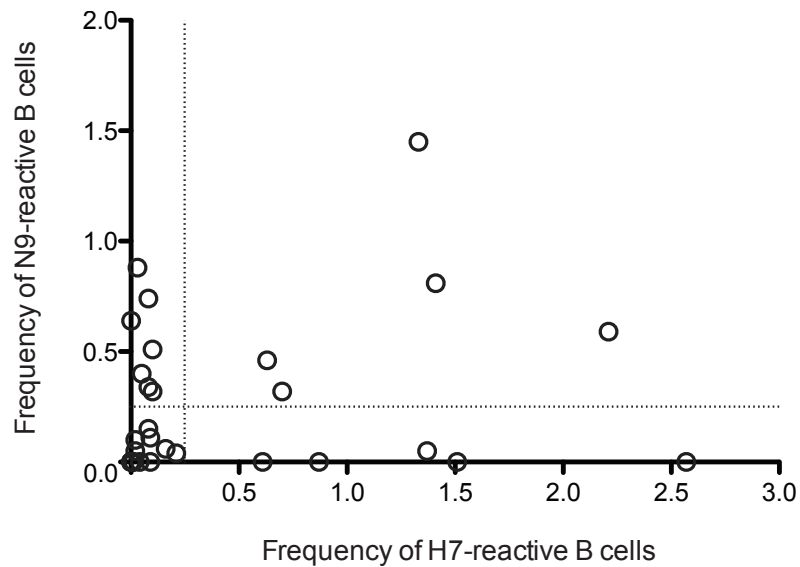
the enzymatic site but with differing binding angles. The potency of the NA inhibitory activity associated with these mAbs appears to depend on the binding angle of each mAb.

I acknowledge Dr. Andrew Ward's group for examining NA antibodies in complex with N9 by negative-stain single-particle electron microscopy (EM), Dr. Sheng Li's group for epitope analysis of N9-reactive mAbs by HDX-MS data, Dr. Ian Wilson's group for providing N9 NA antigen, and the survivors of H7N9 infection who generously donated blood for this study.

### **Comparison of human B cell response to H7 and N9**

We obtained peripheral blood mononuclear cells (PBMCs) from a phase II human clinical trial of monovalent inactivated H7N9 A/Shanghai/02/2013 (A/Sh/2/2013) vaccine. The donors received 2 doses of the vaccine and the PBMC samples were collected on day 0 (day of vaccination) and day 42 post-vaccination. To determine the frequency of B cells encoding antibodies to H7 HA or N9 NA in vaccinated donors, we transformed PBMCs collected on day 42 from 30 donors, using EBV transformation in 384 well plates. The supernatants from transformed B cell lines were screened for the presence of IgGs binding to H7 HA or N9 NA derived from A/Sh/2/2013 by ELISA. Frequency of H7- or N9-reactive B cells was calculated from the total number of transformed B cell colonies on the plate and the number of reactive wells determined by ELISA. Among the 30 donors who received the vaccine, 13 donors responded to either H7 or N9, 5 donors responded well to both H7 and N9, 5 donors responded only to H7 and 7 donors responded only to N9. Because HA is thought to be the primary target for antibodies, it was surprising to see that certain donors responded specifically to N9 but not to H7 (Figure 5-1).

In January 2015, health officials in British Columbia reported the first two human H7N9 cases in North America in two travelers following a trip to Hong Kong and Mainland China (223). The case study reported that both survivors showed seroconversion (> 4-fold increase in antibody titer) to H7N9 by hemagglutination inhibition assay. We obtained PBMC samples from these 2 survivors of natural infection with H7N9 virus (A/British Columbia/1/2015 strain). PBMC samples from the survivors were collected approximately 11 months after recovery from infection. I separately analyzed the B cell frequencies to H7 and N9 in these survivors, similar to the approach used for the H7N9 vaccinee samples. Both survivors had memory B cells secreting IgGs that bound to H7 or N9 at 11 months post-infection. The frequency of H7-reactive B cells for survivors 1 and 2 were 0.38% and 1.45%, respectively. These frequencies are comparable with the H7-reactive B cell frequencies 42 days after vaccination. The frequency of N9-reactive B cells for survivor 1 and 2 were 0.56% and 0.86%, respectively. The N9-reactive frequencies from the two survivors were marginally higher in comparison to the mean frequency calculated from the vaccinated donors (mean 0.27%, n=30). Survivor 1 (Donor 957) showed a better response to N9 NA, while survivor 2 (Donor 958) exhibited higher reactivity to H7 HA.



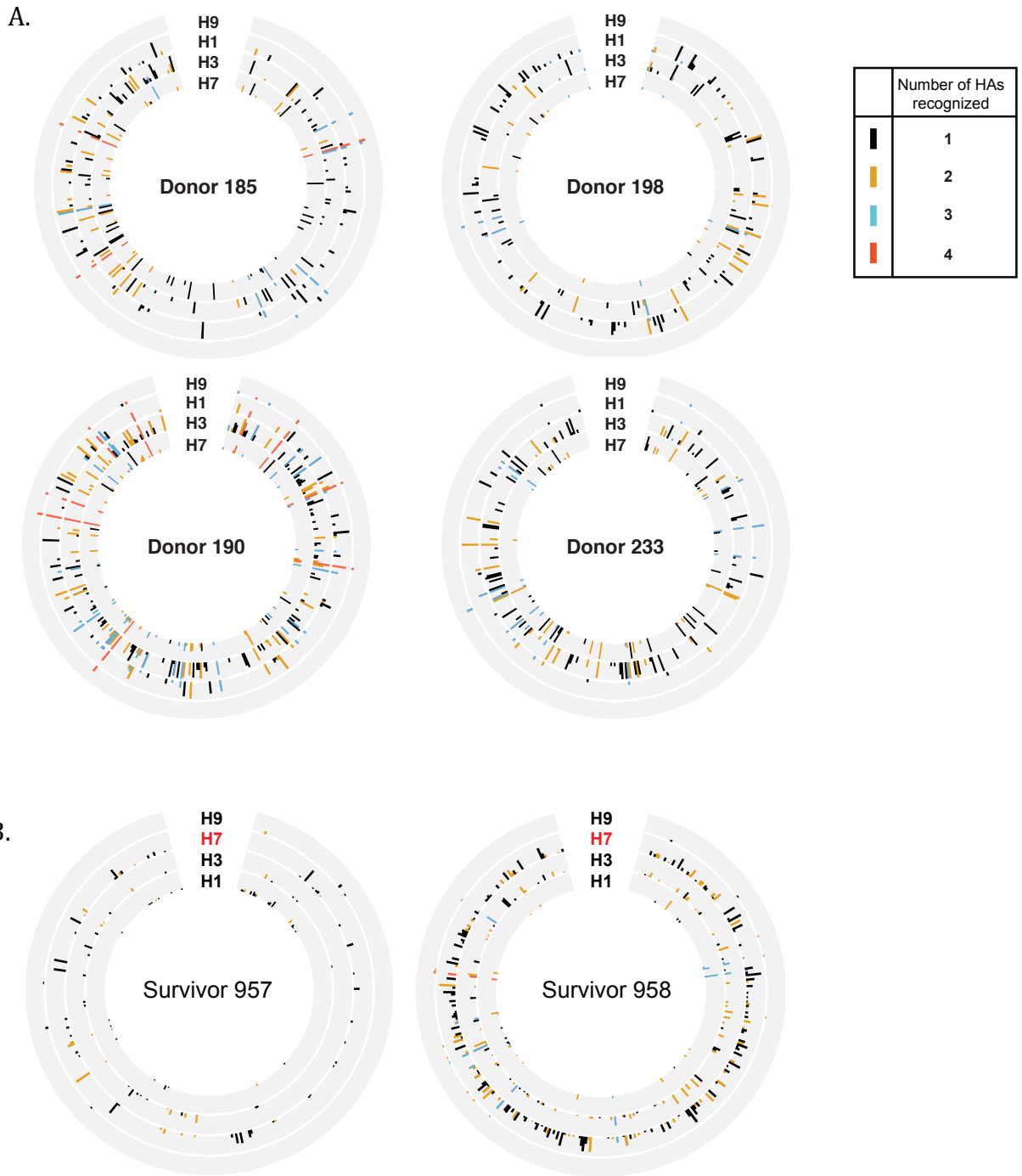
**Figure 5-1. Frequency of H7- and N9-reactive B cells in 30 H7N9 vaccinated donors.** B cell frequency to each antigen was determined by transforming PBMCs from day 42 post-vaccination and screening the transformed B cells supernatants for the presence of H7- or N9- reactive antibodies. Dotted lines indicate threshold of 0.25%.

### Cross-reactive response elicited by H7N9 infection or vaccination

To determine the cross-reactive nature of these H7 and N9 responses, I screened supernatants from EBV-transformed B cells from 12 vaccinated donors and both survivors for the presence of IgGs reactive to group 1 and group 2 HAs: A/Sh/2/2013 or A/New York/55/2004 H7 HAs (H7), A/Hong Kong/1/1968 or A/Victoria/361/2011 H3 HAs (H3), A/California/2009 or A/Texas/36/1991 H1 HAs (H1), or A/turkey/Wisconsin/1/1966 or A/Hong Kong/1073/1999 H9 HA (H9) by ELISA. I performed a similar screen for 2 vaccinated donors and both survivors for presence of IgGs that bound to four NAs belonging to group 1 and 2: A/California/04/2009 (N1), A/Wisconsin/67/2005 (N2), A/Pennsylvania/1/2007 (N8) and A/Sh/2/2013 (N9). The cross-reactive breadth to different HAs and NAs for each donor is represented as a Circos plot (Figure

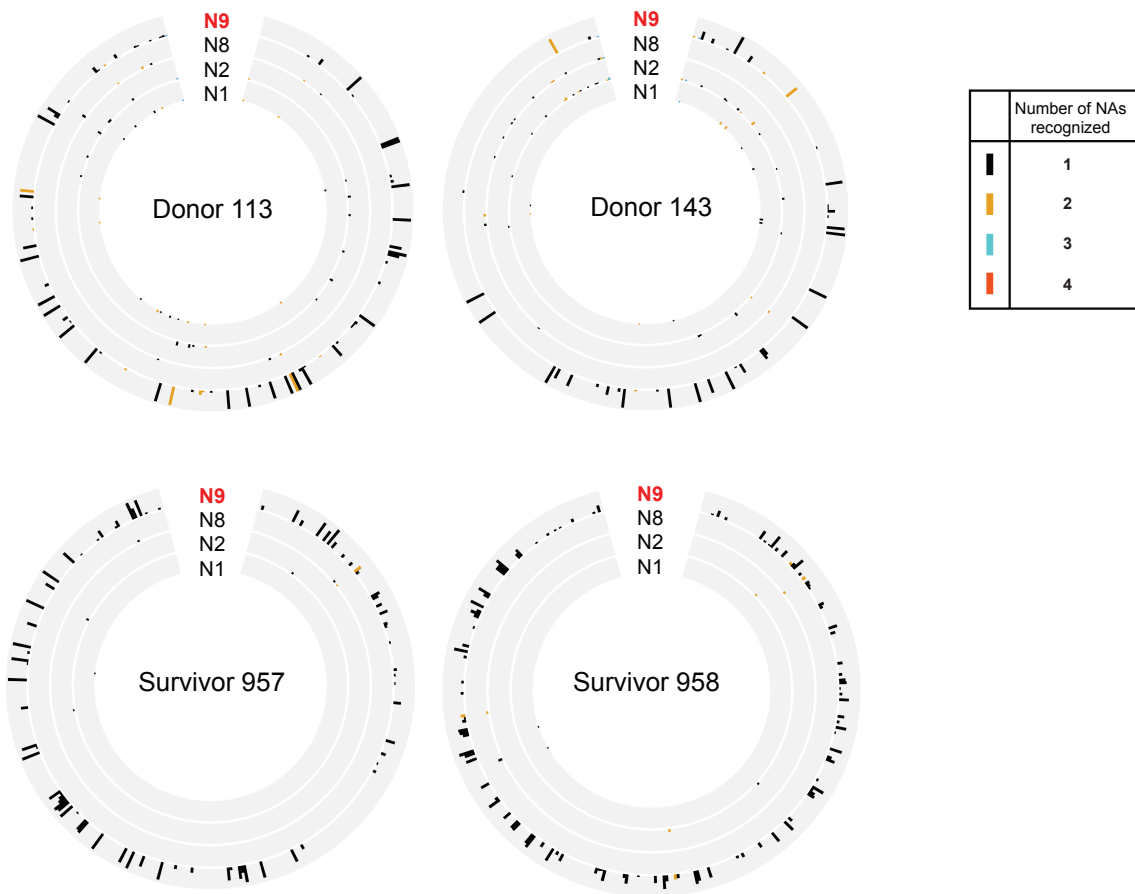
5-2 and 5-3). Each circle on the Circos plot represents reactivity to HA or NA derived from one subtype, the spikes representing the signal from each well of a 384-well ELISA plate. The height of the bar represents the optical density at 405 nm. Presence of IgG was defined as an optical density of greater than two standard deviations above background. Wells with IgGs specific to a single antigen are represented with black bars. Cross-reactivity to two, three or four antigens is indicated by orange, aqua or red bars, respectively.

All vaccinees and survivors exhibited a broad HA response, with varying levels of cross-reactivity observed between individuals (Figure 5-2A and 5-2B). Although reactivity to more than 2 antigens was low, a high percentage of B cells produced IgGs that were H7-H3 or H7-H1 cross-reactive. Other groups also have reported similar findings that demonstrate the development of HA cross-reactive antibodies following vaccination with H7N9. In stark contrast to the HA response, the vaccinated donors exhibited a narrow N9-specific response with negligible cross-reactivity to other NAs. Consistently, the same pattern of N9-specificity also was observed in both the survivors. (Figure 5-3)



**Figure 5-2. Breadth of HA response in H7N9 vaccinees and survivors (A)** Circos plots representing number of B cell lines with reactivity for specified HAs in four representative vaccinees. PBMCs from donors 185, 190, 198, or 233 from day 42 were immortalized with EBV. Transformed B cell supernatants were screened by ELISA for the presence of IgGs that bound to

HAs from H1, H3, H7 and H9. Each circle has 384 positions with each representing one well of a 384-well plate. Each ring represents results from ELISA. The height of the bar represents the optical density of the well at 405 nm. Presence of IgG was defined as an optical density of greater than two standard deviations above background. Black, gold, aqua or coral bars indicate that a well contained IgG that bound to one, two, three, or four HA proteins, respectively. **(B)** Circos plots representing B cell lines with reactivity for specified HAs in two survivors of natural infection.



**Figure 5-3. Breadth of NA response in H7N9 vaccinees and survivors.** Circos plots representing number of B cell lines with reactivity for specified NA in 2 vaccinees (day 42) and 2 survivors. Transformed B cell supernatants were screened by ELISA for the presence of IgGs that bound to HAs from N1, N2, N8 and N9. The number of wells that were reactive against one (black), two (gold), three (aqua), or all four (coral) NAs was counted and indicated in the top portion of the table.

### **Isolation of N9 human antibodies**

Transformed B cells that showed reactivity to N9 were chosen for hybridoma generation to isolate human mAbs to N9 NA. I isolated a panel of 35 mAbs to N9 from a total of four donors (2 vaccinees and 2 survivors) (Figure 5-4). I also isolated an N2 antibody from a survivor to be used for comparative purposes. To determine binding breadth, purified mAbs at a single concentration of 5  $\mu\text{g/mL}$  were tested for binding to NA antigens from representative influenza strains belonging to five different subtypes. As expected, all N9 mAbs showed strong binding to NA derived from N9 A/Sh/2/2013 (the vaccine strain) and most of them also exhibited reactivity to NA from N9 A/Anhui/1/2013. Consistent with the results from the primary analysis with B cell supernatants, the purified mAbs did not show cross-reactivity to NA from other subtypes (Figure 5-4). Two antibodies, designated mAbs NA-111 and NA-126, displayed weak cross-reactivity to other subtypes (O.D. > 1.5). To further examine their binding affinities, I determined the  $\text{EC}_{50}$  values for mAbs to NA from N9 A/Sh/2/2013 by ELISA (Figure 5-5). Twenty-one mAbs showed strong binding to N9 with  $\text{EC}_{50}$  values less than 100 ng/mL. Eleven mAbs exhibited intermediate binding with  $\text{EC}_{50}$  values between 0.1 to 1  $\mu\text{g/mL}$ , and three mAbs displayed weak binding with  $\text{EC}_{50}$  values greater than 1  $\mu\text{g/mL}$ .

### **Functional analysis of N9 mAbs**

I tested each of the 35 N9-specific mAbs for their ability to inhibit the enzymatic activity of N9 from A/Sh/2/2013 using an enzyme-linked lectin assay (ELLA). Fetuin, a heavily sialated glycoprotein, is used as the NA substrate in ELLA. The assay measures the amount of penultimate galactose that is released when NA cleaves the terminal sialic acid on fetuin. Zanamivir, the commercially available neuraminidase activity inhibitor, was used as an assay

positive control for comparative purposes. Among the 35 mAbs, 12 mAbs exhibited complete inhibition of N9 enzymatic activity, with  $IC_{50}$  less than 100 nM (Figure 5-5). These 12 mAbs will be referred to here as neuraminidase inhibiting (NI) mAbs. Interestingly, 6 of the 12 NI mAbs exhibited potent inhibition of N9 activity with  $IC_{50}$  values lower than the zanamivir drug ( $IC_{50}$  of zanamivir is 3.7 nM), while the other six mAbs exhibited  $IC_{50}$  values greater than 3.7 nM. In particular, the activity of mAb NA-80 was remarkable in that it was 9-fold more potent than zanamivir (Figure 5-5). In addition to the 12 mAbs that displayed complete NA inhibition, a few mAbs showed partial inhibition of N9 activity leaving behind a residual uninhibited fraction.

Since the N9 Hb site is implicated to play a role in H7N9 transmission, I examined the ability of N9-specific mAbs to inhibit the hemadsorption activity of this site on A/Sh/2/2013 NA. I did a preliminary analysis to determine the amount of N9 NA-coated paramagnetic beads that is required to hemagglutinate turkey RBCs. Using this predetermined amount of N9-coated beads, I performed an assay for inhibition of NA protein mediated hemagglutination with serial dilution of N9 mAbs. Because zanamivir is a small molecule compound that targets the enzymatic site, it does not have inhibitory activity against the N9 Hb site and was therefore used as an assay negative control. Interestingly, 9 of 12 NI mAbs blocked the NA protein mediated hemagglutination activity at concentrations less than 5  $\mu\text{g}/\text{mL}$  (Figure 5-5). Three other mAbs that displayed partial activity on ELLA also exhibited N9 hemagglutination inhibition activity (Figure 5-5).



Donor	mAb	Optical density of 5 µg/ml mAb binding in ELISA to NA from indicated influenza type group and subtype													
		Group 2							Group 1						
		N9		N2					N1				N4	N8	
		A/Shanghai/2/2013	A/Anhui/1/2013	A/mallard/Netherlands/3/1999	A/Wisconsin/67/2005	A/Brisbane/10/2007	A/shorebird/Delaware/127/1997	A/turkey/Wisconsin/1/1966	A/California/04/2009	A/New Caledonia/20/1999	A/Brisbane/59/2007	A/Puerto Rico/8/1934	A/grey teal/Australia/2/1979	A/equine/Pennsylvania/1/2007	
Vaccinee	143	NA-3	3.7	<	<	<	<	<	<	<	<	<	<	<	<
		NA-4	3.7	<	<	<	<	<	<	<	<	<	<	<	<
		NA-5	3.7	3.7	<	<	<	<	<	<	<	<	<	<	<
	113	NA-16	3.8	1.8	<	<	<	<	<	<	<	<	<	<	<
		NA-17	3.7	2.9	<	<	<	<	<	<	<	<	<	<	<
		NA-22	3.8	3.7	<	<	<	<	<	<	<	<	<	<	<
		NA-37	3.8	3.8	<	<	<	<	<	<	<	<	<	<	<
		NA-45	3.7	<	<	<	<	<	<	<	<	<	<	<	<
		NA-55	3.8	3.7	<	<	<	<	<	<	<	<	<	<	<
		NA-63	3.7	2.2	<	<	<	<	<	<	<	<	<	<	<
		NA-69	3.8	1.1	<	<	<	<	<	<	<	<	<	<	<
		NA-73	3.7	3.7	<	<	<	<	<	<	<	<	<	<	<
		NA-77	3.8	3.8	<	<	<	<	<	<	<	<	<	<	<
		NA-80	3.8	3.8	<	<	<	<	<	<	<	<	<	<	<
NA-81	3.8	2.4	<	<	<	<	<	<	<	<	<	<	<		
NA-86	3.8	3.8	<	<	<	<	<	<	<	<	<	<	<		
Survivor	957	NA-89	3.7	3.5	<	<	<	<	<	<	<	<	<	<	
		NA-93	3.8	3.8	<	<	<	<	<	<	<	<	<	<	
		NA-95	3.7	3.8	<	<	<	<	<	<	<	<	<	<	
		NA-97	3.8	3.8	<	<	<	<	<	<	<	<	<	<	
		NA-108	3.8	3.8	<	<	<	<	<	<	<	<	<	<	
		NA-110	3.8	3.2	<	<	<	<	<	<	<	<	<	<	
		NA-111	3.8	3.8	1.1	<	<	1.0	2.2	1.5	<	1.2	<	0.9	1.4
		NA-121	3.8	3.7	<	<	<	<	<	<	<	<	<	<	<
		NA-126	3.8	3.8	<	<	<	<	<	0.8	0.8	1.9	<	0.9	<
		NA-127	3.7	3.7	<	<	<	<	<	<	<	<	<	<	<
	NA-144	3.8	3.4	<	<	<	<	<	<	<	<	<	<	<	
	958	NA-148	3.8	3.8	<	<	<	<	<	<	<	<	<	<	<
		NA-152	3.8	3.5	<	<	<	<	<	<	<	<	<	<	<
		NA-157	3.8	3.7	<	<	<	<	<	<	<	<	<	0.9	<
NA-164		3.8	3.1	<	<	<	<	<	<	<	<	<	<	<	
NA-171		3.7	3.7	<	<	<	<	1.0	<	<	<	<	<	<	
NA-175		3.8	3.8	<	<	<	<	<	<	<	<	<	<	<	
NA-177	3.7	<	<	<	<	<	<	<	<	<	<	<	<		
NA-181	3.7	1.9	<	<	<	<	<	<	<	<	<	<	<		
NA-169	0.8	<	<	3.8	3.8	3.8	3.8	<	<	0.8	<	0.8	<		

**Figure 5-4. Binding breadth of NA-reactive mAbs isolated from H7N9 survivors and vaccinees.** Purified N9 NA-reactive mAbs at 5 µg/mL were tested for breadth of binding by ELISA, against NAs from vaccine strain and 12 other strains. < symbol indicates optical density below 0.5

MAB	Binding to A/Sh/2/2013, EC <sub>50</sub> (ng/mL)	Inhibition of N9 enzymatic activity by ELLA, IC <sub>50</sub> (nM)	Neuraminidase N9 HAI (µg/mL)
NA-80	40	0.42	0.92
NA-95	75	0.67	>
NA-73	38	0.94	2.7
NA-108	52	1.33	0.92
NA-77	148	2.15	>
NA-22	129	2.66	0.92
NA-121	100	4.22	0.92
NA-181	1,596	6.12	>
NA-3	56	17.5	0.92
NA-63	43	19.1	0.92
NA-45	160	39.1	2.7
NA-157	46	72.9	0.92
NA-17	45	PI	2.7
NA-126	78	PI	2.7
NA-127	48	PI	0.92
Zanamivir	ND	3.71	>

**Figure 5-5. Functional characterization of N9-specific antibodies.** The binding affinities (EC<sub>50</sub>) for N9-reactive mAbs to N9 A/Sh/2/2013 NA were determined by ELISA. The potency (IC<sub>50</sub>) of N9-specific mAbs to inhibit NA enzymatic activity was determined by ELLA assay. PI indicates partial enzymatic inhibition activity (presence of residual uninhibited fraction) in ELLA. The ability of N9-specific mAbs to inhibit N9 hemagglutination activity was determined by HAI assay with turkey blood cells using N9 protein coated beads. > indicates that no HAI activity was detected below 25 µg/mL. ND indicates not determined.

## Epitope mapping of human N9 mAbs

Currently, little is known about the functional epitopes targeted by human NA antibodies. It is not clear if the functional NA mAbs target a single site or bind to multiple distinct epitopes on NA. To evaluate if the human N9 mAbs targeted diverse antigenic regions on NA, I performed a quantitative competition-binding assay using surface plasmon resonance (SPR; using a Wasatch Microfluidics device). I competed 29 human N9-specific mAbs and one murine N9-specific mAb NC10 for binding to N9 from A/Sh/2/2013 (Figure 5-6). The majority of the N9 mAbs that exhibited NA enzymatic inhibition activity blocked binding of each other to the NA antigen and segregated into a single competition-binding group (Figure 5-6). The bulk of the N9-specific mAbs that lacked NI activity segregated into 3 groups: one major competition-binding group and 2 minor groups. Two functional mAbs, NA-95 and NA-3, competed with both NI and non-NI mAbs for binding to N9 NA (Figure 5-6). These results suggest that the functional NI epitopes targeted by N9 mAbs are located in/around a major antigenic region on NA while the majority of the non-NI antibodies seem to target several other distinct sites.

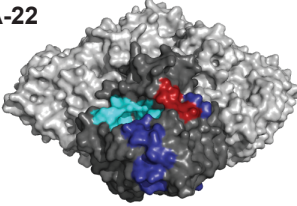

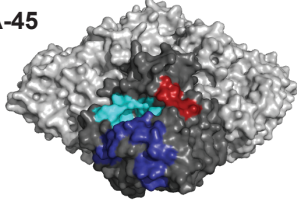

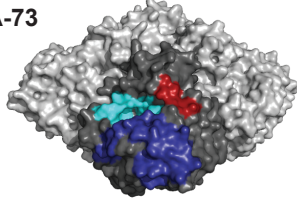

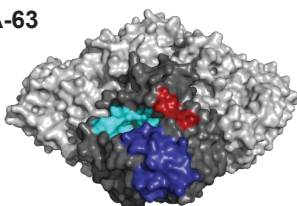
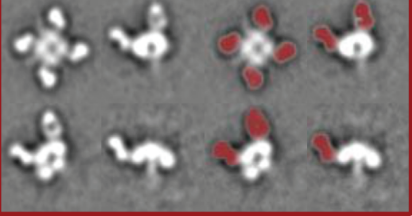
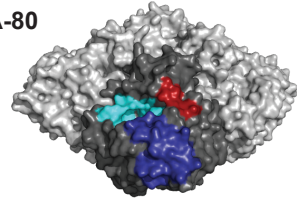
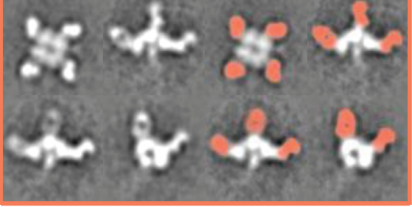
To map the functional epitopes in further detail, we performed DXMS of mAb-NA complexes in collaboration with the laboratory of Dr. Sheng Li at UCSD. For DXMS analysis, N9 from A/Sh/2/2013 was labeled with deuterated water in the presence or absence of NA-3, NA-22, NA-45, NA-63, NA-73, NA-77, NA-80, NA-95, NA-108 or NA-121 mAbs. The N9 NA protein was digested with pepsin, and deuterium labeling of resulting peptides was measured by mass spectrometry. A decrease in deuterium labeling in the presence of a mAb suggests that residues in that peptide were in contact with the mAb. The peptides that exhibited decreased deuterium labeling when incubated with mAb are mapped on the N9 NA tetramer structure (PDB ID: 4MW1) in dark purple (Figure 5-7A). All NI-mAbs decreased deuterium labeling to peptides

in either site A (amino acids 261-301) or site B (amino acids 342-372) or both site A and B, which are situated below the enzymatic site towards the side of the protomer (Figure 5-7A).

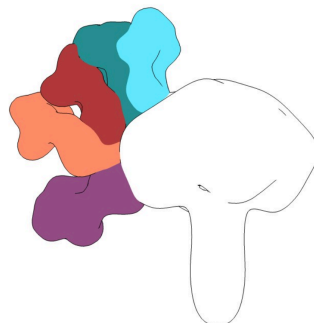
We also performed electron microscopy of N9 NA in complex with Fab fragments of 5 mAbs, NA-22, NA-45, NA-63, NA-73 and NA-80, in collaboration with the laboratory of Dr. Andrew Ward's group. The 2D averages obtained from the EM images for each complex revealed different binding angles for each mAb. MAb NA-45 and NA-73 appear to bind in an almost vertical orientation to the enzymatic site, while NA-63 and NA-80 bind at an inclined angle (Figure 5-7A and 5-7 B). While both NA-63 and NA-80 seem to bind in close proximity to the enzymatic site, their binding poses angles away from each other; mAb NA-80 positions towards the enzymatic site while mAb NA-63 positions away from the enzymatic site (Figure 5-7A). This finding could explain the ability of mAb NA-80 to potently inhibit enzymatic activity ( $IC_{50} = 0.42$  nM), while mAb NA-63 exhibits much lower potency ( $IC_{50} = 19.1$  nM). Surprisingly NA-22 was shown to bind to the side of the NA-protomer away from the enzymatic site and tilting towards the stalk, which would make it impossible to directly or sterically block the enzymatic site. It is possible that mAb NA-22 inhibits both the enzymatic site and the Hb site in an allosteric manner by altering the sites themselves.



A.

DXMS classes	2D class averages
<p data-bbox="412 310 488 331">NA-22</p> 	
<p data-bbox="412 562 488 583">NA-45</p> 	
<p data-bbox="412 804 488 825">NA-73</p> 	
<p data-bbox="412 1045 488 1066">NA-63</p> 	
<p data-bbox="412 1297 488 1318">NA-80</p> 	

B.



**Figure 3. Epitope mapping of N9-specific mAbs by HDX-MS and EM.** (A) On the left is the surface representation of N9 NA tetramer (PDB ID: 4MW1) with the enzymatic site and the Hb site represented in cyan and red, respectively. The HDX-MS predicted epitopes for MAbs NA-22, NA-45, NA-73, NA-63 and NA-80 IgGs are mapped on N9 NA in deep blue. The mAbs are organized into 3 classes based on their HDX-MS predicted epitopes. The 2D class averages of the Fab portions of each N9 mAb bound to N9 NA are shown on left. Fabs NA-22 (purple), NA-45 (green), NA-73 (blue), NA-63 (red) and NA-80 (orange) are colored for clarity. (B) Schematic representation of relative angles of binding to N9 by each N9-reactive Fab. Figure credit for panel B: Hannah Turner (Ward laboratory)

## Discussion

Despite the significant role of NA in pathogenesis, there is very little information about the human antibody response to NA. Here, I have compared the antibody responses to H7 HA and N9 NA following H7N9 vaccination or natural infection, by determining the frequency of B cells reactive to each antigen. Although HA is thought to exhibit immunodominance over NA during influenza infection or vaccination, we identified several donors who did not respond to H7 but exhibited a significant N9 response. Our analysis of cross-reactivity responses in both vaccinees and survivors showed that H7 induced a heterosubtypic HA response, indicating conserved antigenic determinants among HAs. Other groups have also reported similar findings that demonstrate the development of HA cross-reactive antibodies following vaccination with H7N9. There is less known about the nature of cross-reactive responses induced by N9 NA. In contrast to the heterosubtypic HA response, the N9-induced response was very specific to N9 NA, suggesting lack of conserved immunodominant epitopes between N9 NA and NAs (N1 and N2) from seasonal strains. Currently, there is no evidence for NA-based heterosubtypic protection induced by vaccination or natural infection. The only known heterosubtypic NA mAb was obtained by immunizing rabbits with a 9-amino acid long peptide (ILRTQESEC) that is conserved across all NAs. While the rabbit mAb exhibits enzymatic inhibition activity across all NAs, it is possibly unlikely for antibodies targeting this site to be induced by natural infection or

vaccination (224).

In this chapter, I report the isolation of a diverse panel of naturally occurring human N9 reactive mAbs from individuals naturally infected with H7N9 virus or immunized with an experimental H7N9 subunit vaccine. Twelve of thirty-five mAbs exhibited N9 enzymatic inhibition activity; six of these mAbs displayed higher potency than the commercially available NA inhibitor, zanamivir. Specifically, mAbs NA-73, NA-80 and NA-95 are several folds more potent than zanamivir at inhibiting NA enzymatic activity. Additionally, mAbs NA-73 and NA-80 also inhibit N9 sialic-acid binding site. Such mAbs have promising potential as prophylactics or therapeutics. In the wake of the recent emergence of H7N9 drug-resistance to NA inhibitors, these human mAbs could provide an alternative form of therapy against H7N9 infections.

Several groups have mapped the antigenic sites on different NAs including N1, N2 and N9 NA using murine monoclonal antibodies. The most extensive mapping was done in early studies by Webster et al. showing the presence of four antigenic sites on N2 NA; antibodies to two of the four sites inhibited NA enzymatic activity (220). Preliminary epitope analysis of human N9 mAbs by epitope binning studies have shown a similar pattern; mAbs that inhibited enzymatic activity fell into a major competition group 1 and a minor group that overlapped with both group 1 and a 2<sup>nd</sup> major competition group containing antibodies without NI activity. The non-NI mAbs also formed 2 other minor groups. DXMS and EM analysis of N9-specific mAbs have revealed 2 major antigenic sites bound by NI mAbs with different binding angles. MAb NA-22 that binds to the periphery of the bottom surface of the N9 molecule also elicited NA inhibition activity possibly by allosteric effect. Identification of these potent human N9-specific mAbs and their corresponding epitopes on N9 NA allows better understanding of the human antibody response to N9 and provides insight into designing new NA-based vaccines.



## Experimental methods

**Cloning, expression and purification of recombinant neuraminidase proteins.** The N9 protein from A/Shanghai/2/2013 (H7N9) was provided to us by Dr. Ian Wilson's group. The ectodomain plus stalk region (37-465) of NA from the influenza virus A/Shanghai/2/2013 (H7N9) (GISAID accession number EPI\_ISL\_138738) was expressed in a baculovirus expression system in insect cells. The cDNAs corresponding to the NA ectodomain plus stalk region of A/Shanghai/2/2013 (H7N9) were inserted into a baculovirus transfer vector, pFastbacHT-A (Invitrogen) with an N-terminal gp67 signal peptide, a thrombin cleavage site, a His<sub>6</sub>-tag, and an N-terminal tetramerization domain, essentially as previously described (225, 226). For NA molecules from zanamivir-resistant N9 mutant viruses, the M-PIPE mutagenesis method was used to mutate the wild-type N9 plasmid (227). The constructed plasmids were used to transform DH10bac competent bacterial cells by site-specific transposition (Tn-7 mediated) to form a recombinant Bacmid with  $\beta$ -galactosidase blue-white receptor selection. The purified recombinant bacmids were used to transfect Sf9 insect cells for overexpression. NA proteins were produced by inoculating suspension cultures of Sf9 cells with recombinant baculovirus at an MOI of 5-10 and incubating at 28°C while shaking at 110 RPM. After 72 hours, Sf9 cells were removed by centrifugation and supernatants containing secreted, soluble NAs were concentrated and purified by metal affinity chromatography using Ni-nitrilotriacetic acid (NTA) resin (Qiagen). The uncleaved NA ectodomain plus stalk region with tetramerization domain and His-tag were concentrated in 20 mM Tris pH 8.0, 150 mM NaCl.

Additional NA proteins were obtained from BEI resources (Manassas, VA) corresponding to the viruses N9 A/Anhui/1/2013 (catalog number NR-44082), N2 A/mallard/Netherlands/3/1999 (NR-29011), N2 A/Wisconsin/67/2005 (NR-19237), N2 A/Brisbane/10/2007 (NR-43784), N2

A/shorebird/Delaware/127/1997 (NR-657), N2 A/turkey/Wisconsin/1/1966 (NR-43783), N1 A/California/04/2009 (NR-19234), N1 A/New Caledonia/20/1999 (NR-43779), N1 A/Brisbane/59/2007 (NR-43785), N1 A/Puerto Rico/8/1934 (NR-19235), N4 A/grey teal/Australia/2/1979 (NR-656), and N8 A/equine/Pennsylvania/1/2007 (NR-13523)

**Human sample acquisition.** Blood samples from two survivors of natural H7N9 infection, as described (223), were collected approximately 11 months after recovery from infection. The vaccine samples used in this study were from subjects enrolled in a phase II randomized, doubled-blinded, controlled study in healthy adults to assess the safety, reactogenicity, and immunogenicity of a monovalent influenza A/H7N9 virus vaccine at different dosages with or without AS03 or MF59 adjuvant (DMID 13-0033; Identifier: NCT01942265). The details of the clinical trial were described previously (204). Adults between 19 and 64 years of age were eligible to participate, and vaccine was administered at day 0 and day 21. Blood was collected at day 0 and day 42, and peripheral blood mononuclear cells were isolated and cryopreserved until use.

**Hybridoma generation and antibody isolation.** Generation of human hybridoma cell lines secreting human monoclonal antibodies was performed as described previously. On day 8, the supernatants from transformed B cells were used to screen for the presence of heterosubtypic antibodies that bound broadly to NA antigens from N1, N2, N8 or N9 subtypes using a capture ELISA. The recombinant NA antigens used for screening were derived from A/California/04/2009 (N1), A/Wisconsin/67/2005 (N2), A/Pennsylvania/1/2007 (N8) and the vaccine strain A/Shanghai/2/2013 (N9). Purified IgG generated from hybridomas was used for

all the studies.

**Enzyme-Linked Lectin-based Assay (ELLA).** The ability of N9 mAbs to inhibit the enzymatic activity of soluble recombinant NA was assayed by ELLA using fetuin, a heavily sialylated glycoprotein as the NA substrate. 96-well ELISA plates were coated with 100  $\mu$ L of 25  $\mu$ g/mL of fetuin from fetal bovine serum (Sigma-Aldrich, F3004) diluted in 0.1 M PBS and incubated at 4  $^{\circ}$ C for 48 hours. 50  $\mu$ L of three-fold serial dilutions of each antibody starting at a molar concentration of 667 nM (10  $\mu$ g/mL) in PBS was added to 50  $\mu$ L of pre-optimized concentration of soluble NA diluted in PBS containing 0.9 mM  $\text{CaCl}_2$ , 0.5 mM  $\text{MgCl}_2$ , 1% BSA and 0.5% Tween. The fetuin-coated plates were washed and the mAb-NA mixture was added to the plates and incubated for 18 hours at 37  $^{\circ}$ C. The plates were washed 6 times with PBST, and 100  $\mu$ L of HRP-conjugated lectin from *Arachis hypogaea* (Sigma-Aldrich, L7759) at 2.5 mg/ mL was added to the plates and incubated for 2 hours at RT. The plates were washed and 100  $\mu$ L of TMB substrate was added to the plates, and the reaction was stopped with 1N HCl. The optical density values were measured at 450 nm wavelength on a BioTek plate reader. Each dilution was performed in triplicate, and the  $\text{IC}_{50}$  values were calculated in Prism software (GraphPad) using non-linear regression analysis. The experiment was conducted twice independently.

**Neuraminidase N9 hemagglutination inhibition assay.** 50  $\mu$ L of His-tag isolation and pulldown Dynabeads (Invitrogen, 10104D) were washed twice with PBST and blocked with 500  $\mu$ L of 5% non-fat dry milk in PBST for 15 minutes at RT. The beads were washed again and added to 300  $\mu$ g of N9 NA protein from A/Shanghai/2/2013 and incubated overnight on a shaker at 4 degrees. The NA-coated beads were washed, and serial dilutions of NA beads were

incubated with 0.5% turkey blood cells to determine hemagglutination (HA) titer. For HAI assays, 25  $\mu$ L of 4 HA units of the beads were incubated with 25  $\mu$ L of three-fold dilutions of the mAb, starting at 25  $\mu$ g/mL in PBS for 1 hr at 37°C. 50  $\mu$ L of the NA beads-antibody mixture was incubated with turkey red blood cells for 1 hr at RT. The HAI titer was defined as the highest dilution of antibody that inhibited hemagglutination of red blood cells. Each dilution was performed in duplicate.

**Competition-binding groups.** Competition-binding for N9 mAbs was performed using sequential binding on a surface plasmon resonance instrument (Wasatch Microfluidics). All experiments were conducted on a 96-ligand array with N9 NA from A/Shanghai/1/2013 antigen. A heat map was obtained by SPRI-premix experiments in which the first antibody and N9 NA were premixed before adding to the array printed with the second antibodies.

**Epitope mapping using peptide fragmentation and deuterium exchange mass spectrometry.**

To maximize peptide probe coverage, the optimized quench condition was determined prior to deuteration studies (208, 209). In short, NA antigen was diluted with H<sub>2</sub>O buffer (8.3 mM Tris, 150 mM NaCl, in H<sub>2</sub>O, pH 7.15) at 0 °C and then quenched with 0.8% formic acid (v/v) containing various concentration of GuHCl (0.8-6.4 M) and Tris(2-carboxyethyl)phosphine (TCEP) (0.1 or 1.0 M). After incubating on ice for 5 minutes, the quenched samples were diluted 4-fold with 0.8% formic acid (v/v) containing 16.6% (v/v) glycerol and then were frozen at -80 °C until they were transferred to the cryogenic autosampler. 6.4 M GuHCl, 1.0 M TCEP in 0.8% formic acid gave an optimal peptide coverage map.

The samples later were thawed automatically on ice and then immediately passed over an AL-20-pepsin column (16  $\mu$ L bed volume, 30 mg/mL porcine pepsin (Sigma)). The resulting peptides were collected on a C18 trap and separated using a C18 reversed phase column (Vydac) running a linear gradient of 0.046% (v/v) trifluoroacetic acid, 6.4% (v/v) acetonitrile to 0.03% (v/v) trifluoroacetic acid, 38.4% (v/v) acetonitrile over 30 min with column effluent directed into an Orbitrap Elite mass spectrometer (Thermo-Fisher Scientific). Data were acquired in both data-dependent MS:MS mode and MS1 profile mode. Proteome Discoverer software (Thermo Finnigan Inc.) was used to identify the sequence of the peptide ions. DXMS Explorer (Sierra Analytics Inc., Modesto, CA) was used for the analysis of the mass spectra, as described previously (210). The mixtures MAb-NA complexes were incubated at 25 °C for 30 min. All functionally deuterated samples, with the exception of the equilibrium-deuterated control, and buffers were pre-chilled on ice and prepared in the cold room.

Functional deuterium-hydrogen exchange reaction was initiated by diluting free NA or antibody-bound NA stock solution with D<sub>2</sub>O buffer (8.3 mM Tris, 150 mM NaCl, in D<sub>2</sub>O, pDREAD 7.15) at a 1:2 vol/vol ratio. At 10 sec, 100 sec or 1,000 sec, quench was added to the respective samples, and then samples were frozen at -80 °C. In addition, non-deuterated samples, equilibrium-deuterated back-exchange control samples were prepared, as previously described (208, 209, 211). The centroids of the isotopic envelopes of non-deuterated, functionally deuterated, and fully deuterated peptides were measured using DXMS Explorer, and then converted to corresponding deuteration levels with corrections for back-exchange (212).

## CHAPTER VI

### CONCLUSIONS AND FUTURE DIRECTIONS

*“We regret very much the fact that an influenza virologist is unable to live say 200 years, so that he himself would be able to see what has developed from his earlier assumptions.”*

*J. Mulder and J.F.P Hers, Influenza (1972)*

#### **Study of human antibody response to IAVs**

Influenza A viruses are highly contagious pathogens that cause severe disease worldwide with high morbidity and mortality rates. The emergence of new human infections by novel zoonotic IAVs poses a major public threat due to the lack of immunity to these viruses. Vaccination is currently the most effective approach to prevent influenza infection and associated complications. However, the ability of IAVs to continuously mutate and undergo reassortment gives rise to new strains with significant antigenic diversity. As a consequence, current influenza vaccinations offer protection only against strains that are antigenically similar to the vaccine strain. Although antiviral drugs provide broader protection, the emergence of drug resistance is a major drawback. The CDC no longer recommends the use of Adamantanes, a class of drugs that were previously used to treat influenza, due to the prevalence of adamantane-resistance strains. Therefore, there is a strong need for therapeutics and vaccines that can provide broad protection against IAVs.

The study of human antibody responses to IAVs is fundamental for developing broad therapeutics and vaccines because (a) diversity in human antibody response to novel antigens

such as H7 offers new strategies for inducing a cross-reactive response, (b) identification of cross-reactive epitopes facilitate rational design of structure-based broadly protective vaccines (c) identification of broad heterosubtypic antibodies also facilitate the development of antibody-based therapeutics and (d) elucidation of novel mechanisms of antibody-mediated protection identifies new targets for therapeutic intervention. My thesis work has been largely focused on studying human antibody-responses to zoonotic IAVs, H3N2v and H7N9, and discovery of subtype-specific and broadly cross-reactive antibodies to influenza glycoproteins, HA and NA. In this chapter, I have summarized my finding and possible future directions.

### **Human antibody response to H3v HA**

Swine-origin H3N2v viruses are antigenically distinct from H3N2 viruses currently in human circulation. Prior to 2011, transmission of these novel influenza variants from swine to human was rare with only 27 reported cases between 1990 and 2010. Since 2011 there has been a substantial increase in the number of human infections with H3N2v viruses, specifically in children, associated with pig exposure. I screened B cells from adult donors before and after immunization with H3N2v vaccine for secretion of H3v-reactive antibodies. The results showed that most adults had some pre-existing immunity to the H3 variant HA. Isolation and characterization of variant-reactive antibodies isolated from these adult donors revealed antigenic relatedness between H3N2v virus and seasonal strains from 1995-2004, explaining why adults had some prior immunity to these viruses while children were very susceptible. A sudden increase in the number of H3N2v human infections may be due to waning immunity in the adult population.

Although H3N2v HA resembles the older seasonal strain, it has key polymorphisms near

the upper rim of receptor-binding site that makes it antigenically distinct from the current human strains. When donors were immunized with the variant vaccine, they developed a significant antibody response to H3v HA. Studies with EBV-transformed B cell supernatants and purified mAbs showed that the majority of this response was not cross-reactive to the current seasonal strains. These variant-specific antibodies specifically recognized the area around receptor-binding site on the HA head domain and functioned by blocking attachment.

Nonetheless, the vaccinated donors had a small percentage of antibodies (H3v-47, H3v-79, H3v-84, H3v-86 and H3v-95) that showed cross-reactivity against both variant and seasonal H3 HAs. Collectively, data obtained from crystallography, epitope binning, DXMS and EM reconstructions has shown that these cross-reactive antibodies target either the vestigial esterase subdomain of HA head (H3v-47, H3v-84 and H3v-95) or the conserved HA stem (H3v-79 and H3v-86). While HA stem is a known target for broadly neutralizing antibodies, the vestigial esterase domain has not been identified as a target for broad H3 antibodies. Our studies reveal the presence of novel epitopes in the esterase subdomain that are conserved across diverse H3 strains of human- and swine-origin. Development of vaccines that can redirect the immune response away from the highly diverse epitopes around the RBS towards these conserved sites in the esterase domain can provide a much broader protection against diverse H3 strains.

### **Human antibody response to H7 HA and N9 NA**

Wild aquatic birds are the natural reservoir for all influenza subtypes and thought to provide the source of the next pandemic, where all influenza pandemics since 1918 have contained a viral component of avian origin. Vaccine trials for avian IAVs (H5N1, H9N2 and H7) in humans have reported varying efficacies depending on vaccine formulations and route of



administration, but have consistently shown that these vaccines are poorly immunogenic in comparison to seasonal influenza H1 and H3 vaccines. In general, avian IAV vaccines require large protein doses or use of new adjuvants in order to induce protective neutralizing antibody titers. The basis for this poor immunogenicity is not well understood. Previous studies have evaluated the contribution of intrinsic properties of the avian HAs and vaccine formulations on the poor immunogenicity of the vaccine; lower T cell epitope content, receptor binding specificity and vaccine morphology have been suggested to contribute towards the low immunogenicity of the AIV vaccines. It is possible that the lack of prior immunity to antigenically related strains may also be a contributing factor. Because H7 is antigenically very different from the current seasonal strains, the majority of the population is immunologically naïve to H7 HA.

In contrast to the strong response seen in donors who received the unadjuvanted monovalent inactivated H3N2v vaccine, the average response seen after monovalent H7N9 vaccination (both adjuvanted and unadjuvanted groups present in the blinded trial) was relatively mediocre. The response to H7N9 was comprised of both H7-specific antibodies as well as broadly cross-reactive heterosubtypic antibodies. Studies done in collaboration with Natalie Thornburg, alumna of the Crowe laboratory, showed that the H7-specific antibodies isolated from H7N9 vaccinees were significantly less mutated than H1-specific antibodies, broadly neutralizing cross-reactive antibodies, and H7-induced heterosubtypic antibodies compared to their inferred germline genes. This suggests that these H7-specific antibodies were induced as a primary response to the vaccine while the H7-induced heterosubtypic mAbs possibly arose from a secondary response. A similar pattern of H7-specific and cross-reactive response was observed in H7N9 survivors. In contrast to the H7 response, the N9-induced response was comprised of

antibodies reactive only against N9 NA. The N9-specific response was observed in donors who received H7N9 vaccination and in natural survivors of H7N9 infection. Moreover, all of the N9 antibodies isolated from the vaccinees contained very few mutations compared to their germline genes, similar to what was seen for H7-specific antibodies. These results indicate an almost naïve response to the N9 antigen.

### **Future directions: Towards universal influenza vaccines**

The key focus of current influenza research is to develop universal vaccines that provide robust protection against multiple subtypes of influenza. Based on my results and conclusions, I have proposed future directions aimed towards rational design of better vaccines.

### **Induction of broadly cross-reactive antibodies by exposure to H7 HA**

Although H7 HAs belong to a different antigenic clade from H1 or H3 HAs, H7 vaccination elicited high levels of heterosubtypic antibodies with cross-reactivity against H7 and seasonal HAs. The ability of H7 HA to consistently induce a broad heterosubtypic response against group 1 and group 2 HAs unlike any other vaccine, suggests molecular mechanisms and determinants important for eliciting these cross-reactive antibodies. Vaccination strategies that include H7 HA would facilitate induction of heterosubtypic mAbs and enable development of “universal influenza vaccines”. To develop H7-based vaccination strategies, it is important to determine the common structural or antigenic determinants between H7 and the seasonal strains targeted by H7 induced heterosubtypic antibodies. Currently, all known antibodies (except FluA-20) that exhibit cross-reactivity against H3 and H7 HAs bind to the conserved stem domain, which are found at very low frequencies in individuals vaccinated or infected with the seasonal strains. It is unclear if H7 induced cross-reactive mAbs target this stem domain or other conserved epitopes. To determine if these cross-reactive mAbs bound to other conserved

epitopes, I isolated a total of nine cross-reactive HA mAbs from six H7N9 vaccinated donors; Three mAbs displayed binding to HAs within one subtype (either H1 or H3) and six mAbs exhibited cross-reactivity towards more than one subtype (heterosubtypic) (Table 6-1). From preliminary competition binding studies, some of these H7-induced heterosubtypic HA mAbs appear to bind to the head domain rather than the conserved stem domain. Currently, the FluA-20 epitope is the only site on the HA head that is conserved across a majority of the HA subtypes. It is possible that these H7-induced heterosubtypic mAbs bind to the FluA-20 epitope or to a novel conserved epitope on the HA head domain. Detailed epitope analysis of these mAbs by electron microscopy and crystal structures can be used to identify these conserved epitopes.

In order to use a H7 based universal vaccine approach, it is also important to understand if the conserved epitopes targeted by H7 heterosubtypic mAbs translate to *in vivo* protection. From my antibody panel, 8 of 9 of these cross-reactive antibodies did not possess neutralizing activity at mAb concentrations as high as 20  $\mu\text{g}/\text{mL}$ . However, cross-reactive antibodies have been implicated to provide protection by Fc-mediated mechanisms rather than traditional neutralization mechanisms. The next step would be to test the *in vivo* efficacy of these mAbs in mice challenged with representative IAV strains. Based on my research, it is likely that these mAbs will possess *in vivo* efficacy and mediate protection either by Fc-mediated mechanisms or other unique mechanisms such as viral egress. Several antibody Fc mutants that eliminate Fc binding to Fc $\gamma$  receptors have been characterized in the recent years. The contribution of Fc in protection can be evaluated by performing *in vivo* studies comparing the efficacies of the WT and the mutant mAbs. Despite the recent interest in Fc-mediated anti-viral protection, the necessary features required to engage Fc $\gamma$ R have not been identified. One of the factors that have been implicated in Fc $\gamma$ R activation is the orientation of antibody Fc domain in such a way

that the Fc regions of at least 2 antibodies can simultaneously engage and cross-link FcγRs on effector cells. EM analysis of mAbs in complex with antigen and soluble FcγRs will allow us to identify optimal antibody orientations required to activate FcγRs.

Donor	MAb	EC <sub>50</sub> for indicated strain (μg/mL)														
		H1		H2	H3			H5	H7		H9	H13	H14	H16		
		A/California/2009	A/Texas/36/1991	A/Solomon islands/03/2006	A/Singapore/1/1957	A/Hong Kong/1/1968	A/Texas/50/2012	A/Switzerland/9715293/2013	A/Minnesota/11/10	A/Egypt/3300-NAMRU3/2008	A/New York/107/2003	A/Shanghai/2/3013	A/Hong Kong/1073/99	A/gull/Maryland/704/1977	A/mallard duck/Astrakhan/263/1982	A/black-headed gull/Sweden/4/1999
140	FluA-79	>	2.05	>	>	>	>	>	>	>	>	>	>	>	>	>
140	FluA-77	>	0.01	7.22	10.9	>	>	>	>	>	>	>	>	>	>	>
140	FluA-78	>	>	>	>	0.04	0.85	3.33	1.51	>	>	>	>	>	>	>
149	FluA-85	>	>	>	>	>	0.01	0.01	3.17	>	>	>	>	>	>	>
208	FluA-16	>	>	>	>	>	0.94	8.38	>	>	0.01	>	0.71	>	>	>
185	FluA-38	>	>	>	>	0.40	>	>	>	>	1.74	2.71	0.52	>	1.71	>
233	FluA-49	0.54	0.12	0.60	0.04	15.5	>	>	>	0.18	>	>	>	>	>	>
233	FluA-55	0.04	3.38	8.63	5.74	1.46	6.74	>	>	>	>	13.7	0.02	>	9.83	>
154	FluA-75	14.1	1.34	6.21	6.74	0.16	1.92	7.92	>	>	>	>	4.65	>	>	>
185	FluA-45	0.03	2.55	4.10	6.05	0.15	0.08	4.85	3.70	>	>	17.3	0.01	>	14.87	>

### **Broad H3 mAbs that target vestigial esterase domain and inhibit viral egress**

Exposure to H3v HA induced broad H3 mAbs (H3v-47, H3v-84 and H3v-95) that target the vestigial esterase domain on HA head. My analysis of one such mAb H3v-47 revealed that this mAb functions by inhibiting viral egress similar to the function of neuraminidase inhibitors. As the other 2 mAbs, H3v-84 and H3v-95, bind around the same site and show broad H3 activity similar to H3v-47, it is possible that these mAbs also function by inhibiting viral egress. So far, influenza A mAb, H3v-47 and influenza B mAb, CR8071 are the only 2 antibodies that have been shown to function by preventing viral egress and both these mAbs bind to the vestigial esterase site. The prevalence of this mechanism is currently unknown because antibodies to HA are generally assayed only for inhibition of receptor binding or viral fusion. Assessment of egress inhibition by H3v-84 and H3v-95 as well as other vestigial esterase mAbs would help us better understand and appreciate the prevalence of this mechanism.

The exact molecular mechanisms by which HA mAbs play a role in virus release is not completely clear. My work on H3v-47 has shown that inhibition of viral egress by HA mAbs can be achieved by cross-linking HAs on the newly formed virions causing virus aggregation on the cell surface. Another approach is by sterically hindering the NA enzymatic activity. This is feasible due to the close proximity of HA and NA on the surface of the virus. Moreover, the NA protein extends beyond the HA on the virus surface by  $\sim 2$  Å as HA spikes are about 14 Å while NA spikes are about 16 Å from the viral surface. Therefore, antibodies that bind to the HA head domain can potentially inhibit viral egress by sterically hindering the NA-enzymatic site. Indeed, my preliminary analysis of NA enzymatic inhibition by three H3 head domain antibodies by fetuin assay showed that all 3 mAbs possessed some level of NI activity. Analysis of a larger panel of HA head and stem antibodies with known HA epitopes and binding modes can be

performed to demonstrate the epitope dependence of this mechanism. Also, there is little evidence of how this actually occurs on the virus surface. Cryo-EM analysis of influenza virions bound by HA head antibodies can provide high-resolution images of influenza surface proteins bound by mAbs and therefore provide insight into the mechanism of NA inhibition by these HA antibodies. Additionally, NA enzymatic inhibition studies using sialic acid substrates of different sizes will offer details on the accessibility to enzymatic site in presence of HA antibodies. Identifying these novel mechanisms of neutralization mediated by HA antibodies not only offers new targets for therapeutics but also allows better understanding of molecular interactions between viral proteins.

### **Targeting HA trimer interface for heterosubtypic breadth**

Majority of the exposed surface on a HA trimer is highly variable between different HAs except for the receptor binding pocket and the stem region near the fusion peptide. Consequently, the heterosubtypic antibodies that have been isolated so far have targeted these 2 sites. Additionally, the surface of HA monomer occluded within the trimer interface is also well conserved but has been considered inaccessible due to HA trimer stability. In contrast to what was known before, identification of FluA-20 epitope within this trimer interface has revealed unknown dynamic features of the HA protein. This not only reinforces the biological relevance of this epitope but also provides a unique opportunity to study the dynamic features of trimeric HA. We observed that cleavage of HA0 to HA1 and HA2 significantly reduced FluA-20 binding to HA suggesting that the head region of HA protomers are much more dynamic before cleavage. This decrease in the movement of protomers following cleavage was also observed by HDX-MS studies. Changes in temperature or pH could also play a role in increasing breathing (dynamics) of the HA trimer. We can examine this by performing bio-layer interferometry to determine

binding of these mAbs to HA at low pH or at higher temperatures. Additionally, we can also test for neutralization by incubating the mAb with virus at different temperatures and pH before adding the mixture on MDCK cells. Understanding the dynamic features of HA will assist in targeting conserved sites present in the HA trimer interface by vaccines or therapeutics.

## LIST OF PUBLICATIONS

**Sandhya Bangaru**, Travis Nieusma, Nurgun Kose, Natalie J. Thornburg, Jessica A. Finn, Bryan S. Kaplan, Hannah G. King, Vidisha Singh, Rebecca M. Lampley, Gopal Sapparapu, Alberto Cisneros, Kathryn M. Edwards, James C. Slaughter, Srilatha Edupuganti, Lilin Lai, Juergen A. Richt, Richard J. Webby, Andrew B. Ward, and James E. Crowe Jr. Recognition of influenza H3N2 variant virus by human neutralizing antibodies. *Journal of Clinical Investigation Insight* 2016 July;1(10):e86673. doi:10.1172/jci.insight.86673.

Natalie J. Thornburg, Heng Zhang, **Sandhya Bangaru**, Gopal Sapparapu, Nurgun Kose, Rebecca M. Lampley, Robin G. Bombardi, Yingchun Yu, Stephen Graham, Andre Branchizio, Sandra M. Yoder, Michael T. Rock, C. Buddy Creech, Kathryn M. Edwards, David Lee, Sheng Li, Ian A. Wilson, Adolfo García-Sastre, Randy A. Albrecht, and James E. Crowe Jr. H7N9 influenza virus neutralizing antibodies that possess few somatic mutations. *Journal of Clinical Investigation* 2016 Apr 1;126(4):1482-94. doi:10.1172/JCI85317

Keitel WA, Jackson LA, Edupuganti S, Winokur PL, Mulligan MJ, Thornburg NJ, Patel SM, Roupael NG, Lai L, **Bangaru S**, McNeal MM, Bellamy AR, Hill HR; VTEU H3N2v Vaccine Study Work Group. Safety and Immunogenicity of a Subvirion Monovalent Unadjuvanted Inactivated Influenza A(H3N2) Variant Vaccine in Healthy Persons  $\geq 18$  Years Old. *Journal of Infectious Diseases* 2015 Aug 15;212(4):552-61. doi: 10.1093/infdis/jiv056.



## BIBLIOGRAPHY

1. E. D. Kilbourne, in *Influenza*, (Springer, Boston, MA, Boston, MA, 1987), pp. 157–218.
2. A. E. Fiore *et al.*, Prevention and Control of Influenza: Recommendations of the Advisory Committee on Immunization Practices (ACIP), 2008. *MMWR Recomm Rep*, 1–60 (2008).
3. M. B. Rothberg, S. D. Haessler, R. B. Brown, Complications of viral influenza. *The American Journal of Medicine* **121**, 258–264 (2008).
4. W. W. Thompson *et al.*, Estimates of US influenza-associated deaths made using four different methods. *Influenza and Other Respiratory Viruses* **3**, 37–49 (2009).
5. R. E. Shope, Swine influenza : I. experimental transmission and pathology. *J. Exp. Med.* **54**, 349–359 (1931).
6. R. E. Shope, Swine influenza: III. filtration experiments and etiology. *J. Exp. Med.* **54**, 373–385 (1931).
7. W. Smith, C. H. Andrewes, P. P. Laidlaw, A virus obtained from influenza patients. *The Lancet* **222**, 66–68 (1933).
8. T. Francis, A new type of virus from epidemic influenza. *Science* **92**, 405–408 (1940).
9. B. A. Briody, Hemagglutination by influenza virus: I. modification of the O phase of influenza A virus. *J. Infect. Dis.* **83**, 283–287 (1948).
10. B. M. Hause *et al.*, Characterization of a novel influenza virus in cattle and swine: proposal for a new genus in the *Orthomyxoviridae* family. *MBio* **5**, e00031–14 (2014).
11. M. C. Zambon, Epidemiology and pathogenesis of influenza. *Journal of Antimicrobial Chemotherapy* **44**, 3–9 (1999).
12. J. Sui *et al.*, Structural and functional bases for broad-spectrum neutralization of avian and human influenza A viruses. *Nat. Struct. Mol. Biol.* **16**, 265–273 (2009).
13. G. J. Nabel, A. S. Fauci, Induction of unnatural immunity: prospects for a broadly protective universal influenza vaccine. *Nat. Med.* **16**, 1389–1391 (2010).
14. Y. Wu, Y. Wu, B. Tefsen, Y. Shi, G. F. Gao, Bat-derived influenza-like viruses H17N10 and H18N11. *Trends Microbiol.* **22**, 183–191 (2014).
15. D. A. Steinhauer, J. J. Skehel, Genetics of influenza viruses. *Annu. Rev. Genet.* **36**, 305–332 (2002).

16. A. J. W. te Velhuis, E. Fodor, Influenza virus RNA polymerase: insights into the mechanisms of viral RNA synthesis. *Nat. Rev. Microbiol.* **14**, 479–493 (2016).
17. M. L. Li, The active sites of the influenza cap-dependent endonuclease are on different polymerase subunits. *The EMBO Journal* **20**, 2078–2086 (2001).
18. M. Kobayashi, T. Toyoda, A. Ishihama, Influenza virus PB1 protein is the minimal and essential subunit of RNA polymerase. *Archives of Virology* **141**, 525–539 (1996).
19. P. Digard, V. C. Blok, S. C. Inglis, Complex formation between influenza virus polymerase proteins expressed in *Xenopus* oocytes. *Virology* **171**, 162–169 (1989).
20. E. Fodor *et al.*, A single amino acid mutation in the PA subunit of the influenza virus RNA polymerase inhibits endonucleolytic cleavage of capped RNAs. *J. Virol.* **76**, 8989–9001 (2002).
21. Y. Liang, S. Danzy, L. D. Dao, T. G. Parslow, Y. Liang, P. Digard, Ed. Mutational analyses of the influenza A virus polymerase subunit PA reveal distinct functions related and unrelated to RNA polymerase activity. *PLoS ONE* **7**, e29485 (2012).
22. H. Liu, M. L. Grantham, A. Pekosz, Mutations in the influenza A virus M1 protein enhance virus budding to complement lethal mutations in the M2 cytoplasmic tail. *J. Virol.*, JVI.00858–17 (2017).
23. J. J. Skehel, D. C. Wiley, Receptor binding and membrane fusion in virus entry: The influenza hemagglutinin. <http://dx.doi.org/10.1146/annurev.biochem.69.1.531> **69**, 531–569 (2000).
24. P. Palese, K. Tobita, M. Ueda, R. W. Compans, Characterization of temperature sensitive influenza virus mutants defective in neuraminidase. *Virology* **61**, 397–410 (1974).
25. N. Naffakh, A. Tomoiu, M.-A. Rameix-Welti, S. van der Werf, Host Restriction of Avian Influenza Viruses at the Level of the Ribonucleoproteins. *Annu. Rev. Microbiol.* **62**, 403–424 (2008).
26. C. Schroeder, H. Heider, E. M ncke-Buchner, T.-I. Lin, The influenza virus ion channel and maturation cofactor M2 is a cholesterol-binding protein. *Eur Biophys J* **34**, 52–66 (2004).
27. A. García-Sastre *et al.*, Influenza A virus lacking the NS1 gene replicates in interferon-deficient systems. *Virology* **252**, 324–330 (1998).
28. B. G. Hale, R. E. Randall, J. Ortin, D. Jackson, The multifunctional NS1 protein of influenza A viruses. *J. Gen. Virol.* **89**, 2359–2376 (2008).
29. R. E. O'Neill, The influenza virus NEP (NS2 protein) mediates the nuclear export of viral ribonucleoproteins. *The EMBO Journal* **17**, 288–296 (1998).

30. Y. Suzuki, Sialic acid species as a determinant of the host range of influenza A viruses. *J. Virol.* **74**, 11825–11831 (2000).
31. G. N. Rogers, J. C. Paulson, Receptor determinants of human and animal influenza virus isolates: Differences in receptor specificity of the H3 hemagglutinin based on species of origin. *Virology* **127**, 361–373 (1983).
32. T. Ito, Molecular basis for the generation in pigs of influenza A viruses with pandemic potential. *J. Virol.* **72**, 7367–7373 (1998).
33. R. J. Connor, Y. Kawaoka, R. G. Webster, J. C. Paulson, Receptor specificity in human, avian, and equine H2 and H3 influenza virus isolates. *Virology* **205**, 17–23 (1994).
34. M. J. Gething, Studies on the mechanism of membrane fusion: site-specific mutagenesis of the hemagglutinin of influenza virus. *The Journal of Cell Biology* **102**, 11–23 (1986).
35. K. Cross, W. Langley, R. Russell, J. Skehel, D. Steinhauer, Composition and functions of the influenza fusion peptide. *Protein Pept. Lett.* **16**, 766–778 (2009).
36. T. Stegmann, Membrane fusion mechanisms: the influenza hemagglutinin paradigm and its implications for intracellular fusion. *Traffic* **1**, 598–604 (2000).
37. R. A. Lamb, C. D. Richardson, S. L. Zebedee, Influenza virus M2 protein is an integral membrane protein expressed on the infected-cell surface. *Virus Research* **3**, 4 (1985).
38. K. Shimbo, D. L. Brassard, R. A. Lamb, L. H. Pinto, Ion selectivity and activation of the M2 ion channel of influenza virus. *Biophysical Journal* **70**, 1335–1346 (1996).
39. K. Martin, A. Helenius, Nuclear transport of influenza virus ribonucleoproteins: the viral matrix protein (M1) promotes export and inhibits import. *Trends Cell Bio* **2**, 8 (1992).
40. K. Martin, A. Helenius, Transport of incoming influenza virus nucleocapsids into the nucleus. *Trends Cell Bio* **2**, 8 (1992).
41. C. Herz, E. Stavnezer, R. M. Krug, T. Gurney Jr., Influenza virus, an RNA virus, synthesizes its messenger RNA in the nucleus of infected cells. *Cell* **26**, 391–400 (1981).
42. A. J. Hay, B. Lomniczi, A. R. Bellamy, J. J. Skehel, Transcription of the influenza virus genome. *Virology* **83**, 337–355 (1977).
43. S. G. Lazarowitz, P. W. Choppin, Enhancement of the infectivity of influenza A and B viruses by proteolytic cleavage of the hemagglutinin polypeptide. *Virology* **68**, 440–454 (1975).
44. F. X. Bosch, W. Garten, H. D. Klenk, R. Rott, Proteolytic cleavage of influenza virus hemagglutinins: primary structure of the connecting peptide between HA1 and HA2 determines proteolytic cleavability and pathogenicity of avian influenza viruses. *Virology* **113**, 725–735 (1981).

45. Y. Kawaoka, R. G. Webster, Sequence requirements for cleavage activation of influenza virus hemagglutinin expressed in mammalian cells. *PNAS* **85**, 324–328 (1988).
46. A. García-Sastre, Inhibition of interferon-mediated antiviral responses by influenza A viruses and other negative-strand RNA viruses. *Virology* **279**, 375–384 (2001).
47. A. K. Heer *et al.*, TLR signaling fine-tunes anti-influenza B cell responses without regulating effector T cell responses. *J. Immunol.* **178**, 2182–2191 (2007).
48. V. Jeisy-Scott *et al.*, TLR7 recognition is dispensable for influenza virus A infection but important for the induction of hemagglutinin-specific antibodies in response to the 2009 pandemic split vaccine in mice. *J. Virol.* **86**, 10988–10998 (2012).
49. C. W. Potter, J. S. Oxford, Determinants of immunity to influenza infection in man. *British Medical Bulletin* **35**, 69–75 (1979).
50. R. J. Cox, K. A. Brokstad, P. Ogra, Influenza virus: Immunity and vaccination strategies. Comparison of the immune response to inactivated and live, attenuated influenza vaccines. *Scand J Immunol* **59**, 1–15 (2004).
51. B. R. Murphy, M. L. Clements, in *New strategies for oral immunization*, Current Topics in Microbiology and Immunology. (Springer Berlin Heidelberg, Berlin, Heidelberg, 1989), vol. 146, pp. 107–116.
52. C. A. Janeway, P. Travers, M. Walport, J. D. Capra, Immunobiology: The immune System in health and disease (4th edn). *Immunology Today* **21**, 201 (2000).
53. M. E. Ackerman *et al.*, D. C. Douek, Ed. Polyfunctional HIV-specific antibody responses are associated with spontaneous HIV control. *PLoS Pathog.* **12**, e1005315 (2016).
54. M. Bonsignori *et al.*, Antibody-Dependent Cellular Cytotoxicity-Mediating antibodies from an HIV-1 vaccine efficacy trial target multiple epitopes and preferentially use the VH1 gene family. *J. Virol.* **86**, 11521–11532 (2012).
55. M. R. Vogt *et al.*, Poorly neutralizing cross-Reactive antibodies against the fusion loop of west nile virus envelope protein protect in vivo via Fcγ receptor and complement-dependent effector mechanisms. *J. Virol.* **85**, 11567–11580 (2011).
56. S. Greenberg, H. R. Six, S. Drake, R. B. Couch, Cell cytotoxicity due to specific influenza antibody production in vitro after recent influenza antigen stimulation. *PNAS* **76**, 4622–4626 (1979).
57. G. Hashimoto, P. F. Wright, D. T. Karzon, Ability of human cord blood lymphocytes to mediate antibody-dependent cellular cytotoxicity against influenza virus-infected cells. *Infect. Immun.* **42**, 214–218 (1983).
58. S. Jegaskanda, J. T. Weinfurter, T. C. Friedrich, S. J. Kent, Antibody-dependent cellular

- cytotoxicity is associated with control of pandemic H1N1 influenza virus infection of macaques. *J. Virol.* **87**, 5512–5522 (2013).
59. W. He *et al.*, T. S. Dermody, Ed. Broadly neutralizing anti-influenza virus antibodies: Enhancement of neutralizing potency in polyclonal mixtures and IgA backbones. *J. Virol.* **89**, 3610–3618 (2015).
  60. D. Corti *et al.*, A neutralizing antibody selected from plasma cells that binds to group 1 and group 2 influenza A hemagglutinins. *Science* **333**, 850–856 (2011).
  61. D. J. DiLillo, G. S. Tan, P. Palese, J. V. Ravetch, Broadly neutralizing hemagglutinin stalk-specific antibodies require Fc $\gamma$ R interactions for protection against influenza virus in vivo. *Nat. Med.* **20**, 143–151 (2014).
  62. D. J. DiLillo, P. Palese, P. C. Wilson, J. V. Ravetch, Broadly neutralizing anti-influenza antibodies require Fc receptor engagement for in vivo protection. *J. Clin. Invest.* **126**, 605–610 (2016).
  63. E. D. Kilbourne, Influenza pandemics of the 20th century. *Emerging Infect. Dis.* **12**, 9–14 (2006).
  64. J. K. Taubenberger, D. M. Morens, Influenza: The once and future pandemic. *Public Health Reports* **125**, 15–26 (2010).
  65. D. M. Morens, J. K. Taubenberger, A. S. Fauci, The persistent legacy of the 1918 influenza virus. *N Engl J Med* **361**, 225–229 (2009).
  66. R. G. Webster, M. Yakhno, V. S. Hinshaw, W. J. Bean, K. Copal Murti, Intestinal influenza: Replication and characterization of influenza viruses in ducks. *Virology* **84**, 268–278 (1978).
  67. G. S. Freidl *et al.*, Influenza at the animal-human interface: a review of the literature for virological evidence of human infection with swine or avian influenza viruses other than A(H5N1). *Euro Surveill.* **19**, 8–26 (2014).
  68. G. Neumann, Y. Kawaoka, Transmission of influenza A viruses. *Virology* **479-480**, 234–246 (2015).
  69. J. A. Belser, C. B. Bridges, J. M. Katz, T. M. Tumpey, Past, present, and possible future human infection with influenza virus A subtype H7. *Emerging Infect. Dis.* **15**, 859–865 (2009).
  70. R. A. M. Fouchier *et al.*, Avian influenza A virus (H7N7) associated with human conjunctivitis and a fatal case of acute respiratory distress syndrome. *Proc. Natl. Acad. Sci. U.S.A.* **101**, 1356–1361 (2004).
  71. Transmission of H7N7 avian influenza A virus to human beings during a large outbreak in commercial poultry farms in the Netherlands. (2004) (available at

<http://www.sciencedirect.com/science/article/pii/S014067360415589X>).

72. R. Gao *et al.*, Human Infection with a Novel Avian-Origin Influenza A (H7N9) Virus. *N Engl J Med* **368**, 1888–1897 (2013).
73. A. D. Iuliano *et al.*, Increase in human infections with avian influenza A(H7N9) virus during the fifth epidemic — China, October 2016–February 2017. *MMWR Morb. Mortal. Wkly. Rep.* **66**, 254–255 (2017).
74. B. Liu *et al.*, Clusters of human infections with avian influenza A(H7N9) virus in China, March 2013 to June 2015. *J. Infect. Dis.* **216**, S548–S554 (2017).
75. D. Liu *et al.*, Origin and diversity of novel avian influenza A H7N9 viruses causing human infection: phylogenetic, structural, and coalescent analyses. *The Lancet* **381**, 1926–1932 (2013).
76. Y. Wang *et al.*, Towards a better understanding of the novel avian-origin H7N9 influenza A virus in China. *Scientific Reports* **3**, f2222 (2013).
77. Genetic analysis of novel avian A(H7N9) influenza viruses isolated from patients in China, February to April 2013. **18**, 20453 (2013).
78. I. H. Brown, The pig as an intermediate host for influenza A viruses between birds and humans. *International Congress Series* **1219**, 173–178 (2001).
79. G. J. D. Smith *et al.*, Origins and evolutionary genomics of the 2009 swine-origin H1N1 influenza A epidemic. *Nature* **459**, 1122–1125 (2009).
80. K. P. Myers, Cases of swine influenza in humans: a review of the literature. *Clin. Infect. Dis.* **44**, 1084–1088 (2007).
81. S. Lindstrom *et al.*, Human infections with novel reassortant influenza A(H3N2)v viruses, United States, 2011. *Emerging Infect. Dis.* **18**, 834–837 (2012).
82. L. Finelli, D. L. Swerdlow, The emergence of influenza A (H3N2)v virus: what we learned from the first wave. *Clin. Infect. Dis.* **57 Suppl 1**, S1–3 (2013).
83. B. Shu *et al.*, Genetic analysis and antigenic characterization of swine origin influenza viruses isolated from humans in the United States, 1990-2010. *Virology* **422**, 151–160 (2012).
84. K. Waalen, A. Kilander, S. G. Dudman, Age-dependent prevalence of antibodies cross-reactive to the influenza A (H3N2) variant virus in sera collected in Norway in 2011. *Euro Surveill.* (2012).
85. D. M. Skowronski *et al.*, Cross-reactive and vaccine-induced antibody to an emerging swine-origin variant of influenza A virus subtype H3N2 (H3N2v). *J. Infect. Dis.* **206**, 1852–1861 (2012).

86. I. A. Wilson, J. J. Skehel, D. C. Wiley, Structure of the haemagglutinin membrane glycoprotein of influenza virus at 3 Å resolution. *Nature* **289**, 366–373 (1981).
87. W. Weis *et al.*, Structure of the influenza virus haemagglutinin complexed with its receptor, sialic acid. *Nature* **333**, 426–431 (1988).
88. C. M. Carr, P. S. Kim, A spring-loaded mechanism for the conformational change of influenza hemagglutinin. *Cell* **73**, 823–832 (1993).
89. Y. Ha, D. J. Stevens, J. J. Skehel, D. C. Wiley, X-ray structures of H5 avian and H9 swine influenza virus hemagglutinins bound to avian and human receptor analogs. *Proc. Natl. Acad. Sci. U.S.A.* **98**, 11181–11186 (2001).
90. S. J. Gamblin, J. J. Skehel, Influenza hemagglutinin and neuraminidase membrane glycoproteins. *J. Biol. Chem.* **285**, 28403–28409 (2010).
91. M. Matrosovich *et al.*, Early alterations of the receptor-binding properties of H1, H2, and H3 avian influenza virus hemagglutinins after their introduction into mammals. *J. Virol.* **74**, 8502–8512 (2000).
92. J. Stevens, O. Blixt, J. C. Paulson, I. A. Wilson, Glycan microarray technologies: tools to survey host specificity of influenza viruses. *Nat. Rev. Microbiol.* **4**, 857–864 (2006).
93. T. M. Tumpey *et al.*, A two-amino acid change in the hemagglutinin of the 1918 influenza virus abolishes transmission. *Science* **315**, 655–659 (2007).
94. G. N. Rogers *et al.*, Single amino acid substitutions in influenza haemagglutinin change receptor binding specificity. *Nature* **304**, 76–78 (1983).
95. P. B. Rosenthal *et al.*, Structure of the haemagglutinin-esterase-fusion glycoprotein of influenza C virus. *Nature* **396**, 92–96 (1998).
96. R. J. Russell *et al.*, H1 and H7 influenza haemagglutinin structures extend a structural classification of haemagglutinin subtypes. *Virology* **325**, 287–296 (2004).
97. C. Dreyfus, D. C. Ekiert, Structure of a classical broadly neutralizing stem antibody in complex with a pandemic H2 influenza virus hemagglutinin. *J. Virol.* **87**, 7149–7154 (2013).
98. M. Knossow, J. J. Skehel, Variation and infectivity neutralization in influenza. *Immunology* **119**, 1–7 (2006).
99. A. G. Schmidt *et al.*, Preconfiguration of the antigen-binding site during affinity maturation of a broadly neutralizing influenza virus antibody. *Proc. Natl. Acad. Sci. U.S.A.* **110**, 264–269 (2013).
100. R. Yoshida *et al.*, P. Palese, Ed. Cross-protective potential of a novel monoclonal antibody directed against antigenic site B of the hemagglutinin of influenza A viruses.

- PLoS Pathog.* **5**, e1000350 (2009).
101. D. Fleury *et al.*, A complex of influenza hemagglutinin with a neutralizing antibody that binds outside the virus receptor binding site. *Nat. Struct. Mol. Biol.* **6**, 530–534 (1999).
  102. Structure of antigenic sites on the haemagglutinin molecule of H5 avian influenza virus and phenotypic variation of escape mutants. **83**, 2497–2505 (2002).
  103. T. Ohkura *et al.*, Epitope mapping of neutralizing monoclonal antibody in avian influenza A H5N1 virus hemagglutinin. *Biochem. Biophys. Res. Commun* **418**, 38–43 (2012).
  104. D. C. Wiley, I. A. Wilson, J. J. Skehel, Structural identification of the antibody-binding sites of Hong Kong influenza haemagglutinin and their involvement in antigenic variation. *Nature* **289**, 373–378 (1981).
  105. A. J. Caton, G. G. Brownlee, J. W. Yewdell, W. Gerhard, The antigenic structure of the influenza virus A/PR/8/34 hemagglutinin (H1 subtype). *Cell* **31**, 417–427 (1982).
  106. R. G. Webster, W. G. Laver, Determination of the number of nonoverlapping antigenic areas on Hong Kong (H3N2) influenza virus hemagglutinin with monoclonal antibodies and the selection of variants with potential epidemiological significance. *Virology* **104**, 139–148 (1980).
  107. B. Brandenburg *et al.*, P. Digard, Ed. Mechanisms of hemagglutinin targeted influenza virus neutralization. *PLoS ONE* **8**, e80034 (2013).
  108. D. C. Ekiert *et al.*, Antibody recognition of a highly conserved influenza virus epitope. *Science* **324**, 246–251 (2009).
  109. D. Corti *et al.*, Heterosubtypic neutralizing antibodies are produced by individuals immunized with a seasonal influenza vaccine. *J. Clin. Invest.* **120**, 1663–1673 (2010).
  110. M. Throsby *et al.*, D. Unutmaz, Ed. Heterosubtypic neutralizing monoclonal antibodies cross-protective against H5N1 and H1N1 recovered from human IgM+ memory B cells. *PLoS ONE* **3**, e3942 (2008).
  111. Broadly cross-reactive antibodies dominate the human B cell response against 2009 pandemic H1N1 influenza virus infection. **208**, 181–193 (2011).
  112. R. H. E. Friesen *et al.*, A common solution to group 2 influenza virus neutralization. *Proc. Natl. Acad. Sci. U.S.A.* **111**, 445–450 (2014).
  113. D. C. Ekiert *et al.*, A Highly Conserved Neutralizing Epitope on Group 2 Influenza A Viruses. *Science* **333**, 843–850 (2011).
  114. G. S. Tan *et al.*, Characterization of a broadly neutralizing monoclonal antibody that targets the fusion domain of group 2 influenza A virus hemagglutinin. *J. Virol.* **88**,



- 13580–13592 (2014).
115. C. Dreyfus *et al.*, Highly conserved protective epitopes on influenza B viruses. *Science* **337**, 1343–1348 (2012).
  116. G. Nakamura *et al.*, An in vivo human-plasmablast enrichment technique allows rapid identification of therapeutic influenza A antibodies. *Cell Host & Microbe* **14**, 93–103 (2013).
  117. Y. Wu *et al.*, A potent broad-spectrum protective human monoclonal antibody crosslinking two haemagglutinin monomers of influenza A virus. *Nat. Commun.* **6**, ncomms8708 (2015).
  118. N. L. Kallewaard *et al.*, Structure and function analysis of an antibody recognizing all influenza A subtypes. *Cell* **166**, 596–608 (2016).
  119. J. Lee *et al.*, Molecular-level analysis of the serum antibody repertoire in young adults before and after seasonal influenza vaccination. *Nat. Med.* **22**, 1456–1464 (2016).
  120. S. A. Valkenburg *et al.*, Stalking influenza by vaccination with pre-fusion headless HA mini-stem. *Scientific Reports* **6**, srep22666 (2016).
  121. H. M. Yassine *et al.*, Hemagglutinin-stem nanoparticles generate heterosubtypic influenza protection. *Nat. Med.* **21**, 1065–1070 (2015).
  122. A. Impagliazzo *et al.*, A stable trimeric influenza hemagglutinin stem as a broadly protective immunogen. *Science* **349**, 1301–1306 (2015).
  123. R. Nachbagauer *et al.*, A chimeric haemagglutinin-based influenza split virion vaccine adjuvanted with AS03 induces protective stalk-reactive antibodies in mice. *npj Vaccines* **1**, npjvaccines201615 (2016).
  124. J. N. Varghese, P. M. Colman, Three-dimensional structure of the neuraminidase of influenza virus A/Tokyo/3/67 at 2.2 Å resolution. *J. Mol. Biol.* **221**, 473–486 (1991).
  125. M. N. Matrosovich, T. Y. Matrosovich, T. Gray, N. A. Roberts, H. D. Klenk, Neuraminidase is important for the initiation of influenza virus infection in human airway epithelium. *J. Virol.* **78**, 12665–12667 (2004).
  126. L. J. Mitnaul *et al.*, Balanced hemagglutinin and neuraminidase activities are critical for efficient replication of influenza A virus. *J. Virol.* **74**, 6015–6020 (2000).
  127. M. J. Sylte, D. L. Suarez, in *New strategies for oral immunization*, Current Topics in Microbiology and Immunology. (Springer Berlin Heidelberg, Berlin, Heidelberg, 2009), vol. 333, pp. 227–241.
  128. J. N. Varghese, P. M. Colman, A. van Donkelaar, T. J. Blick, J. L. McKimm-Breschkin, Structural evidence for a second sialic acid binding site in avian influenza virus

- neuraminidases. *PNAS* **94**, 11808–11812 (1997).
129. W. G. Laver, P. M. Colman, R. G. Webster, V. S. Hinshaw, G. M. Air, Influenza virus neuraminidase with hemagglutinin activity. *Virology* **137**, 314–323 (1984).
  130. D. J. Benton, S. A. Wharton, S. R. Martin, J. W. McCauley, B. R. G. Williams, Ed. Role of neuraminidase in influenza A (H7N9) virus receptor binding. *J. Virol.* **91**, e02293–16 (2017).
  131. B. R. Murphy, J. A. Kasel, R. M. Chanock, Association of serum anti-neuraminidase antibody with resistance to influenza in man. *N Engl J Med* **286**, 1329–1332 (1972).
  132. T. Wohlbold, F. Krammer, In the shadow of hemagglutinin: A growing interest in influenza viral neuraminidase and its role as a vaccine antigen. *Viruses* **6**, 2465–2494 (2014).
  133. L. Couzens *et al.*, An optimized enzyme-linked lectin assay to measure influenza A virus neuraminidase inhibition antibody titers in human sera. *J. Virol. Methods* **210**, 7–14 (2014).
  134. R. B. Couch *et al.*, Randomized comparative study of the serum antihemagglutinin and antineuraminidase antibody responses to six licensed trivalent influenza vaccines. *Vaccine* **31**, 190–195 (2012).
  135. M. R. Laguio-Vila *et al.*, Comparison of serum hemagglutinin and neuraminidase inhibition antibodies after 2010-2011 trivalent inactivated influenza vaccination in healthcare personnel. *Open Forum Infectious Diseases* **2**, ofu115–ofu115 (2015).
  136. Y. Shoji *et al.*, An influenza N1 neuraminidase-specific monoclonal antibody with broad neuraminidase inhibition activity against H5N1 HPAI viruses. *Human Vaccines* **7**, 199–204 (2014).
  137. H. Wan *et al.*, Molecular basis for broad neuraminidase immunity: conserved epitopes in seasonal and pandemic H1N1 as well as H5N1 influenza viruses. *J. Virol.* **87**, 9290–9300 (2013).
  138. T. J. Wohlbold *et al.*, Vaccination with adjuvanted recombinant neuraminidase induces broad heterologous, but not heterosubtypic, cross-protection against influenza virus infection in mice. *MBio* **6**, e02556–14 (2015).
  139. C. Scholtissek, V. S. Hinshaw, C. W. Olsen, *Influenza in pigs and their role as the intermediate host* (Textbook of Influenza, 1998).
  140. Update: Influenza A (H3N2)v transmission and guidelines - five states, 2011. *MMWR Morb. Mortal. Wkly. Rep.* **60**, 1741–1744 (2012).
  141. S. Lindstrom *et al.*, Human infections with novel reassortant influenza A(H3N2)v viruses, United States, 2011. *Emerging Infect. Dis.* **18**, 834–837 (2012).

142. Antibodies cross-reactive to influenza A (H3N2) variant virus and impact of 2010-11 seasonal influenza vaccine on cross-reactive antibodies-United States. **11**, 20131083–20131083 (2012).
143. N. N. Zhou *et al.*, Emergence of H3N2 reassortant influenza A viruses in North American pigs. *Vet. Microbiol.* **74**, 47–58 (2000).
144. N. N. Zhou, Genetic reassortment of avian, swine, and human influenza A viruses in American pigs. *J. Virol.* **73**, 8851–8856 (1999).
145. R. J. Webby, Evolution of swine H3N2 influenza viruses in the United States. *J. Virol.* **74**, 8243–8251 (2000).
146. Antibodies cross-reactive to influenza A (H3N2) variant virus and impact of 2010-11 seasonal influenza vaccine on cross-reactive antibodies - United States. *MMWR Morb. Mortal. Wkly. Rep.* **61**, 237–241 (2012).
147. B. F. Koel *et al.*, Substitutions near the receptor binding site determine major antigenic change during influenza virus evolution. *Science* **342**, 976–979 (2013).
148. M. J. Choi *et al.*, Live animal markets in Minnesota: A potential source for emergence of novel influenza A viruses and interspecies Transmission. *Clin. Infect. Dis.* **61**, civ618–1362 (2015).
149. B. Manicassamy *et al.*, R. A. M. Fouchier, Ed. Protection of mice against lethal challenge with 2009 H1N1 influenza A virus by 1918-like and classical swine H1N1 based vaccines. *PLoS Pathog.* **6**, e1000745 (2010).
150. M. I. Nelson *et al.*, Y. Kawaoka, Ed. Multiple reassortment events in the evolutionary history of H1N1 influenza A virus since 1918. *PLoS Pathog.* **4**, e1000012 (2008).
151. A. L. Vincent, W. Ma, K. M. Lager, B. H. Janke, J. A. Richt, in *Advances in virus research*, Advances in Virus Research. (Elsevier, 2008), vol. 72, pp. 127–154.
152. B. Lina *et al.*, S-OtrH3N2 viruses: use of sequence data for description of the molecular characteristics of the viruses and their relatedness to previously circulating H3N2 human viruses. *Euro Surveill.* **16**, 20039 (2011).
153. W. A. Keitel *et al.*, Safety and immunogenicity of a subvirion monovalent unadjuvanted inactivated influenza A(H3N2) variant vaccine in healthy persons  $\geq 18$  years old. *J. Infect. Dis.* **212**, 552–561 (2015).
154. S. A. Smith *et al.*, Persistence of circulating memory B cell clones with potential for dengue virus disease enhancement for decades following infection. *J. Virol.* **86**, 2665–2675 (2012).
155. C. Suloway *et al.*, Automated molecular microscopy: The new Legimon system. *J. Struct. Biol.* **151**, 41–60 (2005).

156. N. R. Voss, C. K. Yoshioka, M. Radermacher, C. S. Potter, B. Carragher, DoG Picker and TiltPicker: Software tools to facilitate particle selection in single particle electron microscopy. *J. Struct. Biol* **166**, 205–213 (2009).
157. M. Hohn *et al.*, SPARX, a new environment for Cryo-EM image processing. *J. Struct. Biol* **157**, 47–55 (2007).
158. M. van Heel, G. Harauz, E. V. Orlova, R. Schmidt, M. Schatz, A new generation of the IMAGIC image processing system. *J. Struct. Biol* **116**, 17–24 (1996).
159. G. Tang *et al.*, EMAN2: An extensible image processing suite for electron microscopy. *J. Struct. Biol* **157**, 38–46 (2007).
160. S. J. Ludtke, P. R. Baldwin, W. Chiu, EMAN: Semiautomated software for high-resolution single-particle reconstructions. *J. Struct. Biol* **128**, 82–97 (1999).
161. A. G. S. C. Jansen, E. A. M. Sanders, A. W. Hoes, A. M. van Loon, E. Hak, Influenza- and respiratory syncytial virus-associated mortality and hospitalisations. *Eur. Respir. J.* **30**, 1158–1166 (2007).
162. M. K. Iwane *et al.*, Population-based surveillance for hospitalizations associated with respiratory syncytial virus, influenza virus, and parainfluenza viruses among young children. *Pediatrics* **113**, 1758–1764 (2004).
163. L. Simonsen *et al.*, Impact of influenza vaccination on seasonal mortality in the US elderly population. *Arch. Intern. Med.* **165**, 265–272 (2005).
164. D. J. Smith *et al.*, Mapping the antigenic and genetic evolution of influenza Virus. *Science* **305**, 371–376 (2004).
165. C. A. Russell *et al.*, The global circulation of seasonal influenza A (H3N2) viruses. *Science* **320**, 340–346 (2008).
166. L. Blanton *et al.*, Update: influenza activity--United states and worldwide, May 24-September 5, 2015. *MMWR Recomm Rep* **64**, 1011–1016 (2015).
167. S. Salzberg, The contents of the syringe. *Nature* **454**, 160–161 (2008).
168. T. D'Mello *et al.*, Update: Influenza activity--United States, September 28, 2014-February 21, 2015. *MMWR Morb. Mortal. Wkly. Rep.* **64**, 206–212 (2015).
169. K. Hutchings, Circulation of drifted influenza A(H3N2)viruses in the EU/EEA —22 December 2014. Stockholm: ECDC, 2014. (2014).
170. M. A. Jhung, S. Epperson, M. Biggerstaff, D. Allen, A. Balish, Outbreak of variant influenza A(H3N2) virus in the United States. *Clin. Infect. Dis.* **57**, 1703–1712 (2013).
171. T. J. Wohlbold *et al.*, D. S. Lyles, Ed. Hemagglutinin stalk- and neuraminidase-specific

- monoclonal antibodies protect against lethal H10N8 influenza virus infection in mice. *J. Virol.* **90**, 851–861 (2016).
172. S. Jegaskanda *et al.*, Cross-reactive influenza-specific antibody-dependent cellular cytotoxicity antibodies in the absence of neutralizing antibodies. *J. Immunol.* **190**, 1837–1848 (2013).
173. V. C. Huber, J. M. Lynch, D. J. Bucher, J. Le, D. W. Metzger, Fc receptor-mediated phagocytosis makes a significant contribution to clearance of influenza virus infections. *J. Immunol.* **166**, 7381–7388 (2001).
174. F. Cox *et al.*, HA antibody-mediated Fc $\gamma$ RIIIa activity is both dependent on FcR engagement and interactions between HA and sialic acids. *Front. Immunol.* **7**, 1333 (2016).
175. S. Bangaru *et al.*, Recognition of influenza H3N2 variant virus by human neutralizing antibodies. *JCI Insight* **1**, e86673 (2016).
176. R. Yoshida *et al.*, P. Palese, Ed. Cross-protective potential of a novel monoclonal antibody directed against antigenic site B of the hemagglutinin of influenza A viruses. *PLoS Pathog.* **5**, e1000350 (2009).
177. C. E. Mullarkey *et al.*, Broadly neutralizing hemagglutinin stalk-specific antibodies induce potent phagocytosis of immune complexes by neutrophils in an Fc-dependent manner. *MBio* **7**, e01624–16 (2016).
178. W. He *et al.*, Epitope specificity plays a critical role in regulating antibody-dependent cell-mediated cytotoxicity against influenza A virus. *Proc. Natl. Acad. Sci. U.S.A.* **113**, 11931–11936 (2016).
179. B. D. Wines *et al.*, Dimeric Fc $\gamma$ R ectodomains as probes of the Fc receptor function of anti-influenza virus IgG. *J. Immunol.* **197**, 1507–1516 (2016).
180. P. S. Lee, I. A. Wilson, in *Influenza Pathogenesis and Control - Volume II*, Current Topics in Microbiology and Immunology. (Springer International Publishing, Cham, 2014), vol. 386, pp. 323–341.
181. D. Fleury, R. S. Daniels, J. J. Skehel, M. Knossow, T. Bizebard, Structural evidence for recognition of a single epitope by two distinct antibodies. *Proteins: Struct., Funct., Genet.* **40**, 572–578 (2000).
182. A complex of influenza hemagglutinin with a neutralizing antibody that binds outside the virus receptor binding site. **6**, 530–534 (1999).
183. X. Zhu, Y.-H. Guo, T. Jiang, Y.-D. Wang, A unique and conserved neutralization epitope in H5N1 influenza viruses identified by an antibody against the A/Goose/Guangdong/1/96 hemagglutinin. *J. Virol.* **87**, 12619–12635 (2013).

184. J. Stevens *et al.*, Structure and receptor specificity of the hemagglutinin from an H5N1 influenza virus. *Science* **312**, 404–410 (2006).
185. Z. Otwinowski, W. Minor, in *Macromolecular Crystallography Part A*, Methods in Enzymology. (Elsevier, 1997), vol. 276, pp. 307–326.
186. A. J. McCoy *et al.*, Phaser crystallographic software. *J. Appl. Crystallogr.* **40**, 658–674 (2007).
187. P. Emsley, B. Lohkamp, W. G. Scott, K. Cowtan, IUCr, Features and development of Coot. *Acta Crystallogr. D Biol. Crystallogr.* **66**, 486–501 (2010).
188. P. D. Adams *et al.*, PHENIX: a comprehensive Python-based system for macromolecular structure solution. *Acta Crystallogr. D Biol. Crystallogr.* **66**, 213–221 (2010).
189. I. K. McDonald, J. M. Thornton, Satisfying hydrogen bonding potential in proteins. *J. Mol. Biol.* **238**, 777–793 (1994).
190. S. Sheriff, W. A. Hendrickson, J. L. Smith, Structure of myohemerythrin in the azidomet state at 1.7/1.3 Å resolution. *J. Mol. Biol.* **197**, 273–296 (1987).
191. M. L. Connolly, IUCr, Analytical molecular surface calculation. *J. Appl. Crystallogr.* **16**, 548–558 (1983).
192. K. R. Abhinandan, A. C. R. Martin, Analysis and improvements to Kabat and structurally correct numbering of antibody variable domains. *Mol. Immunol.* **45**, 3832–3839 (2008).
193. V. B. Chen *et al.*, MolProbity: all-atom structure validation for macromolecular crystallography. *Acta Crystallogr. D Biol. Crystallogr.* **66**, 12–21 (2010).
194. Y. Bao *et al.*, The influenza virus resource at the National Center for Biotechnology Information. *J. Virol.* **82**, 596–601 (2008).
195. R. C. Edgar, MUSCLE: multiple sequence alignment with high accuracy and high throughput. *Nucl. Acids Res.* **32**, 1792–1797 (2004).
196. D. C. Ekiert *et al.*, Cross-neutralization of influenza A viruses mediated by a single antibody loop. *Nature* **489**, 526–532 (2012).
197. P. S. Lee *et al.*, Heterosubtypic antibody recognition of the influenza virus hemagglutinin receptor binding site enhanced by avidity. *Proc. Natl. Acad. Sci. U.S.A.* **109**, 17040–17045 (2012).
198. P. E. Leon *et al.*, Optimal activation of Fc-mediated effector functions by influenza virus hemagglutinin antibodies requires two points of contact. *PNAS* **113**, E5944–E5951 (2016).

199. F. Krammer, N. Pica, R. Hai, I. Margine, P. Palese, Chimeric hemagglutinin influenza virus vaccine constructs elicit broadly protective stalk-specific antibodies. *J. Virol.* **87**, 6550 (2013).
200. J. Steel *et al.*, Influenza virus vaccine based on the conserved hemagglutinin stalk domain. *MBio* **1**, e00018–10–e00018–10 (2010).
201. Y. Lu, J. P. Welsh, J. R. Swartz, Production and stabilization of the trimeric influenza hemagglutinin stem domain for potentially broadly protective influenza vaccines. *Proc. Natl. Acad. Sci. U.S.A.* **111**, 125–130 (2014).
202. J. W. Yewdell, A. Taylor, A. Yellen, A. Caton, W. Gerhard, Mutations in or near the fusion peptide of the influenza virus hemagglutinin affect an antigenic site in the globular region. *J. Virol.* **67**, 933–942 (1993).
203. J. Van Dongen, A. W. Langerak, M. Brüggemann, ... standardization of PCR primers and protocols for detection of clonal immunoglobulin and T-cell receptor gene recombinations in suspect lymphoproliferations: report .... *MMWR Recomm Rep* (2003).
204. N. J. Thornburg *et al.*, H7N9 influenza virus neutralizing antibodies that possess few somatic mutations. *Journal of Clinical Investigation* **126**, 1482–1494 (2016).
205. X. Brochet, M.-P. Lefranc, V. Giudicelli, IMGT/V-QUEST: the highly customized and integrated system for IG and TR standardized V-J and V-D-J sequence analysis. *Nucl. Acids Res.* **36**, W503–8 (2008).
206. V. Giudicelli, M.-P. Lefranc, IMGT/junctionanalysis: IMGT standardized analysis of the V-J and V-D-J junctions of the rearranged immunoglobulins (IG) and T cell receptors (TR). *Cold Spring Harbor Protocols* **2011**, 716–725 (2011).
207. G. R. McLean, A. Nakouzi, A. Casadevall, N. S. Green, Human and murine immunoglobulin expression vector cassettes. *Mol. Immunol.* **37**, 837–845 (2000).
208. S. Li *et al.*, Mechanism of intracellular camp sensor Epac2 activation cAMP-induced conformational changes identified by amide hydrogen/deuterium exchange mass spectrometry (DXMS). *J. Biol. Chem.* **286**, 17889–17897 (2011).
209. S. Hsu *et al.*, Structural insights into glucan phosphatase dynamics using amide hydrogen–deuterium exchange mass spectrometry. *Biochemistry* **48**, 9891–9902 (2009).
210. Y. Hamuro *et al.*, Mapping Intersubunit Interactions of the Regulatory Subunit (RI $\alpha$ ) in the Type I Holoenzyme of Protein Kinase A by Amide Hydrogen/Deuterium Exchange Mass Spectrometry (DXMS). *J. Mol. Biol.* **340**, 1185–1196 (2004).
211. W. D. Lu, T. Liu, S. Li, V. L. Woods, V. Hook, The prohormone proenkephalin possesses differential conformational features of subdomains revealed by rapid H-D exchange mass spectrometry. *Protein Science* **21**, 178–187 (2012).

212. Z. Zhang, D. L. Smith, Determination of amide hydrogen exchange by mass spectrometry: A new tool for protein structure elucidation. *Protein Science* **2**, 522–531 (1993).
213. N. Xiang *et al.*, Assessing change in avian influenza A(H7N9) Virus infections during the fourth epidemic — China, September 2015–August 2016. *MMWR Morb. Mortal. Wkly. Rep.* **65**, 1390–1394 (2016).
214. C. J. Henry Dunand *et al.*, Both neutralizing and non-neutralizing human H7N9 influenza vaccine-induced monoclonal antibodies confer protection. *Cell Host & Microbe* **19**, 800–813 (2016).
215. J. Wang *et al.*, S. Perlman, Ed. Characterization of two human monoclonal antibodies neutralizing influenza a H7N9 viruses. *J. Virol.* **89**, 9115–9118 (2015).
216. L. Liu *et al.*, Induction of broadly cross-reactive stalk-specific antibody responses to influenza group 1 and group 2 hemagglutinins by natural H7N9 virus infection in humans. *J. Infect. Dis.* **215**, 518–528 (2017).
217. S. Rockman *et al.*, Neuraminidase-inhibiting antibody is a correlate of cross-protection against lethal H5N1 influenza virus in ferrets immunized with seasonal influenza vaccine. *J. Virol.* **87**, 3053–3061 (2013).
218. A. S. Monto *et al.*, Antibody to influenza virus neuraminidase: an independent correlate of protection. *J. Infect. Dis.* **212**, 1191–1199 (2015).
219. G. M. Air, M. C. Els, L. E. Brown, W. G. Laver, R. G. Webster, Location of antigenic sites on the three-dimensional structure of the influenza N2 virus neuraminidase. *Virology* **145**, 237–248 (1985).
220. R. G. Webster, L. E. Brown, W. G. Laver, Antigenic and biological characterization of influenza virus neuraminidase (N2) with monoclonal antibodies. *Virology* **135**, 30–42 (1984).
221. R. L. Malby *et al.*, The structure of a complex between the NC10 antibody and influenza virus neuraminidase and comparison with the overlapping binding site of the NC41 antibody. *structure* **2**, 733–746 (1994).
222. W. R. Tulip, J. N. Varghese, W. G. Laver, R. G. Webster, P. M. Colman, Refined crystal structure of the influenza virus N9 neuraminidase-NC41 Fab complex. *J. Mol. Biol.* **227**, 122–148 (1992).
223. D. M. Skowronski *et al.*, Avian influenza A(H7N9) virus infection in 2 travelers returning from China to Canada, January 2015. *Emerging Infect. Dis.* **22**, 71–74 (2016).
224. T. M. Doyle *et al.*, Universal anti-neuraminidase antibody inhibiting all influenza A subtypes. *Antiviral Research* **100**, 567–574 (2013).



225. X. Zhu, X. Xu, I. A. Wilson, Structure determination of the 1918 H1N1 neuraminidase from a crystal with lattice-translocation defects. *Acta Crystallogr. D Biol. Crystallogr.* **64**, 843–850 (2008).
226. X. Zhu *et al.*, Influenza virus neuraminidases with reduced enzymatic activity that avidly bind sialic acid receptors. *J. Virol.* **86**, 13371–13383 (2012).
227. H. E. Klock, S. A. Lesley, in *High throughput protein expression and purification*, Methods in Molecular Biology. (Humana Press, Totowa, NJ, 2009), vol. 498, pp. 91–103.